공학석사 학위청구논문

Evaluation of Wind Pressure Coefficients of Greenhouses using Wind Tunnel Test and Numerical Model

풍동 실험과 수치 모델에 의한 온실 풍압 계수 평가

2015 년 8 월

서울대학교 대학원

생태조경 · 지역시스템공학부 지역시스템공학전공

김 락 우

Evaluation of Wind Pressure Coefficients of Greenhouses using Wind Tunnel Test and Numerical Model

풍동 실험과 수치 모델에 의한 온실 풍압 계수 평가

지도 교수 이 인 복

이 논문을 공학석사 학위논문으로 제출함
2015 년 8 월

서울대학교 대학원
생태조경 · 지역시스템공학부 지역시스템공학전공
김 락 우

김락우의 공학석사 학위논문을 인준함
2015 년 8 월

위 원 장 _____ (인)

부위원장 _____ (인)

위 원 _____ (인)

Abstract

In the case of South Korea, greenhouse cultivation area has greatly increased with the introduction of greenhouse modernization policy by Korean government since the beginning of the 1990s. In addition, the Korean government recently announced a new development plan for a large-scale greenhouse complex to harvest higher value-added vegetables. However, many conventional greenhouses collapsed in a series of natural disasters ever year because a greenhouse facility is classified as a light-weight structure that is vulnerable to heavy wind loads. Therefore, reference to the newly modified greenhouse design standards, especially for reclaimed lands, has been required to ensure structural safety on strong winds.

In this study, to evaluate the structural safety of greenhouses according to the wind characteristics of the reclaimed lands, the wind pressure coefficients of the commercial single-span greenhouse facilities, such as Even-span, Three-quarter, Peach and Mono-span types, were measured according to various wind direction and design factors, such as the roof slope and the radius of the curvature of the roof materials. Additionally, for computing wind pressure coefficients of multi-span greenhouses, accuracy of 3D designed CFD model was initially evaluated using the measured results of Even-span and Peach type greenhouses.

Firstly, the wind environments of the reclaimed lands were designed in wind tunnel. Variations in the windward terrain roughness of the target reclaimed lands were also computed to design the wind and turbulence intensity profiles based on ESDU. Next, the wind pressure coefficients of typical single-span greenhouses in Korea were measured according to the wind direction, roof slope and radius of the curvature of the roof. From the wind tunnel measurement, when the wind blows perpendicularly to the sidewall of the greenhouse (0 and 180° wind directions), a relatively large pressure variation was generated near the eaves of the greenhouse;

these large pressure differences can cause the collapse and permanent strain of the framework of the greenhouse. The wind direction on the local wind pressure was influential; therefore, consideration of the local pressure acting on the surface of the facilities is critical in establishing safe design criteria, especially glazing bars and coverings. From the results, the wind pressure coefficients of 4 types of greenhouses built in reclaimed lands were proposed in terms of structural safety and cladding design.

For CFD validations, CFD computed and WT measured results were compared with each other, and especially y^+ values were mainly considered to find optimum conditions of first grid height. CFD computed y^+ value almost exactly corresponded with the measured results as first grid height at 1.5×10^{-4} m. As a result, 1.5×10^{-4} m was selected for the first grid height. Computational domain and grid independence tests were also conducted to determine the domain size, the grid size. The length of upstream part was fixed at 3H, and the length of the side and the upper part was determined to be 5H and 5H, respectively. The length of downstream was determined to be 15H because the CFD model accurately predicted 10H above. The accuracy of the CFD model improved as the grid size decreased. The grid size was designed as 1.0×10^{-2} m based on a grid independence test. From a given standard, an appropriate turbulence model was selected according to the wind direction and the type and the environmental conditions of greenhouse. SST $k-\omega$ model was determined as a turbulence model for CFD validation because the statistical indices in SST $k-\omega$ model were generally higher than that in other turbulence models. Finally, the simulated and measured wind pressure coefficients were compared using statistical indices. The CFD validation model made accurate predictions under all experimental conditions. It was determined that the CFD validation model was appropriate for estimating the wind pressure coefficient.

Keywords : Computational fluid dynamics, CFD validation model, Single-span Greenhouse, Wind pressure coefficient, Wind tunnel test
Student Number : 2013-23257

Contents

Abstract i
Contents iii
List of Tables v
List of Figures viii

1. Introduction 1

2. Literature review 4
2.1 Field experiment and Wind tunnel test 4
2.2 Computational fluid dynamics 5

3. Materials and Methods 7
3.1 Target reclaimed lands 8
3.2 Target greenhouses 9
3.2.1 Target greenhouses for wind tunnel test 9
3.2.2 Target greenhouses for validation of CFD model 13
3.3 Experimental wind tunnel 14
3.4 ESDU (Engineering Sciences Data Unit) 15
3.5 Wind pressure coefficients 17
3.6 CFD simulation 18
3.7 The law of the wall 19
3.8 Wall roughness 21
3.9 Design of the wind environment 22
3.9.1 ESDU design of the wind environment of reclaimed land 22
3.9.2 Design of wind Environment in the wind tunnel 25
3.9.3 Design of wind environment in CFD simulation 28
3.10 Experimental design 30
3.10.1 Experimental design of the wind tunnel test 30
3.10.2 Experimental conditions of the CFD simulation 41
3.9 Accuracy analysis of CFD model 47

4. Results and Discussions 50
4.1 Wind pressure coefficients in terms of the structural design 50
4.1.1 Even-span type greenhouses 50
4.1.2 Three-quarter type greenhouses 56
4.1.3 Peach type greenhouses 62
4.1.4 Mono-span type greenhouses 67
4.2 Local wind pressure coefficients in terms of cladding design 73
4.2.1 Even-span type greenhouses 73
4.2.2 Three-quarter type greenhouses 74
4.2.3 Peach type greenhouses 75
4.2.4 Mono-span type greenhouses 76
4.3 Overall evaluation of the wind pressure coefficients for structural and cladding design 77
4.4 Development of CFD model for predicting distribution of wind pressure on greenhouse 84
4.4.1 Comparison of wind pressure coefficients according to y^+ value 84
4.4.2 Comparison of wind pressure coefficients for decision of domain size 89
4.4.3 Comparison of wind pressure coefficients for grid independence 101
4.4.4 Comparison of wind pressure coefficients according to turbulence model 103
4.5 Wind pressure coefficient computed from CFD validation model 107

5. Conclusions 111

References 114

Abstract (Korean) 122

List of Tables

Table 1 Total reclaimed land area and greenhouse complex area, as announced by the Korean government 8
Table 2 Design information of the Even-span and Three-quarter type greenhouses for wind tunnel test 10
Table 3 Design information of Peach type and Mono-span type greenhouses for wind tunnel test..... 12
Table 4 Design information of Even-span and Peach type greenhouses for validation of CFD model 14
Table 5 Design characteristics of the wind tunnel test..... 31
Table 6 The constant input values for the CFD model..... 41
Table 7 Experimental conditions for computational domain size tests..... 45
Table 8 Area-weighted averaged wind pressure coefficients of the RW and RL sections (wind direction was 0°) and the RS sections (wind direction was 90°) for the Type PC-R5000 model..... 67
Table 9 Measured local wind pressure coefficients of Even-span type greenhouses (Type-EV-D26) according to the designed wind directions..... 74
Table 10 Measured local wind pressure coefficients of Three-quarter type greenhouses (Type-TQ-D26) according to the designed wind directions..... 75
Table 11 Measured local wind pressure coefficients of Peach type greenhouses (Type-PC-R5000) according to the designed wind directions 76
Table 12 Measured local wind pressure coefficients of Mono-span type greenhouses (Type-MS-D26) according to the designed wind directions..... 77
Table 13 Suggestion of the wind pressure coefficients of Even-span type greenhouses for structural design..... 78

Table 14 Suggestion of the wind pressure coefficients of Even-span type greenhouses for cladding design 79
Table 15 Suggestion of wind pressure coefficients of Three-quarter type greenhouses for structural design 80
Table 16 Suggestion of wind pressure coefficients of Three-quarter type greenhouses for cladding design 81
Table 17 Suggestion of the wind pressure coefficients of Peach type greenhouses for structural design 82
Table 18 Suggestion of the wind pressure coefficients of Peach type greenhouses for cladding design 83
Table 19 Suggestion of the wind pressure coefficients of Mono-span type greenhouses for structural design 83
Table 20 Suggestion of the wind pressure coefficients of Mono-span type greenhouses for cladding design 84
Table 21 R^2 values between CFD computed and WT measured wind pressure coefficients of Type-EV-D22 according to first grid height when the wind direction was 0° 89
Table 22 R^2 and d values between CFD computed and WT measured wind pressure coefficients of Type-EV-D22 according to length of downstream parts when the wind direction was 0° 99
Table 23 R^2 and d values between CFD computed and WT measured wind pressure coefficients of Type-EV-D22 according to length of side and upper parts when the wind direction was 0° 100
Table 24 R^2 values between CFD computed and WT measured wind pressure coefficients of Type-EV-D22 according to grid size when the wind direction was 0° 103

Table 25 Statistical indices between CFD computed and WT measured wind pressure coefficients of Even-span type greenhouses according to turbulence model when the wind directions were 0 and 90° 104
Table 26 Statistical indices between CFD computed and WT measured wind pressure coefficients of Peach type greenhouses according to turbulence model when the wind directions were 0 and 90° 106

List of Figures

Fig. 1 Location of the 7 target reclaimed lands and 9 KMA weather stations 9
Fig. 2 Schematic diagram of the target single-span greenhouses (a) Even-span and (b) Three-quarter types 11
Fig. 3 Schematic diagram of the target single-span greenhouses (a) Peach and (b)Mono-span types 13
Fig. 4 Schematic diagram of the experimental Eiffel-type wind tunnel (Unit: mm) 15
Fig. 5 Concept of the wind pressure coefficients 18
Fig. 6 Dimensionless velocity profile for a turbulent boundary layer (White., 1991) 20
Fig. 7 Example of the land-use categorization to determine the windward surface roughness in Saemanguem reclaimed land according to the wind direction 24
Fig. 8 Design process of the vertical wind and turbulence intensity profiles over terrain with roughness changes for the wind tunnel test 24
Fig. 9 Design of the vertical wind and turbulence intensity profiles using roughness blocks, spires, and barriers in the wind tunnel 26
Fig. 10 Comparison of the vertical wind profiles as computed by the ESDU and designed at the wind tunnel (a), the vertical turbulence intensity profiles as computed by the ESDU and designed at the wind tunnel (b) and measured power spectral density (c) 28
Fig. 11 Comparison of the vertical wind profiles as computed by the ESDU and designed in CFD simulation (a) and the vertical k, ϵ, ω profiles designed in CFD simulation (b) 30
Fig. 12 Scaled Peach type greenhouse model (Type-PC-R6000) and Multi-channel pressure scanner (Scanivalve Inc., USA) 32
Fig. 13 Examples of the location of the measuring points for pressure coefficients and the definition of monitoring lines for the scaled peach-type greenhouse model (Type-PC-R6000) 34

Fig. 14 Regional definition of each surface of scaled Even-span type greenhouses for wind pressure analyses of the structural design ((a) and (b)) and cladding design ((c) and (d)) 37
Fig. 15 Regional definition of each surface of scaled Three-quarter type greenhouses for wind pressure analyses of the structural design ((a), (b) and (c)) and cladding design ((d), (e) and (f)) 38
Fig. 16 Regional definition of each surface of scaled Peach type greenhouses for wind pressure analyses of the structural design ((a) and (b)) and cladding design ((c) and (d)) 39
Fig. 17 Regional definition of each surface of scaled Mono span type greenhouses for wind pressure analyses of the structural design ((a), (b) and (c)) and cladding design ((d), (e) and (f)) 40
Fig. 18 1.5×10^{-4} m (a), 1.5×10^{-3} m (b) and 1.5×10^{-2} m (c) of first gird height in near wall region 43
Fig. 19 Computation domain size suggested through the empirical and experimental methods 45
Fig. 20 1.0×10^{-2} m (a), 2.5×10^{-2} m (b), 4.0×10^{-2} m (c) and 5.5×10^{-2} m (d) of grid size around greenhouse for grid independence test (Type-EV-D22) 46
Fig. 21 Measured wind pressure coefficients of each monitoring row for the Type-EV-D26 model when the wind directions were 0° (a) and 90° (b) 52
Fig. 22 Distribution of the wind pressure coefficients for Type-EV-D26 when the wind direction was 0° 53
Fig. 23 Distribution of the wind pressure coefficients for Type-EV-D26 when the wind direction was 90° 53
Fig. 24 Area-weighted averaged wind pressure coefficients according to the roof slope and section of the Even-span type greenhouses when the wind directions were 0° (a) and 90° (b) 55

Fig. 25 Measured wind pressure coefficients of each monitoring row for the Type-TQ-D26 model when the wind directions were 0° (a), 90° (b) and 180° (c) 58
Fig. 26 Distribution of the wind pressure coefficients for Type-TQ-D26 when the wind direction was 0° 58
Fig. 27 Distribution of the wind pressure coefficients for Type-TQ-D26 when the wind direction was 90° 59
Fig. 28 Distribution of the wind pressure coefficients for Type-TQ-D26 when the wind direction was 180° 59
Fig. 29 Area-weighted averaged wind pressure coefficients according to the roof slope and section of the Three-quarter type greenhouses when the wind directions were 0° (a), 90° (b) and 180° (c) 61
Fig. 30 Measured wind pressure coefficients of each monitoring row for the Type-PC-R5000 model when the wind directions were 0° (a) and 90° (b) 63
Fig. 31 Distribution of the wind pressure coefficients for Type-PC-R5000 when the wind direction was 0° 64
Fig. 32 Distribution of the wind pressure coefficients for Type-PC-R5000 when the wind direction was 90° 64
Fig. 33 Area-weighted averaged wind pressure coefficients according to the radius of the curvature of roof and the section of Peach type greenhouses when the wind directions were 0° (a) and 90° (b) 66
Fig. 34 Measured wind pressure coefficients of each monitoring row for the Type-MS-D26 model when the wind directions were 0° (a), 90° (b) and 180° (c) 69
Fig. 35 Distribution of the wind pressure coefficients for Type-MS-D26 when the wind direction was 0° 70

Fig. 36 Distribution of the wind pressure coefficients for Type−MS−D26 when the wind direction was 90° 70
Fig. 37 Distribution of the wind pressure coefficients for Type−MS−D26 when the wind direction was 180° 70
Fig. 38 Area−weighted averaged wind pressure coefficients according to the roof slope and section of Mono−span type greenhouses when the wind directions were 0° (a), 90° (b) and 180° (c) 72
Fig. 39 Distributions of y^+ value of Type−EV−D22 as first grid heights were 1.5 × 10^{-4} m (a), 1.5 × 10^{-3} m (b) and 1.5 × 10^{-2} m (c) when the wind direction was 0° 86
Fig. 40 Comparison between CFD computed and WT measured wind pressure coefficients of Type−EV−D22 according to first grid heights when the wind direction was 0° (a) Standard k−ε model (b) RNG k−ε model (c) Realizable k−ε model (d) Standard k−ω (e) SST k−ω model 88
Fig. 41 Vector of wind velocity at central surface of computational domain according to length of downstream part when greenhouse type was Type−EV−D22, and the wind direction was 0° (a) 5H, (b) 10H, (c) 15H, (d) 20H and (d) 25H 91
Fig. 42 Comparison between CFD computed and WT measured wind pressure coefficients of Type−EV−D22 according to length of downstream part when the wind direction was 0° (a) Standard k−ε model (b) RNG k−ε model (c) Realizable k−ε model (d) Standard k−ω (e) SST k−ω model 93
Fig. 43 Comparison between CFD computed and WT measured wind pressure coefficients of Type−EV−D22 according to length of side part when the wind direction was 0° (a) Standard k−ε model (b) RNG k−ε model (c) Realizable k−ε model (d) Standard k−ω (e) SST k−ω model 95

Fig. 44 Comparison between CFD computed and WT measured wind pressure coefficients of Type−EV−D22 according to length of upper part when the wind direction was 0° (a) Standard k−ε model (b) RNG k−ε model (c) Realizable k−ε model (d) Standard k−ω (e) SST k−ω model 97
Fig. 45 Finally determined computational domain size in CFD simulation 100
Fig. 46 Scatter diagram between CFD computed and WT measured wind pressure coefficients of Type−EV−D22 as grid sizes were 1.0×10^{-2} m (a), 2.5×10^{-2} m (b), 4.0×10^{-2} m (c) and 5.5×10^{-2} m (d) when the wind direction was 0° 102
Fig. 47 Comparison between CFD computed and WT measured wind pressure coefficients of Even−span type greenhouses using CFD validation model when the wind directions were 0° (a) and 90° (b) 108
Fig. 48 Comparison between CFD computed and WT measured wind pressure coefficients of Peach type greenhouses using CFD validation model when the wind directions were 0° (a) and 90° (b) 110

1. Introduction

Vegetable and flower consumptions have increased following the social craze about the improvement of diet. In particular, the vegetable consumption per capita in South Korea has steadily increased from 59.9 kg in 1970 to 170 kg in 2013 (Statistics Korea, 2014). In response to these situations, most of the rural farmers recognized importance of protected cultivation that can more efficiently and stably cultivate high-quality crops throughout the year by taking advantage of four clearly distinguishable seasonal climate in Korea. Greenhouse industry is able to most efficiently achieve environment-friendly and high-tech agriculture (Rural Development Administration, 2007). In the case of South Korea, greenhouse cultivation area has greatly increased with the introduction of greenhouse modernization policy by Korean government since the beginning of the 1990s. Current greenhouse cultivation area reached a total 52,530 ha in 2012 in accordance with enlargement and corporatization of greenhouse (Ministry of Agriculture, Food and Rural Affairs of Korea, 2014). The total agricultural economic production in the country was 41.1 billion US dollars in 2013, and the horticultural industry accounted for approximately 14% of the total agricultural production; the steady economic growth of this industry has been predicted (Statistics Korea, 2014).

On the other hand, South Korea is surrounded by sea on three sides with many islands and tidal flats. For this situation, the reclamation project have been made over a long period of time. Especially, Saemangeum reclamation project consisting of a site of about 40,100 ha has been promoted at Gunsan, Kimje and Buan, Jeollabuk-do Province. The Korean government recently announced a new development plan for a large-scale greenhouse complex to harvest higher value-added vegetables: 5,185 ha of high-tech horticulture facilities on 12 reclaimed lands for overseas and domestic markets (Ministry of Agriculture, Food and Rural Affairs,

2014).

In South Korea, greenhouse has been constructed based on various domestic greenhouse standards such as the 'Design Guide for Greenhouse Structures' (Rural Research Institute, 1995), 'Standards and Explanations of Greenhouse Structural Design' (Ministry of Agriculture, Food and Rural Affairs of Korea, 1995), 'Korean Building Code Structural' (Ministry of Land, Infrastructure and Transport, 2009) and so on. However, domestic greenhouse standards are not well-defined in terms of design criteria for wind load while this current version was made more than 20 years ago. The greenhouse facilities are especially classified as a light-weight structures with a low safety factor, and these structures are highly vulnerable to heavy wind loads compared to general buildings. Due to this, many conventional greenhouses collapsed in a series of natural disasters ever year. For example, the amount of damage by Typhoon Muifa in 2011 was reported to be about 42.08 ha and 4.1 million US dollar (Ministry of Public Safety and Security of Korea, 2012). Especially, the wind environments of the reclaimed land are entirely different from those of the inland area; a strong wind velocity is due to the relatively mild surface roughness and is also frequently influenced by the turbulent behavior of convection from coastal regions. The return period of strong winds or huge typhoons and has been recently shortened due to the global and local climatic changes, especially in the west coastal regions of the country, where the bulk of the reclaimed lands are located (Korea Meteorological Administration, 2014). Therefore, economic loss due to the destruction of farm houses and greenhouses by strong winds is a critical problem for the horticultural industry. Consequently, the suggestion of newly modified greenhouse design standards, especially for reclaimed lands, has been required to secure the structural safety in response to the strong wind environment, while the preliminary data collection of wind pressure and wind pressure coefficients on greenhouse structure should take precedence.

In this study, the object was to establish newly modified greenhouse design standards. As a fundamental study, the wind

pressure coefficients of the commercial single-span greenhouse facilities, such as Even-span, Three-quarter, Peach and Mono-span types, were measured according to various wind direction and design factors, such as the roof slope and the radius of the curvature of the roof materials. Additionally, for computing wind pressure coefficients of multi-span greenhouses, CFD validations were performed using the wind tunnel test measurement in order to improve reliability of CFD designed model. As a first step, the wind environments of the target reclaimed lands were designed in the wind tunnel using ESDU. Variations in the upwind terrain roughness of the target regions were considered to accurately design the wind and turbulence intensity profiles in the wind tunnel and CFD simulation. Then, considering the blockage ratio of the wind tunnel, limitations of simultaneous measurements for a number of points and cost problems, the experiments were conducted based on various single-span greenhouses. Measured wind pressure coefficient data according to the each environmental condition were analyzed in terms of structural design and the cladding design of the greenhouse to secure the structural safety under strong wind conditions. After wind tunnel test, wind tunnel measured results were compared to the CFD computed results to predict wind pressure coefficient in various conditions. In order to improve the reliability of CFD model, results was made relative comparison according to y^+ value, computational domain test, grid independence test and turbulence model.

2. Literature review

2.1 Field experiment and Wind tunnel test

Evaluation of structural stability of the greenhouse has been made through field experiment and wind tunnel test. Various field experiments have been conducted to investigate the characteristics of the wind pressure acting on low building, such as greenhouse. Wells and Hoxey (1980) investigated the wind loads on 5 different forms of glass-covered greenhouses under natural wind conditions, and Hoxey and Richardson (1983; 1984) measured the wind loads on plastic film and arch type greenhouses, which represented commercial greenhouses in the U.K. Mehta et al. (1992) measured roof corner pressures at several taps in field. Richardson (1993) also measured the external and internal wind pressure coefficient distribution of single-span plastic film livestock buildings to support a "European code of practice for the design of tunnel buildings." Richards and Hoxey (2012) measured pressures on the vertical and horizontal central lines of the 6m cube. Field experiment is reliable method in terms of using full scale greenhouse model. In contrast, these approaches have shown various experimental limitations: 1) difficulties in acquiring aerodynamic data due to unstable external weather conditions; 2) difficulties in the simultaneous measurement of wind pressure on large surfaces of greenhouse with multiple measurement points; and 3) time- and labor-consuming problems. In this sense, the wind tunnel has been regarded as an economical and accurate alternative for conducting aerodynamic research and obtaining sufficient quantitative data to support design decisions (Lee et al., 2003) compared to field experiments. The wind tunnel has been widely used to investigate the physical characteristics of the target structure in response to the designed artificial wind environment in the fields of civil engineering. Castro and Robins (1977) conducted investigation of the flow around surface-mounted cubes in in uniform and turbulent flows, coupled with pressure

measurements. Tahouri et al. (1990) conducted wind tunnel measurements of mean surface pressure distributions on models in three turbulent boundary layers to study the influence of the approach flow parameters. Robertson et al. (2002) compared the external and internal mean pressure coefficient of a large scale model of an arched polytunnel structure and a flat roof shade house structure. Uematsu et al. (2009) analyzed the effect of sidewall openings on the wind loads and the resultant responses of pipe-framed greenhouses, and Richards et al. (2007) conducted wind tunnel modelling of low building, such as cube. Moriyama et al. (2010) measured the effect of the distance and the number of pipe houses on wind pressure coefficient.

2.2 Computational fluid dynamics (CFD)

The wind tunnel test also has experimental limitations: 1) sensitivity to similarity law; 2) the limited number of channel for simultaneous measurement; 3) the limited size of a greenhouse model due to blockage ratio; 4) cost for manufacturing a greenhouse model under various experimental conditions; and 5) time and labor consumed. Especially, conducting a wind tunnel test for large-sized multi-span greenhouses is very difficult in terms of getting reliable results because of blockage ratio of the wind tunnel, the limitations of simultaneous measurements, and the cost problems associated with manufacturing greenhouse scaled models. For these reasons, computational fluid dynamics (CFD) has been effectively and widely used to obtain reliable data quantitatively as well as qualitatively. Various CFD studies have been actively conducted to measure the wind pressure of Semicircular, Even-span and Venlo type greenhouses. Mathews and Meyer (1987; 1988) predicted the wind loads on a semicircular greenhouse through two dimensional numerical modeling, and Mathews et al. (1988) evaluated the wind pressure distribution of various types of greenhouses. Hoxey et al. (1993) analyzed geometric parameters that affect wind loads on low-rise portal framed buildings using two-dimensional CFD

simulation. Mistriotis et al. (1997) and Reichrath and Davies (2002) simulated the wind pressure coefficients of Venlo type greenhouse. Reichrath and Davies (2002) especially compared the results according to turbulence models such as the Standard $k-\varepsilon$ turbulence model and the RNG $k-\varepsilon$ turbulence model. Mistriotis and Briassoulis (2002) calculated the external and the internal pressure coefficients of a tunnel greenhouse depending on ventilation opening configuration. The results were compared with the Eurocode-1 (1995) and the European standard prEN13031-1 (1999). CFD validation of those studies was conducted by comparing with the results of the field experiment done by Wells and Hoxey (1980) and Hoxey and Richardson (1983; 1984). However, these studies have shown various experimental limitations. Although the computed values were mainly in agreement with the measured values, there was about 0.5 or more of gap and other trend between the measured and the computed wind pressure coefficients at windward. Moreover, the studies analyzed the wind pressure using only two dimensional simulations with a single wind direction as well as the limited and simple structure of greenhouses.

3. Materials and Methods

In this study, wind pressure coefficients of 4 representative single-span greenhouses (Even-span, Three-quarter (Korean Greenhouse design standards for glass type greenhouse, 1997-451, Ministry of Land, Infrastructure and Transport, Korea), Peach (Specification and Drawings of Horticulture facility, 2010-128, Ministry of Agriculture, Food and Rural Affairs, Korea) and Mono-span (Specification and Drawings of Horticulture facility, 2014-78, Ministry of Agriculture, Food and Rural Affairs, Korea) types) were investigated using a large-sized wind tunnel test. Wind pressure coefficients were measured and later analyzed according to the design factors of the greenhouse and the given wind conditions. The ESDU code (Engineering Sciences Data Unit, E0108, IHS, UK) was used to design the vertical wind and turbulence intensity profiles reflecting the multiple surface roughness of windward accurately. The measured wind pressure coefficients were analyzed in terms of the (i) structural design and (ii) cladding design.

CFD model was designed for the purpose of evaluating on structural design of greenhouse by wind pressure in various conditions. Firstly, CFD model was designed for predicting wind pressure. CFD validations according to y^+ value, computational domain and grid independence tests were conducted by comparing between CFD computed and wind tunnel measured results of Even-span greenhouse (Type-EV-D22), which has a 22° roof slope when the wind direction was 0° to the side wall. From CFD model designed from a given first grid height, the domain size and the grid size, the results of Even-span and Peach type greenhouses were also relatively compared to find optimum conditions of turbulence model. The wind pressure coefficients were predicted from the validated CFD model, and the computed and measured wind pressure coefficients were quantitatively compared using statistical indices.

3.1 Target reclaimed lands

The target sites were total 7 representative reclaimed lands in South Korea where the Korean government announced the development plan for high-tech and large-scale greenhouse complex for the overseas and domestic markets: the Sihwa, Hwaong, Sukmoon, Iweon, Goheung, Saemanguen and Yeongsanggang reclaimed lands. Weather data, such as the wind direction and wind speed, of the target reclaimed lands were gathered from the 9 weather observation stations of the KMA (Korean Meteorological Administration) near the target sites. Fig. 1 illustrates the location of the 7 target reclaimed lands and 9 weather observation stations. Each geographical characteristic within a 50-km radius of the studied sites and weather data with a certified analysis process from the KMA weather observation stations were used for the input data of the ESDU model. Table 1 shows the total planning area of each reclaimed land and the area of the greenhouse complex, as announced by the Korean government.

Table 1 Total reclaimed land area and greenhouse complex area, as announced by the Korean government

Reclaimed lands	Total area (ha)	Planning area for greenhouse complex (ha)
Sihwa	3,636	416
Hwaong	4,482	600
Sukmoon	1,968	488
Iweon	847	300
Goheung	2,075	200
Saemanguem	8,570	2,600
Yeongsanggang	7,049	520

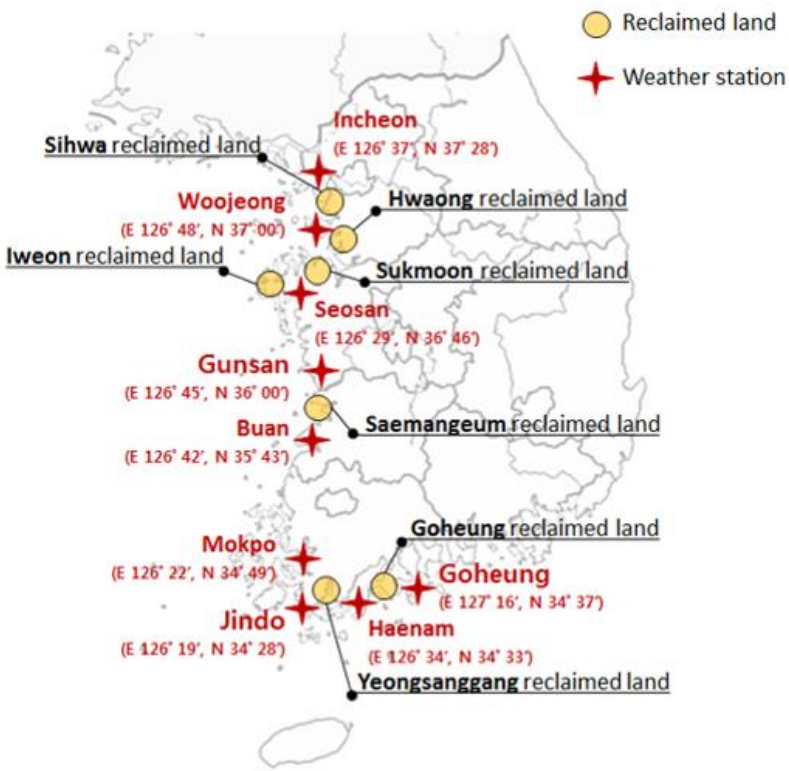

Fig. 1 Location of the 7 target reclaimed lands and 9 KMA weather stations

3.2 Target greenhouses

3.2.1 Target greenhouses for wind tunnel test

The target facilities included 4 types of single-span greenhouses; Even-span, Three-quarter, Peach and Mono-span type greenhouses, which are widely and commonly used in South Korea.

Single-span Even-span type (Fig. 2 (a)) and Three-quarter type (Fig. 2 (b)) greenhouses are typical glass-covered greenhouses, and their specific experimental design data are shown in Table 2. The roof slopes of both of the greenhouse types were used as experimental variables to investigate the variance in the wind pressure coefficients; the height of the ridge of both of the

greenhouses depended on the variables of the roof slope.

Table 2 Design information of the Even-span and Three-quarter type greenhouses for wind tunnel test

Single-span and Even-span type greenhouse
(Korean greenhouse design standards for glass-type greenhouses, 1997-451, Ministry of Land, Infrastructure and Transport, Korea)

Cases	Eave height (m)	Ridge height (m)	Width (m)	Length (m)	Roof slope (°)
Type-EV-D22	2.0	3.41	7.0	44.0	22
Type-EV-D24		3.56			24
Type-EV-D26		3.71			26
Type-EV-D28		3.86			28
Type-EV-D30		4.02			30
Type-EV-D32		4.19			32

Single-span, Three-quarter type greenhouse
(Korean greenhouse design standards for glass-type greenhouses, 1997-451, Ministry of Land, Infrastructure and Transport, Korea)

Cases	Eave height (m)	Ridge height (m)	Width (m)	Length (m)	Roof slope (°)
Type-TQ-D22	2.0	4.12	7.0	44.0	22
Type-TQ-D24		4.36			24
Type-TQ-D26		4.56			26
Type-TQ-D28		4.79			28
Type-TQ-D30		5.03			30
Type-TQ-D32		5.28			32

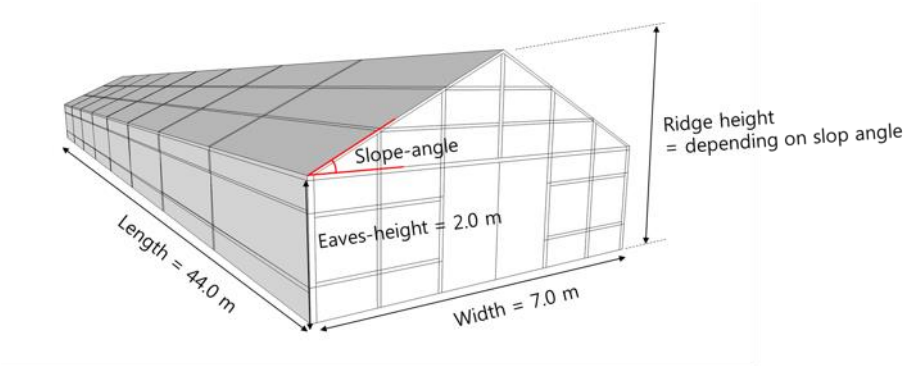

(a) Even-span type greenhouse

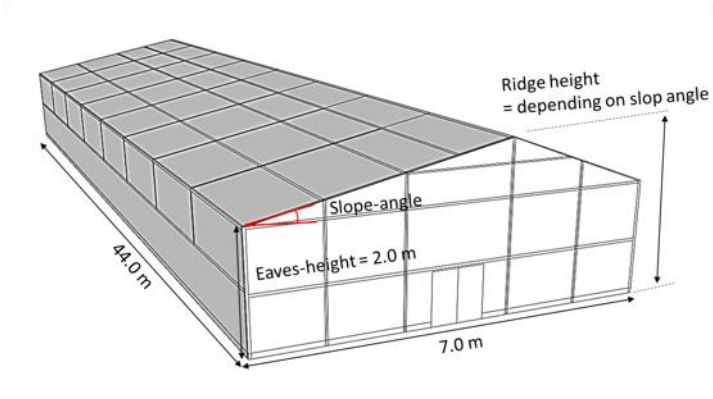

(b) Three-quarter type greenhouse

Fig. 2 Schematic diagram of the target single-span greenhouses (a) Even-span and (b) Three-quarter types

Single-span Peach type (Fig. 3 (a)) and Mono-span type (Fig. 3 (b)) greenhouses are a type of sheet-plastic-film greenhouses, and their specific experimental design data are shown in Table 3. In the case of the Peach type greenhouse, the radius of the curvature of the roof was designed as the experimental variable, ranging from 4,000 to 6,500 mm at regular intervals. The roof slope was used as an experimental variable for Mono-span type greenhouses; the height of the ridge depended on the scale of the roof slope angle, as shown in Table 3.

Table 3 Design information of Peach type and Mono-span type greenhouses for wind tunnel test

Single-span, Peach type greenhouse (Specification and Drawings of Horticulture facility, 2010-128, Ministry of Agriculture, Food and Rural Affairs, Korea)					
Cases	Eave height (m)	Ridge height (m)	Width (m)	Length (m)	Curvature radius of the roof (mm)
Type-PC-R4000	1.6	3.5	7.0	44.0	4,000
Type-PC-R4500					4,500
Type-PC-R5000					5,000
Type-PC-R5500					5,500
Type-PC-R6000					6,000
Type-PC-R6500					6,500

Single-span, Mono-span type greenhouse (Specification and Drawing of Horticulture facility, 2014-78, Ministry of Agriculture, Food and Rural Affairs, Korea)					
Cases	Eave height (m)	Ridge height (m)	Width (m)	Length (m)	Roof slope (°)
Type-MS-D22	2.0	3.41	3.5	3.5	22
Type-MS-D24		3.56			24
Type-MS-D26		3.71			26
Type-MS-D28		3.86			28
Type-MS-D30		4.02			30
Type-MS-D32		4.19			32

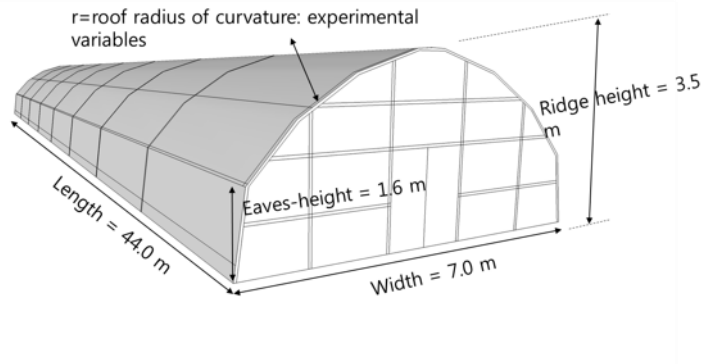

(a) Peach type greenhouse

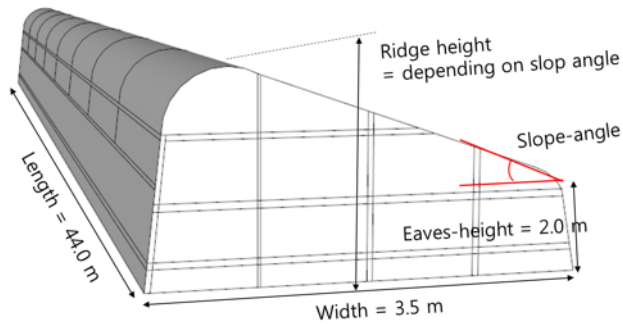

(b) Mono-span type greenhouse

Fig. 3 Schematic diagram of the target single-span greenhouses (a) Peach and (b) Mono-span types

3.2.2 Target greenhouses for validation of CFD model

Even span type and Peach type single-span greenhouses, typical greenhouse models in South Korea, were selected as target greenhouses. The roof slopes of Even-span type greenhouse were used as experimental variables to validate various environmental conditions. In the case of Peach type greenhouse, the radiuses of the curvature of the roof were used as experimental variables. The length of two types of greenhouse was designed by 44.0 m considering the blockage ratio of the wind tunnel, as shown in Table 4.

Table 4 Design information of Even-span and Peach type greenhouses for validation of CFD model

Single-span and Even-span type greenhouse (Korean greenhouse design standards for glass-type greenhouses, 1997-451, Ministry of Land, Infrastructure and Transport, Korea)					
Cases	Eave height (m)	Ridge height (m)	Width (m)	Length (m)	Roof slope (°)
Type-EV-D22	2.0	3.41	7.0	44.0	22
Type-EV-D26		3.71			26
Type-EV-D30		4.02			30

Single-span, Peach type greenhouse (Specification and Drawings of Horticulture facility, 2010-128, Ministry of Agriculture, Food and Rural Affairs, Korea)					
Cases	Eave height (m)	Ridge height (m)	Width (m)	Length (m)	Curvature radius of the roof (mm)
Type-PC-R4000	1.6	3.5	7.0	44.0	4,000
Type-PC-R5000					5,000
Type-PC-R6000					6,000

3.3 Experimental wind tunnel

The wind tunnel has been widely used to investigate various factors, including the structural safety of buildings related to strong wind and residential stability in the wind environment of rural and civil areas, by artificially controlling the wind conditions. In this study, the wind pressure coefficients on single-span greenhouses was measured in an Eiffel-type large sized wind tunnel (TESolution, Co., Anseong City, Gyeonggi-do, Korea). The size of the test section of the experimental wind tunnel was 8.0 m wide, 2.5 m high and 23.2 m long, and Fig. 4 depicts the schematic diagram of the experimental wind tunnel. The diameter of the turntable of the test section is 3.0 m, and it can revolve $\pm 270^{\circ}$ for measurement, while it is used for changing wind direction. Three suction-type wind blowers with a 1.5 m diameter are installed. The performance of the wind blowers is

1,200 rpm at maximum; it can produce a velocity magnitude at the test section ranging from 0.3 to 11.5 m s^{-1}.

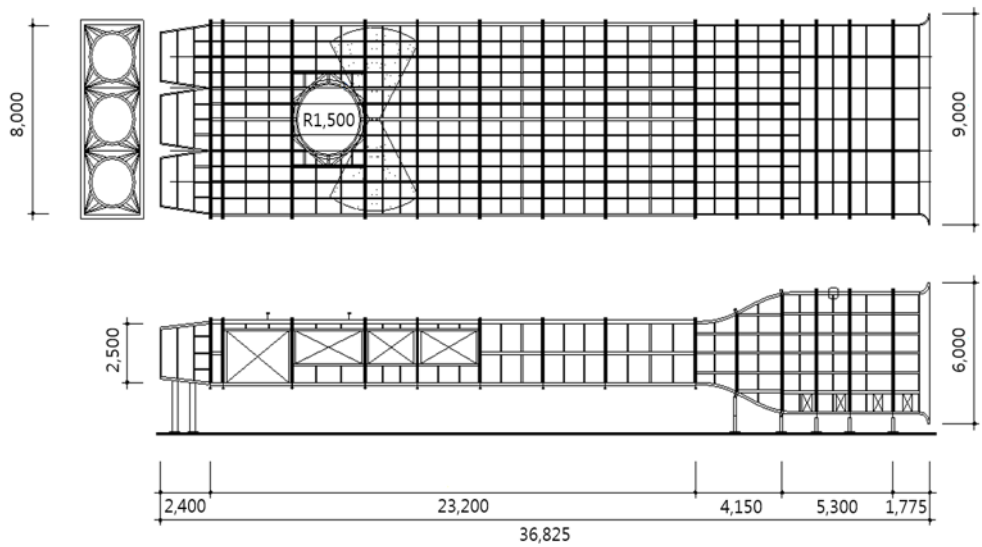

Fig. 4 Schematic diagram of the experimental Eiffel-type wind tunnel (Unit: mm)

3.4 ESDU (Engineering Sciences Data Unit, 84011 and 84030, IHS, UK)

The wind characteristics near the ground show turbulent behavior in space and time because of the surface friction force and horizontal drag forces. The topographic effects, surface roughness and atmospheric stability are the main factors determining the characteristics of the vertical wind profile. Among these factors, the effects of atmospheric stability is not highly influential to the formation of the vertical wind profile when the wind blows with relatively higher velocities to the target area. Especially under strong wind conditions, the atmospheric stability is close to a neutrally stable status; thus, it can be generally ignored. Greenhouse facilities are usually located at the lower part of the atmospheric boundary layer (e.g., less than 5 m high), where the effects of friction and viscosity are influential; therefore, the design of accurate vertical

wind and turbulence intensity profiles is very challenging for investigating the wind pressure acting on greenhouse surface. The vertical wind profile can be generally expressed in two ways: log-law (Jackson, 1981) and power-law (Irwin, 1979). However, both methods are only applicable when the surface roughness of the windward area is fully simple and uniform; if there are multiple surface roughness in the windward area, both methods cannot accurately realize the actual characteristics of the wind profiles.

In this study, the ESDU VIEWpac E0108 (Engineering Sciences Data Unit, IHS, UK) code, which was programmed based on ESDU (Engineering Sciences Data Unit, IHS, UK) 84011 and 84030, was used to design the vertical wind profile and turbulence intensity profiles of 7 target reclaimed lands, reflecting the various changes in the surface roughness of the windward regions. In the fields of wind and civil engineering, ESDU has been widely and recently used to accurately realize the complexity of the wind characteristics in the atmospheric boundary layer (Wang, 2005; Drew et al., 2013; Shademan et al., 2014; Blackman et al., 2015; Li et al., 2015). Based on the ESDU 84011 and 84030 theorem, "Hourly mean wind speeds", "expected maximum τ-second gust occurring in a given period" and "turbulence intensities" can be computed considering such factors as topographical effects, complexities of the surface roughness, and appearance frequency of the gust. The ESDU code uses the wind speed profile factor (K) to calculate the vertical wind profile, which is defined as follows:

$$\mathrm{K} = \frac{\hat{V}_{zx}}{V_{10r}} = \frac{V_{zx}}{V_{10r}} \tag{1}$$

Where, K is the wind speed profile factor (dimensionless), V_{zx} is an hourly mean wind speed (wind speed averaged over 1 hour at height z when the site is a distance x downwind of a change in terrain roughness, m s^{-1}), $\hat{V}_{zx}$ is an expected (or mean) maximum gust speed at height z (averaged over τ seconds, occurring in period of 1 hour when the site is a distance x downwind of a change in terrain

roughness; when τ=3600 s, $\hat{V}_{zx}$ becomes the hourly mean wind speed, V_{zx}, m s^{-1}), and V_{10r} is a reference wind speed: the hourly mean value at z=10 m over flat over country terrain (m s^{-1}).

V and $\hat{V}$ can be expressed using peak factor, g, and turbulence intensity, I.

$$\frac{\hat{V}}{V} = 1 + \mathrm{gI} \tag{2}$$

Where, $\mathrm{g} = 4.2\exp(-0.08\mathrm{k}^3 + 0.17\mathrm{k}^2 - 0.3\mathrm{k})$ and $k = 1 + \log_{10}\tau$

The turbulence intensity is defined as the ratio of the standard deviation of the wind-fluctuating components of the wind speed to the mean hourly wind speed at the same height and under the same conditions (ESDU 84030, IHS, UK).

$$I_{zx} = \frac{\sigma_{zx}}{V_{zx}} = \left(\frac{K_{1sec}}{K_{3600}} - 1\right) \Big/ 3.40 \tag{3}$$

Where, I_{zx} is the turbulence intensity at height z above size and distance x downwind of change in terrain roughness (dimensionless), K_{1sec} is the wind speed profile factor when the gust averaging time is 1 second, K_{3600} is the wind speed profile factor when the gust averaging time is 1 hour, and σ_{zx} is a standard deviation of the wind-fluctuating component of wind speed (m s^{-1}).

3.5 Wind pressure coefficients

Wind pressure coefficients (Fig. 5) can be defined as a dimensionless function of the wind pressure difference and dynamic pressure measuring at the average roof height of the greenhouse based on the Bernoulli theorem

$$C_p = \frac{P}{q_H} = \frac{p_P - p_\infty}{\frac{1}{2}\rho {V_\infty}^2} \quad (4)$$

Where, C_p is an average wind pressure coefficient at an arbitrary point p (dimensionless), P is a pressure difference (Pa), q_H is a dynamic pressure as measured at the average roof height of the greenhouse (Pa), p_P is a static pressure at an arbitrary point p (Pa), and p_∞ is a static pressure at windward regions located far from the greenhouse model (Pa).

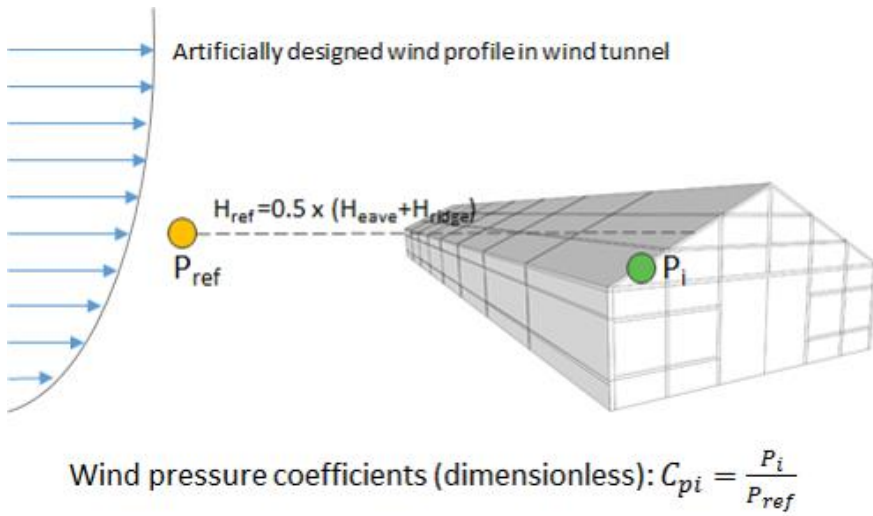

Fig. 5 Concept of the wind pressure coefficients

3.6 CFD simulation

CFD simulation has been variously used for solving heat transfer, mass transfer, chemical reaction and other problems in the field of mechanics, aeronautics and chemical engineering. CFD simulation has been also variously utilized in the studies of agricultural facility such as air conditioning, heating, ventilation and wind pressure in greenhouse and livestock house.

CFD simulation numerically solved the Reynolds-averaged form of the Navier-Stokes equations (Launder and Spalding, 1974) within each cell in the domain (Lee and Short, 2000). The flow of fluid and

energy in CFD simulation is computed using a nonlinear partial difference equation based on the law of conservation of mass, momentum and energy. A mass conservation equation can be applied to a physical phenomenon irrespective of steady state, viscosity and compressibility. The momentum conservation equation is commonly known as the Navier-Stokes equation. The energy conservation equation indicates a relation of energy exchange in a physical system (Launder and Spalding, 1974). In this study, commercial CFD package FLUENT (ver. 15.0, ANSYS Inc., PA, USA) was used for approximately computing the governing equation of fluid flow. FLUENT has been widely used for analysis of physical phenomena such as turbulent flow, steady state, heat transfer, multi-phase flow and others. Also, FLUENT solves numerical value through discretization process using finite volume method.

3.7 The law of the wall

The 'Wall' generally causes turbulent momentum and thermal boundary layers. As turbulence and flow in the near wall region are different from those of overlap and outer layer, special treatments in the near wall region are necessary to accurately predict wind pressure coefficients. Prandtl (1925) originally postulated that, for flows near the wall region, the mixing length is proportional to distance from the wall. This postulate is well-known as the 'law of the wall', which has been observed in the near wall regions (Wilcox., 2006). The near-wall region was composed of three part; 1) Sublayer ($u^+ = y^+$); 2) Log layer ($u^+ = \frac{1}{\kappa}\ln y^+ + B$); 3) Outerlayer (Fig. 6).

Where, u^+ is dimensionless velocity, y^+ is dimensionless distance from wall, κ is karman factor (about 0.41), B is dimensionless constant (5.0 ~ 5.4).

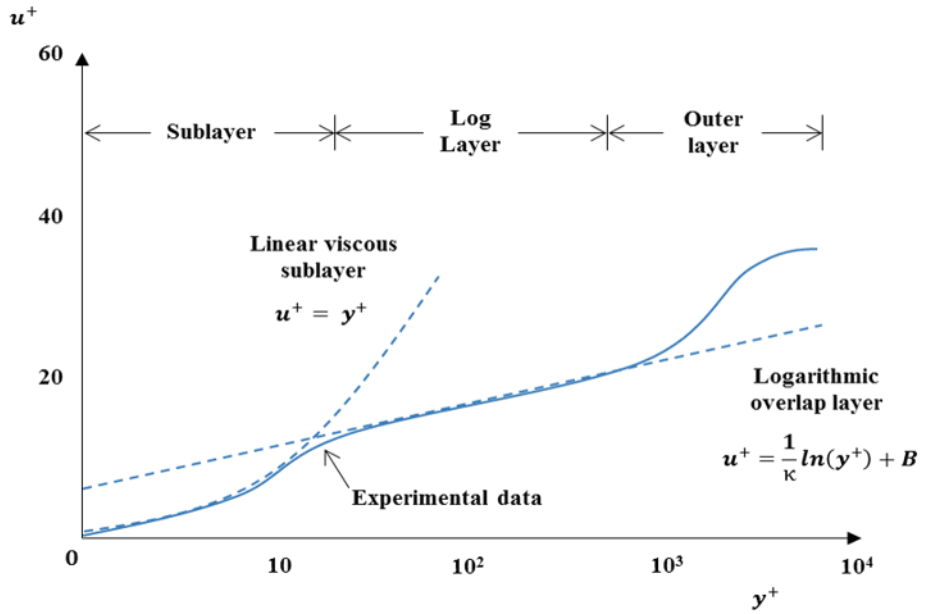

Fig. 6 Dimensionless velocity profile for a turbulent boundary layer (White., 2007)

Eq. (5) and Eq. (6) provide equation of u^+ and y^+.

$$u^+ = \frac{u}{u_\tau} \tag{5}$$

$$y^+ = \frac{y u_\tau}{v} \tag{6}$$

Where, u is velocity (m s^{-1}), u_τ is wall friction velocity (m s^{-1}), y is distance from wall (m), v is kinetic viscosity (m^2 s^{-1}).

An accurate near-wall modeling is important to the success of CFD simulation because the solution of gradients is very high in a wall-bounded flow. A fine grid for near-wall modeling is required to resolve the steep profile in the near wall region. However, to apply this, the number of grid increased in the complex and large domain. It is also often necessary for modeling and computing complex and irregular geometries. To improve the accuracy of analysis in the near

wall region, FLUENT has suggested the Wall Functions model and the standard of grid according to turbulence model. In the case of Standard Wall Functions and Non-Equilibrium Wall Functions, the first grid cell needs to be $30 < y^+ < 300$. In the case of Enhanced Wall Treatment and k-ω model, y^+ should be below 5 (ANSYS manual., 2012).

3.8 Wall roughness

The wall function is generally used for replacing the wall roughness caused by obstacles such as structures, trees, etc. Wall roughness is generally expressed by the aerodynamic roughness length (y_0) and the equivalent sand grain roughness height for the ABL ($k_{s,ABL}$). $k_{s,ABL}$ (large-scale roughness) is typically higher than y_0 in the atmospheric boundary layer (e.g. 0.03 m < y_0 < 2 m (Wieringa, 1992), 0.9 m < $k_{s,ABL}$ < 60 m). k_s (small-scale roughness) is also generally quite small on the surface of the obstacles such as walls, roofs, etc. and the surfaces between those obstacles such as streets, grass plains, etc. (e.g. 0 m < k_s < 0.1 m) (Blocken et al. 2007). The logarithmic law for a rough wall is presented in Eq. (8) (Cebeci and Bradshaw, 1977).

$$k_s^+ = \frac{u^* k_s}{\upsilon} \tag{7}$$

$$\frac{U}{u^*} = \frac{1}{\kappa}\ln\left(\frac{u^* y}{\upsilon}\right) + B - \Delta B\left(k_s{}^+\right) \tag{8}$$

Where, aero dynamically smooth ($k_s{}^+ < 2.25$), transitional ($2.25 \leq k_s{}^+ < 90$), and fully rough ($90 \leq k_s{}^+$).

In FLUENT, Eq. (8) is expressed in fully rough as Eq. (9).

$$\frac{U}{u^*} = \frac{1}{\kappa}\ln\left(\frac{u^* y}{\upsilon C_s k_s{}^+}\right) + 5.43 \tag{9}$$

Where, C_s is roughness constant.

And, there are relations between k_s and y_0 in FLUENT.

$$k_s = \frac{9.793 y_0}{C_s} \tag{10}$$

According to the study of Blocken et al. (2007), four requirements should be simultaneously satisfied. First, high grid resolution is satisfied in the vertical direction close to the bottom of the computational domain. Second, the wall roughness of upstream and downstream region is horizontally homogeneous. Third, the distance y_p from the center point P of the wall-adjacent cell to the wall is larger than k_s. Finally, there are relations between y_0 and k_s. However, it is generally impossible to satisfy four requirements because the grid resolution is quite high satisfying $y_p > k_s$. For these reasons, the maximum k_s was applied within the limit of the required resolution in this study.

3.9 Design of the wind environment

3.9.1 ESDU design of the wind environment of reclaimed land

The vertical wind profile and turbulence intensity profile were designed to reflect the geographical characteristics of the 7 target reclaimed lands in South Korea. The surface roughness of the windward regions of each target reclaimed land was first categorized based on the ESDU procedure. Google maps and GIS data were used to define the change in the surface roughness of the target regions within a 50 km radius, and the decision was made to categorize the geographical characteristics, such as land use, with the help of the expert groups who belong to same research project (PJ009492, Rural Development Administration, Korea). Fetch (x) information, which means the horizontal distance from the representative point of

the each windward region to the point of the each reclaimed land, was also calculated based on Google maps. Databases for each reclaimed land were constructed based on the mentioned categorized surface roughness of each windward region and calculated fetch information. These data were used for input sources of the ESDU VIEWpac E0108 code to compute the vertical wind and turbulence intensity profiles. The profiles of the 7 target reclaimed lands were computed according to various wind directions, the distribution of surface roughness at windward regions and fetch information; then, representative wind and turbulence intensity profiles for each reclaimed land were introduced following selection criteria. The strongest wind and turbulence intensity profiles for each reclaimed land were selected to analyze the structural stability of the greenhouse facilities. Finally, for the purpose of designing the wind tunnel test, a representative "Alpha (α)" value that can embrace the entire range of the introduced profiles was suggested to be 0.15 by the expert groups who belong to the same mentioned research project (PJ009492, Rural Development Administration, Korea). Fig. 7 shows one example of the categorization of land use to determine the surface roughness in Saemanguem reclaimed land with the help of Google maps and GIS data, and Fig. 8 shows the design process of the wind and turbulence intensity profiles for the wind tunnel test in this study.

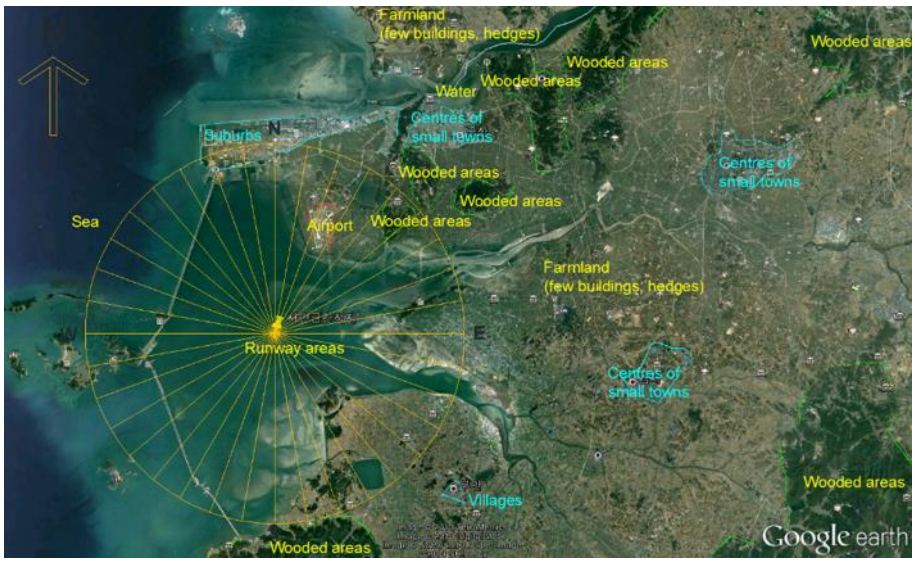

Fig. 7 Example of the land-use categorization to determine the windward surface roughness in Saemanguem reclaimed land according to the wind direction

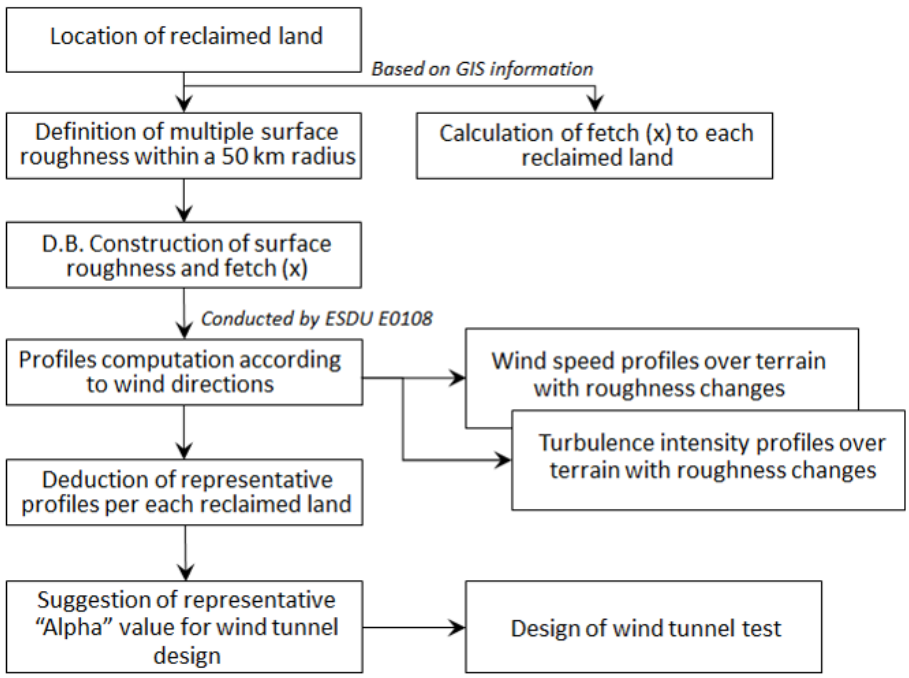

Fig. 8 Design process of the vertical wind and turbulence intensity profiles over terrain with roughness changes for the wind tunnel test

3.9.2 Design of wind environment in the wind tunnel

To designate the experimental atmospheric boundary layer in the wind tunnel artificially, the ESDU computed the vertical wind and turbulence intensity profiles that were designed using roughness blocks, spires and barriers through trial and error. Spires and roughness blocks have been widely used to create the proper wind profiles through the process of the deficit of momentum flux and pressure drop along the test section. Spires were particularly designed by an equation in the research paper of Irwin (1981) and Lee et al. (2004). The "Alpha (α)" value for the design of the wind tunnel test, including the installation of spires, was determined to be 0.15 based on the pre-results as written in the previous sections. Fig. 9 shows the design works of the vertical wind and turbulence intensity profiles as derived from the ESDU model using roughness blocks, spires and barriers. The experimental wind velocity magnitude was set at 6.0 m s^{-1} at the average roof height ((eave height + ridge height)/2) of the scaled greenhouse model.

(a) Design of wind and turbulence intensity profile
using roughness block, spires and barriers in wind tunnel

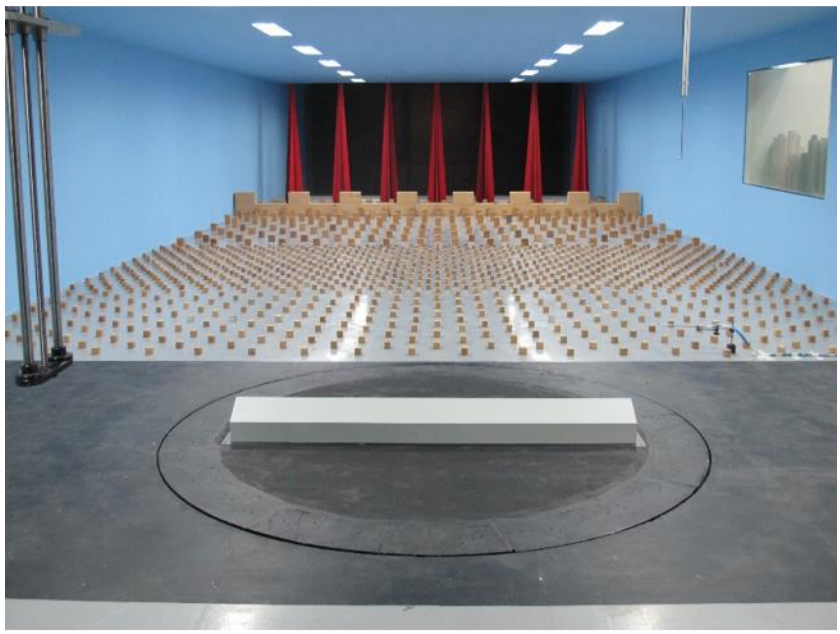

(b) Final view of installation of block, spires
and barriers in wind tunnel

Fig. 9 Design of the vertical wind and turbulence intensity profiles using roughness blocks, spires, and barriers in the wind tunnel

Fig. 10 describes both the measured vertical wind profile in the wind tunnel and the computed wind profile using ESDU (a) and the measured and computed vertical turbulence intensity profiles (b) and power spectral density measured at the average roof height of the greenhouse model (c). From the comparative analysis, each designed profile the in wind tunnel coincided with the computed profiles, reflecting the characteristics of the reclaimed land quite well, especially at the lower level where the scaled greenhouse was located. The average errors between wind tunnel test and ESDU were 4.42% for the vertical wind profile and 3.17% for the vertical turbulence intensity profile.

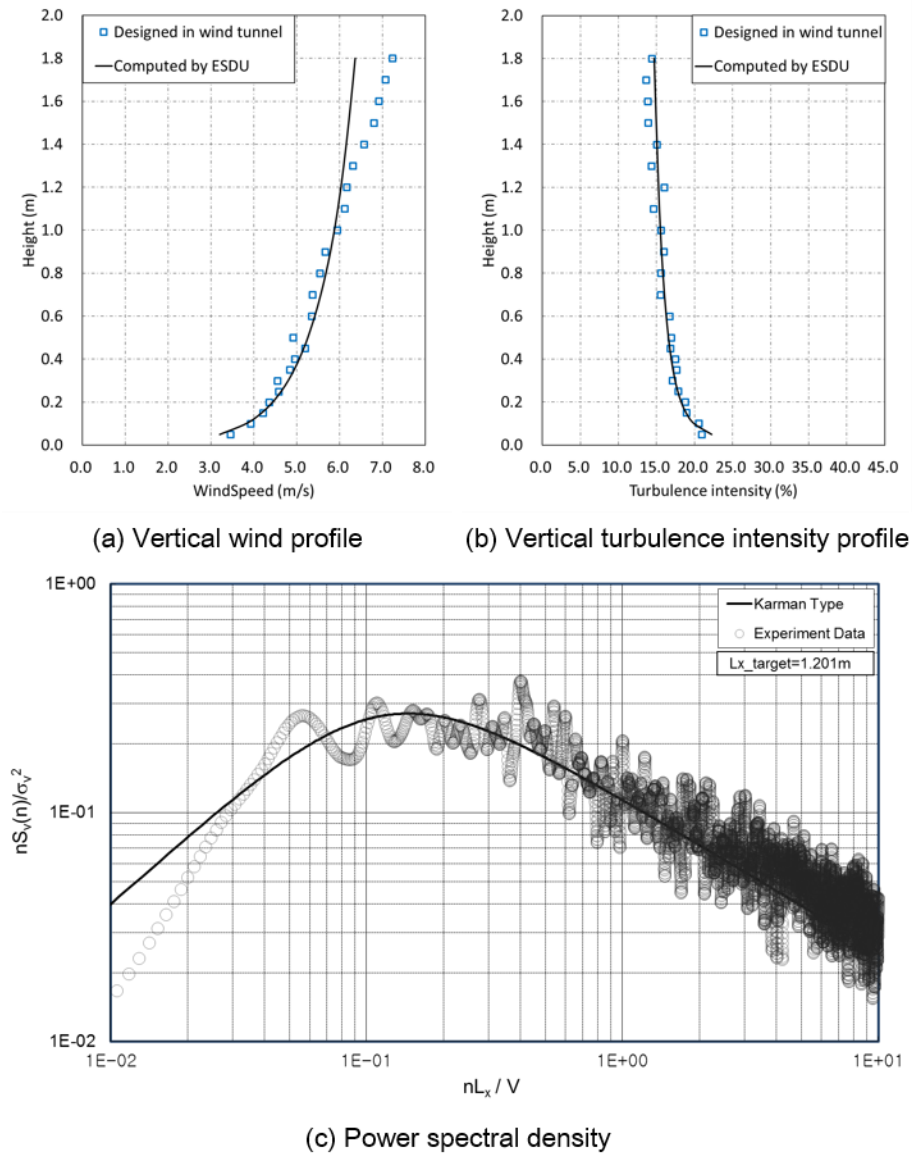

Fig. 10 Comparison of the vertical wind profiles as computed by the ESDU and designed at the wind tunnel (a), the vertical turbulence intensity profiles as computed by the ESDU and designed at the wind tunnel (b) and measured power spectral density (c)

3.9.3 Design of wind environment in CFD simulation

Vertical wind, turbulent kinetic energy and turbulent energy dissipation profile were used to design the experimental atmospheric boundary layer in CFD simulation. The equation for profile was

applied according to study of Richards (1989) based on Harris and Deaves (1981) model. These equations of profiles are generally simplified when the height of computational domain is lower than the ABL height (Richards and Hoxey, 1993).

$$U(y) = \frac{u^*}{\kappa} \ln\left(\frac{y + y_0}{y_0}\right) \tag{11}$$

$$k(y) = \frac{u^{*2}}{\sqrt{C_\mu}} \tag{12}$$

$$\epsilon(y) = \frac{u^{*3}}{\kappa(y + y_0)} \tag{13}$$

$$\omega(y) = \frac{\epsilon}{C_\mu k} \tag{14}$$

Where, y_0 is roughness length (0.03) (m), C_μ is dimensionless constant (0.09).

The profile computed from this equation was an input in CFD simulation through user-defined function (UDF) that was written in C-language. Fig. 11 shows both the vertical wind profile in CFD simulation and the computed wind profile using ESDU (a) and vertical k, ϵ, ω profiles (b).

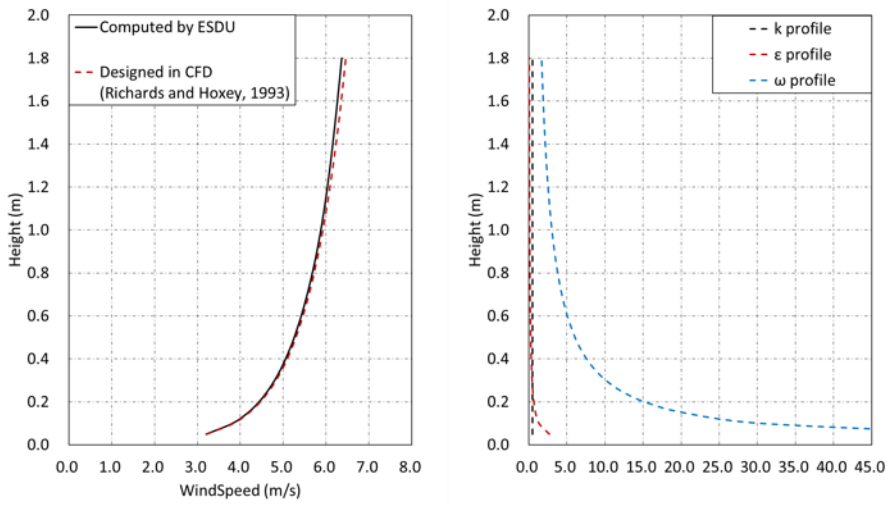

(a) Vertical wind profile (b) Vertical k, ε, ω profile

Fig. 11 Comparison of the vertical wind profiles as computed by the ESDU and designed in CFD simulation (a) and the vertical k, ϵ, ω profiles designed in CFD simulation (b)

3.10 Experimental design

3.10.1 Experimental design of the wind tunnel test

One of the most essential factors for conducting a successful wind tunnel test is to achieve the similarity law. In this study, the geometrical similarity was set to 1:20 considering the blockage ratios. The blockage ratio, which is defined as the ratio of the cross-sectional areas of the scaled greenhouse to that of the wind tunnel, was measured below 5%. Based on the similarity law, the wind velocity scale that was derived based on the Froude number and the time scale were set at 1:6 and 1:3.33, respectively. Table 5 briefly presents the design characteristics of the wind tunnel test.

Table 5 Design characteristics of the wind tunnel test

Contents	
Length scale	1:20
Wind velocity scale	1:6
Time scale	1:3.33
Sampling frequency	625 Hz
Number of moving average	188
Number of measurement trial	5
Wind velocity	6 m s^{-1} (at the average roof height of the greenhouse model)
Wind direction	0, 22.5, 45, 67.5 and 90° to the side wall of the greenhouse

Fig. 12 illustrates one of the scaled experimental greenhouse models: (a) Peach type (Type-PC-R6000) and (b) installation scene of the Multi-channel pressure scanner (ZOC33/64Px×8, Scanivalve, Inc., USA) for measuring the wind pressure acting on the surface of the greenhouse model in this study. Many tiny holes on the greenhouse surface were connected to the pressure scanner using tubes as shown in Fig. 12 (b).

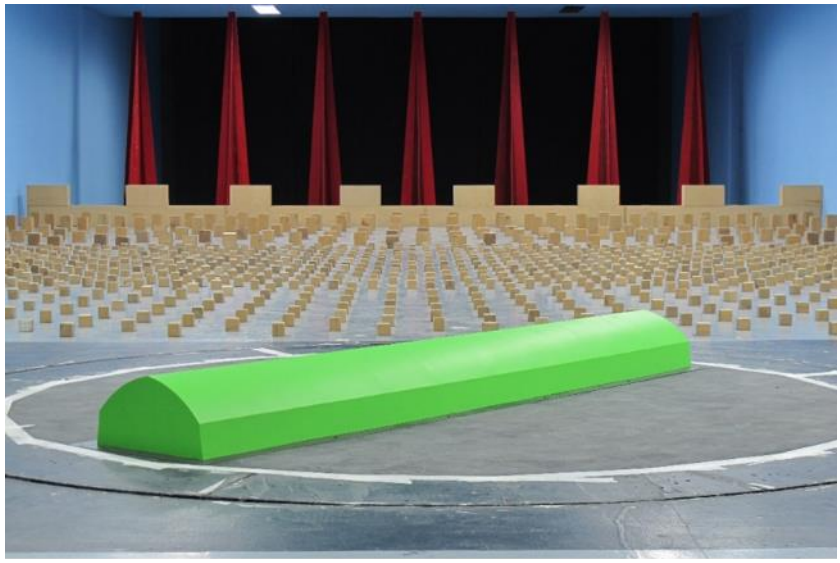

(a) Scaled Peach type greenhouse model (Type-PC-R6000)

(b) Installation of Multi-channel pressure scanner
(Scanivalve inc., USA)

Fig. 12 Scaled Peach type greenhouse model (Type-PC-R6000) and Multi-channel pressure scanner (Scanivalve Inc., USA)

A maximum of 444 pressure measuring taps were installed on the surface of the scaled experimental greenhouse model. The number of measuring points varied according to the design factor, such as the roof slope and the radius of the curvature of the roof.

Each pressure-measuring tap was connected to a multi-channel pressure scanner via pressure tubes and a pressure transmission correction system. Fig. 13 shows one example of the location of pressure-measuring taps for Peach type greenhouses (Type-PC-R6000). The taps were intensively located at the local edge regions of the greenhouse model to investigate the distribution of the local wind pressure coefficients. Additionally, as shown in Fig 13, monitoring rows (from C01 to C15) were defined in the direction of the longitudinal ways of the greenhouse model to analyze the tendencies of the local pressure coefficients according to the designed wind directions. The wind directions varied from 0 to 90° to the side wall of the greenhouse (hereinafter, 0° means that the wind blows perpendicular to the side walls of the greenhouse) at intervals of 22.5° (Table 5 and Fig. 12). For the scaled models of Three-quarter and Mono-span type greenhouses, additional wind directions (from 90 to 180°) were used to consider the asymmetric shape of the models.

The total number of investigated experimental cases was 168 considering the type of the single-span greenhouse model, design factors such as the roof slope angle and the radius of curvature of the roof (Table 2 and 3), and wind direction (Table 5). The pressure coefficients were measured for 300 seconds in the wind tunnel, and then the average wind pressure of each measuring tap was determined by the data-logger through the moving averaging process.

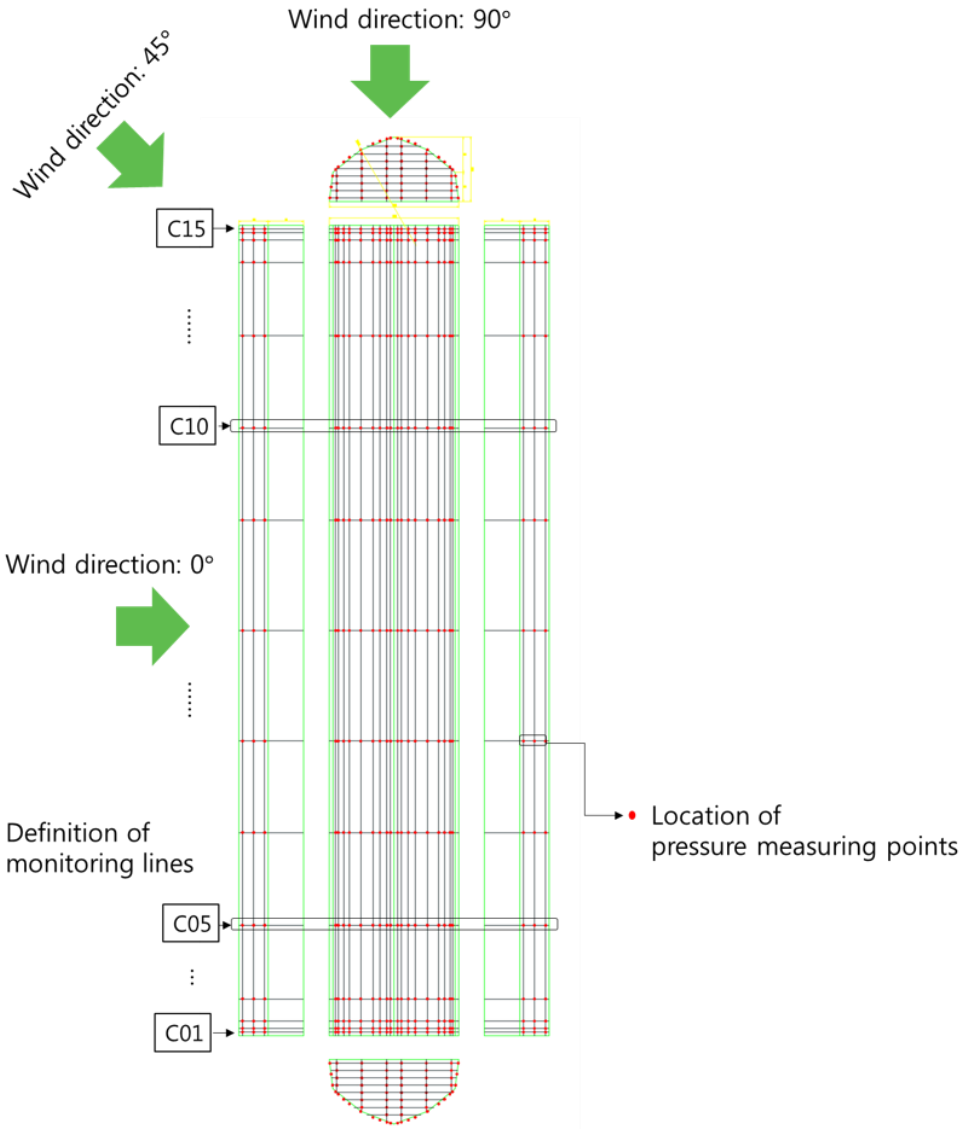

Fig. 13 Examples of the location of the measuring points for pressure coefficients and the definition of monitoring lines for the scaled peach-type greenhouse model (Type-PC-R6000)

The framework of the greenhouse generally functions to support the whole greenhouse structure and share the wind and snow loads. Therefore, an evaluation of the loads and bending moments acting on the greenhouse framework is very important in examining the structural safety of the facility. From the various advanced studies and greenhouse standards (NEN-EN, 2002; KBC, 2009), the

maximum positive or negative pressure causing strong bending moments is generally observed at the surface of the greenhouse when the wind directions are 0 and 90° to the side wall of the greenhouse. In the case of greenhouse cladding, the maximum pressure can be intensively acted on certain local regions for every different wind direction, especially in regions near the edge of the ridge and eaves of the greenhouse. Therefore, various wind directions should be considered to evaluate the durability of the greenhouse cladding. As mentioned above, pressure evaluations for safety of the structural design and cladding design have different mechanisms; thus, pressure analyses should be accomplished in two ways. In this study, the measured wind pressure coefficients at each surface of the greenhouse were analyzed to investigate the structural design of the greenhouse at 0 and 90° wind directions to the side wall of the greenhouse, whereas the maximum wind pressure coefficients at each local surface according to various wind directions were analyzed to propose an accurate local wind pressure coefficients for the cladding design of the greenhouse.

To analyze the tendencies of the sectional and local wind pressure coefficients, a name was given to each part of the wall and roof surface, as shown in Fig. 14 (Even-span type greenhouse) based on the size of the "eaves height" and "wind direction." The regional definitions that are shown in (a) and (b) of Fig. 14 are for the evaluation of the structural design while (c) and (d) for the cladding design. For the 0° wind direction to the side wall, the wall surface of the windward side was represented by W_W (Wall-windward), and that of the leeward side was defined as W_L (Wall-leeward) ((a) of Fig. 14). The roof surface on the windward and leeward sides was represented by R_W (Roof-windward) and R_L (Roof-leeward), respectively. Both walls were located at the end parts of the greenhouse and were also defined as E_S (End-side). As shown in (b) of Fig. 14, for the 90° wind direction to the side wall, the surfaces of the side walls and roof walls were represented by W_S and R_S, respectively, and the end walls on the windward and leeward

sides as E_W and E_L. For the specific analysis of the local wind pressure coefficients of the greenhouse model, a more detailed subdivision based on the “eaves height; h” and “wind direction” was conducted as shown in (c) and (d) of Fig. 14.

Fig. 15, 16 and 17 also describe the definition of each surface of the Three-quarter, Peach and Mono-span type greenhouses, respectively.

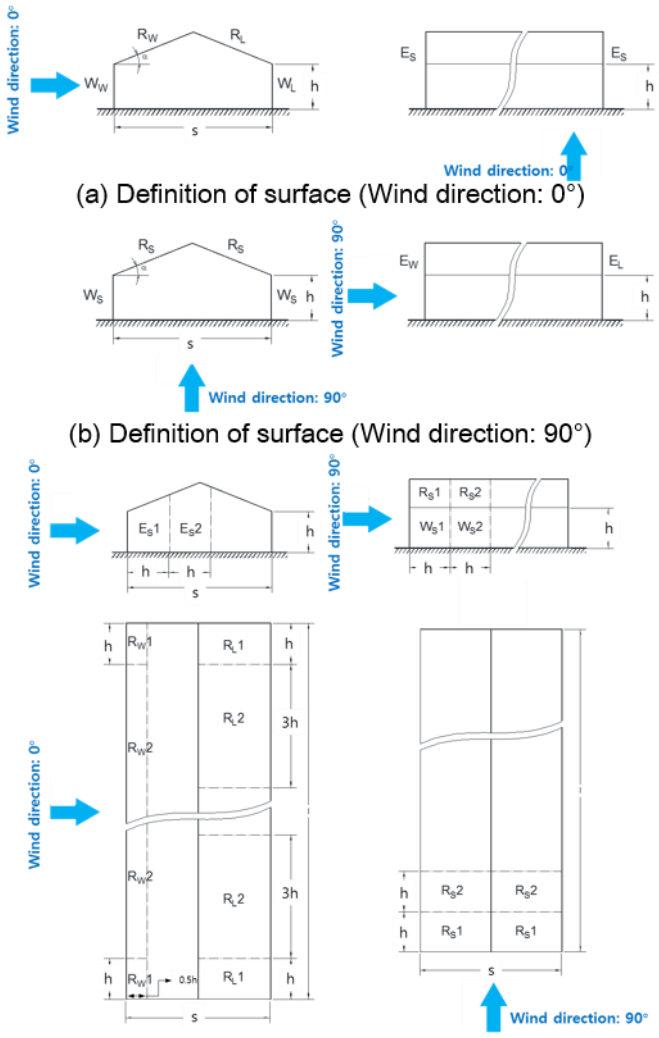

Fig. 14 Regional definition of each surface of scaled Even-span type greenhouses for wind pressure analyses of the structural design ((a) and (b)) and cladding design ((c) and (d))

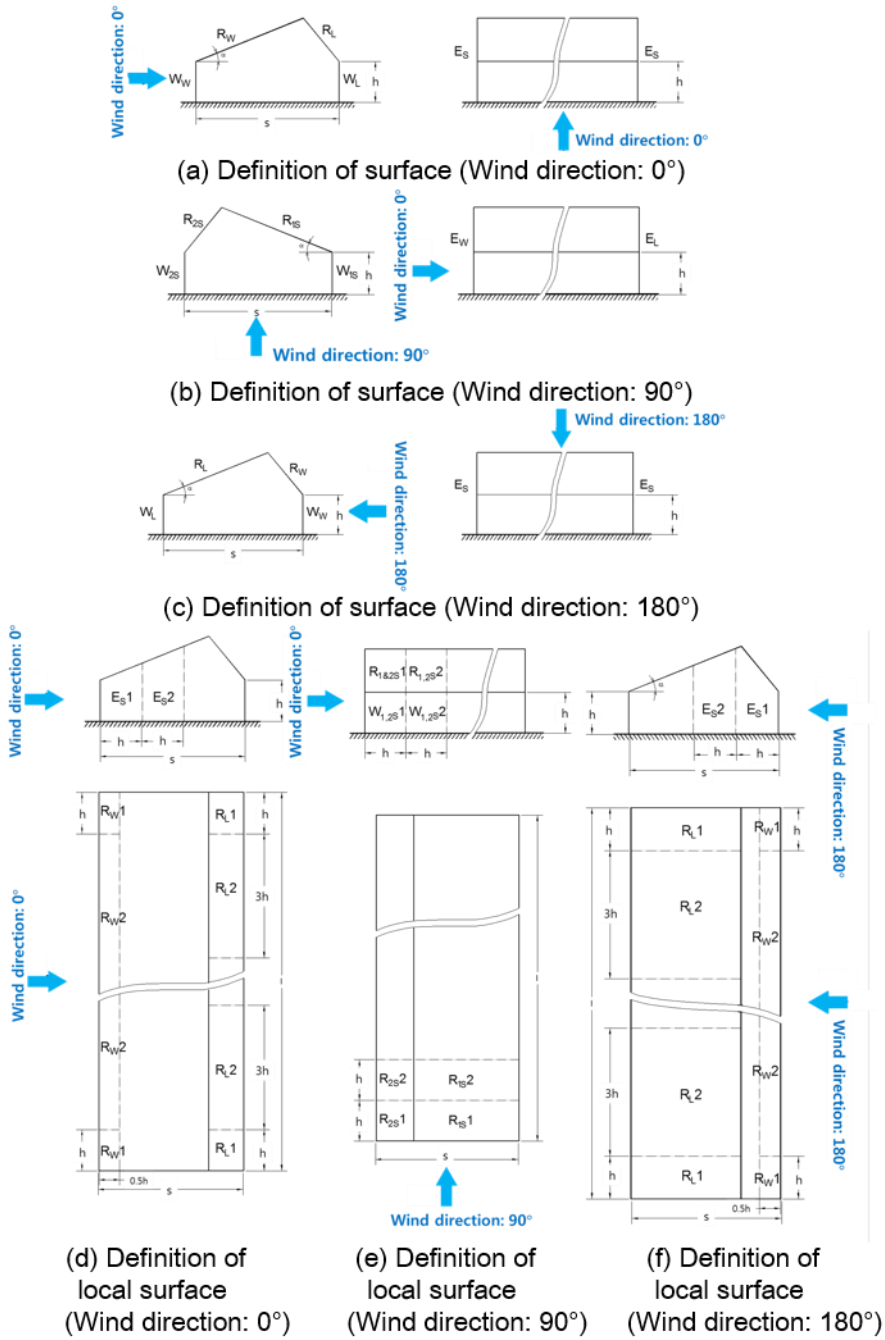

Fig. 15 Regional definition of each surface of scaled Three-quarter type greenhouses for wind pressure analyses of the structural design ((a), (b) and (c)) and cladding design ((d), (e) and (f))

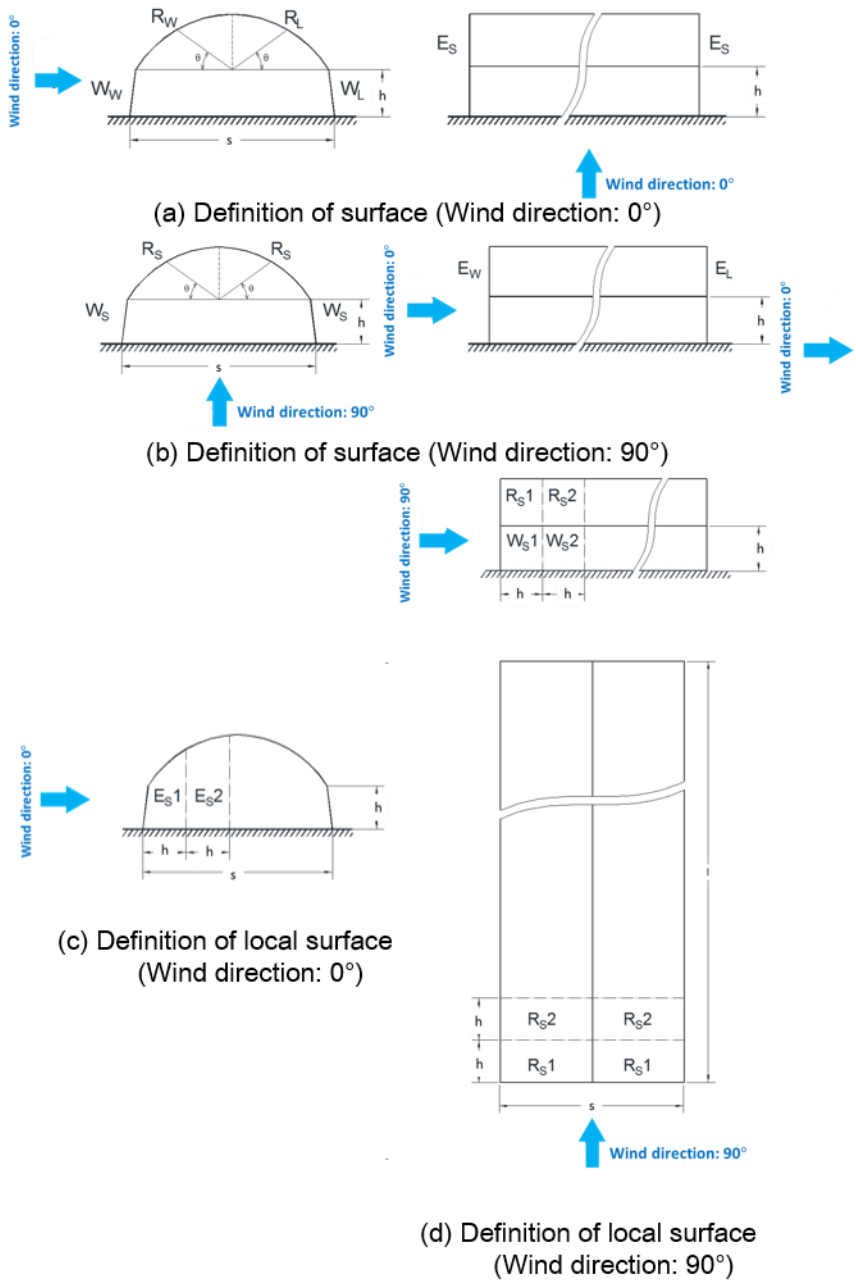

Fig. 16 Regional definition of each surface of scaled Peach type greenhouses for wind pressure analyses of the structural design ((a) and (b)) and cladding design ((c) and (d))

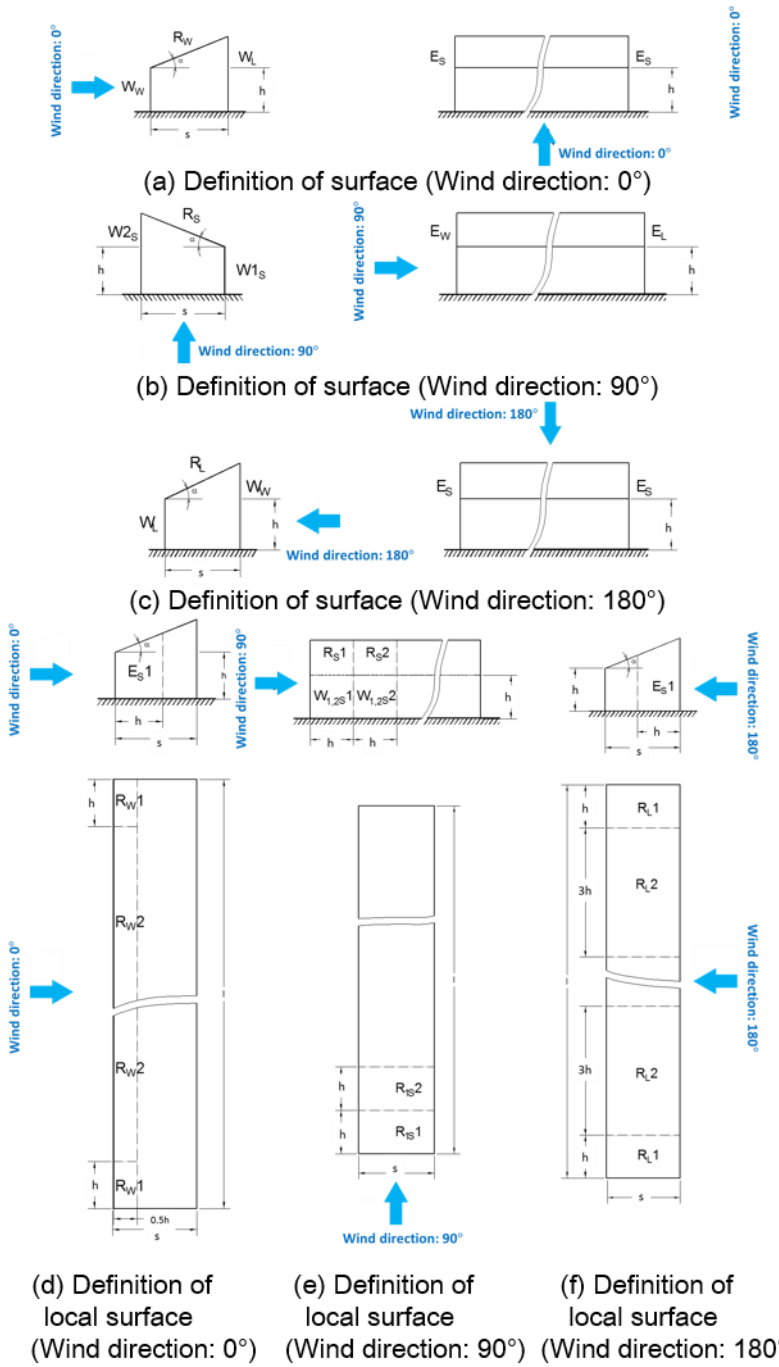

Fig. 17 Regional definition of each surface of scaled Mono span type greenhouses for wind pressure analyses of the structural design ((a), (b) and (c)) and cladding design ((d), (e) and (f))

3.10.2 Experimental conditions of the CFD simulation

In this study, the energy conservation equation was not solved because there was a little impact on the temperature for wind pressure. The pressure-based solver and SIMPLE (Semi-Implicit Method for Pressure-Linked Equations) algorithm were used for flexibility of analysis procedure and convergence. The input data for the profile was applied through the aforementioned equation for profile. The air density was 1.225 kgm^{-3}, and the air viscosity was 1.7894×10^{-5} under the assumption that the air is in incompressible fluid form. Since the wind velocity of the reclaimed land is very high, there is a possibility that the number of grids increased excessively in order to meet y^+ value. For this reason, the scale model in CFD simulation was used for calculating the wind pressure of single-span greenhouses. The constant input values for the CFD model is presented in Table 6.

Table 6 The constant input values for the CFD model

Factor	Value	Unit
Wind velocity	Wind profile	$m\ s^{-1}$
Turbulence kinetic energy	Turbulence kinetic energy profile	$m^2\ s^{-2}$
Specific dissipation rate	Specific dissipation rate profile	s^{-1}
Operating Pressure	101325	Pa
Gravitational Acceleration	9.81	$m\ s^{-2}$
Air density	1.225	$Kg\ m^{-3}$
Air viscosity	1.7894×10^{-5}	$Kg\ m^{-1}\ s^{-1}$

For CFD validations, the CFD computed and the wind tunnel measured results were compared according to y^+ value, the computational domain and the grid independence tests when the

greenhouse type was Even-span greenhouse (Type-EV-D22), which has a 22° roof slope, and the wind direction was 0° to the side wall.

The wind pressure coefficients according to y^+ values were computed using five turbulence models in order to find the optimum condition of the first grid height. The Low-Reynolds number regions were autonomously analyzed in a turbulence model based on k-ω model, while the wall functions for analyzing low Reynolds number regions were used in the case of turbulence model based on k-ε model. In this study, enhanced wall treatment, which was highly efficient wall functions in the near wall region, was applied for deriving more accurate results. Total 3 cases of first gird heights were selected for considering effects of y^+ values, and first grid heights were 1.5×10^{-4}, 1.5×10^{-3} and 1.5×10^{-2} m, respectively (Fig. 18).

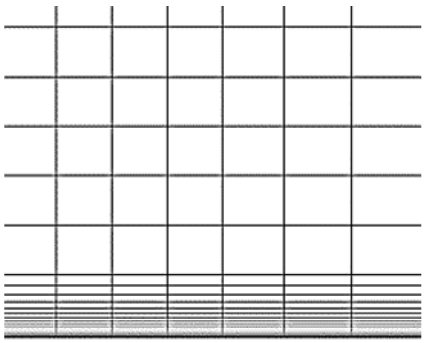

(a) 1.5 × 10^{-4} m of first grid height

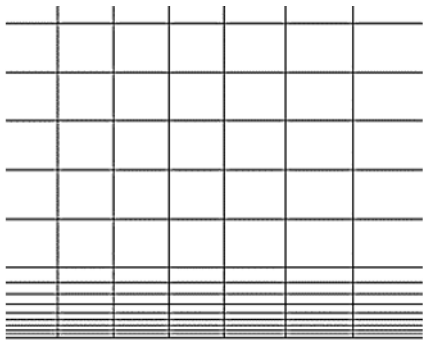

(b) 1.5 × 10^{-3} m of first grid height

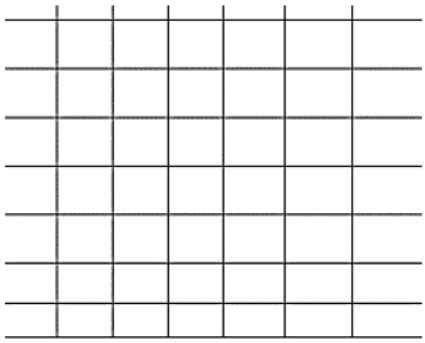

(c) 1.5 × 10^{-2} m of first grid height

Fig. 18 1.5 × 10^{-4} m (a), 1.5 × 10^{-3} m (b) and 1.5 × 10^{-2} m (c) of first gird height in near wall region

The detailed standards of domain size were not available until now, and the computational domain size has been approximately suggested through empirical and experimental methods (Bournet et al., 2007; Bournet and Boulard, 2010; Franke et al., 2004; Tominaga et al., 2008) (Fig. 19). In this study, a computational domain was designed to apply vertical profiles around the greenhouse. The computational domain consisted of four parts; 1) the upstream part for approaching vertical profiles; 2) the central part for computing wind pressure coefficients of single-span greenhouses; 3)the downstream part for stability of flow; 4) the side and the upper part for preventing blockage. The domain size has been generally determined from the height of structure or obstacle because the airflow reaches the farthest when separation of airflow was generated at the maximum height of structure. For these reasons, a

computational domain test was conducted according to the height of greenhouses (hereinafter, H). As noted earlier, it is difficult to satisfy $y_p > k_s$ when grid resolution is quite high. Because of these limitations, the internal boundary layer was consistently developed as the wind profile moved downstream. In this study, the length of the upstream was maximally reduced to 3 times the height of the greenhouse model (3H) in order to prevent development of internal boundary layer. The length of the downstream, side and upper part need to be thoroughly determined because they have a great effect on convergence and accuracy of the computing. A total of five cases of the length of downstream part were selected in the range of 5H to 25H at an interval of 5H, and total three cases of lengths of side and upper parts were designed from 5H to 15H at an interval of 5H, respectively (Table 7).

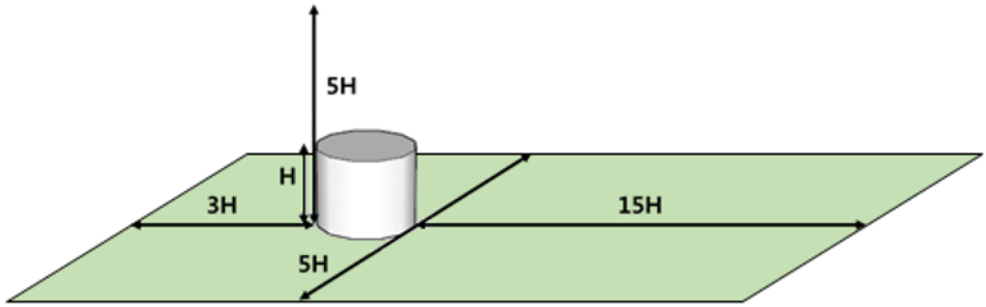

(a) Computational domain determined by height of structure
(Bournet et al., 2007; Bournet and boulard, 2010;
Franke et al., 2004; Tominaga et al., 2008)

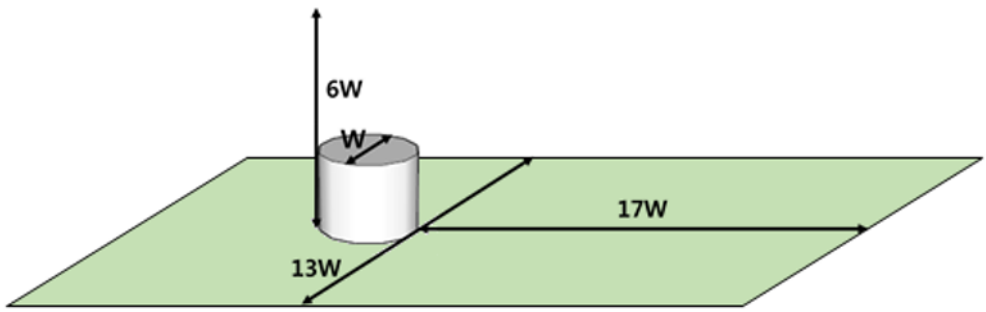

(b) Computational domain determined by width of structure
(Hefny and ooka, 2008)

Fig. 19 Computation domain size suggested through the empirical and experimental methods

Table 7 Experimental conditions for computational domain size tests

Length of upstream parts	Length of downstream parts	Length of side parts	Length of upper parts
3H	5H	5H	5H
	10H	10H	10H
	15H	15H	15H
	20H		
	25H		

For the purpose of efficiency and accuracy of computation, a grid independence test was conducted for determining the grid size around the greenhouse according to five turbulence models. This study selected the total 4 cases of grid size, which were designed on the surface of the greenhouse model. Grid sizes were classified into 1.0×10^{-2} m, 2.5×10^{-2} m, 4.0×10^{-2} m and 5.5×10^{-2} m based on the length of one side of grid, respectively (Fig. 20). In the case of grid size of 1.0×10^{-2} m, which was the smallest grid for effective computing and the total number of grid was about 1.30 million. When the grid size was 2.5×10^{-2} m, 4.0×10^{-2} m and 5.5×10^{-2} m, the total number of grids was 0.61, 0.24 and 0.12 million, respectively. The total number of grid decreased remarkably according to the increasing gird size.

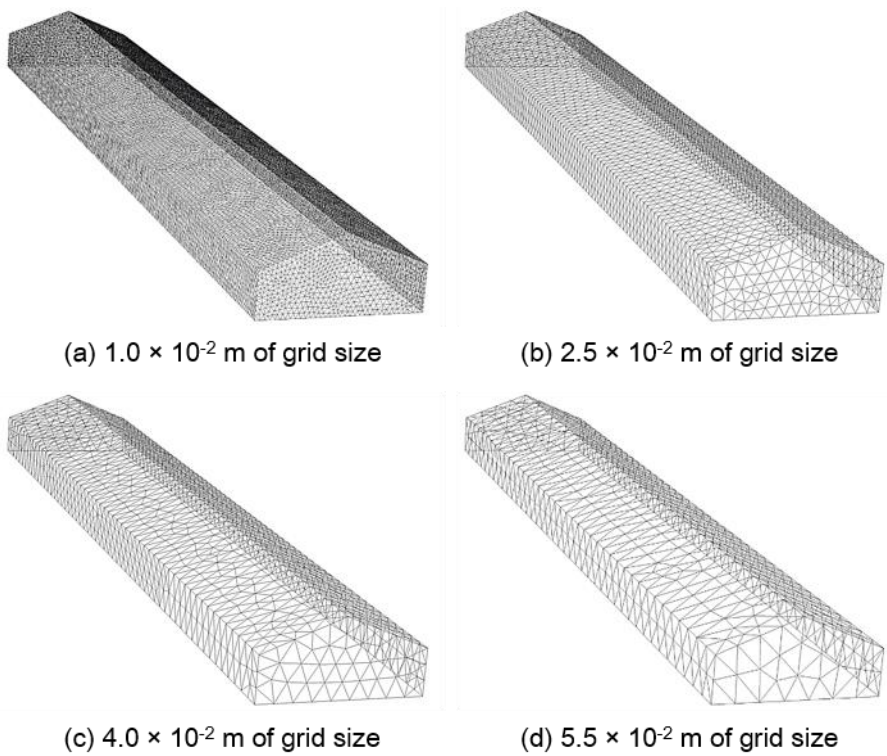

Fig. 20 1.0×10^{-2} m (a), 2.5×10^{-2} m (b), 4.0×10^{-2} m (c) and 5.5×10^{-2} m (d) of grid size around greenhouse for grid independence test (Type-EV-D22)

After y^+ values, computational domain and grid independence tests, CFD models were designed by given first grid height, domain size and grid size. From these CFD models, the results of Even-span and Peach type greenhouses were also relatively compared in order to find optimum conditions of turbulence model. The flow of fluid in natural phenomenon is generally dominated by turbulence that affects separation, recirculation and reattachment. Turbulence is one of the important issues to more accurately predicting natural phenomena because turbulence flow has larger transport coefficients and resistance than laminar flow. In CFD simulation, turbulence flow is approximately computed using a turbulence model because turbulence flow is not constant in time and space with irregular three-dimensional flow. Various turbulence models have been developed to this date. Appropriate turbulence model must be selected according to the characteristics of turbulence model and environmental conditions in order to improve the accuracy of CFD results. In this study, Standard k-ε, RNG k-ε, Realizable k-ε, Standard k-ω and SST k-ω turbulence model as RANS (Reynolds Averaged Navier-Stokes) model were used for validation of CFD model. Lastly, an appropriate turbulence model was also selected as a result of validation.

3.11 Accuracy analysis of CFD model

A relationship between simulated and measured values need to be sufficiently expressed. The simulated values also have to be evaluated whether they can effectively predict the measured values. For these reasons, various statistical indices have been used in validation studies. Most studies on CFD simulations have validated the simulated values through visual analysis and R^2 (coefficient of determination). However, there is a limit to determine the accuracy of CFD model using visual analysis and R^2. In this study, R^2, RSR (root mean square error-observations standard deviation ratio) and d (Index of agreement) as statistical indices were used for accuracy analysis of simulated values.

R^2 has a value in the range of 0 to 1, indicating similarity of the measured values and the simulation values. R^2 does not represent the degree of error but trends. When R^2 is closer to 1, it means that the simulated values correspond to the trend of the measured values.

$$R^2 = \left(\frac{\sum_{i=1}^{n}\left(Y_i^{obs} - \overline{Y^{obs}}\right)\left(Y_i^{sim} - \overline{Y^{sim}}\right)}{\sqrt{\sum_{i=1}^{n}\left(Y_i^{obs} - \overline{Y^{obs}}\right)}\sqrt{\sum_{i=1}^{n}\left(Y_i^{sim} - \overline{Y^{sim}}\right)}} \right)^2 \quad (15)$$

Where, Y_i^{obs} is $i-$th measured value, $\overline{Y^{obs}}$ is average measured value, Y_i^{sim} is $i-$th simulated value, $\overline{Y^{sim}}$: average simulated value.

RSR is a statistical index standardizing the RMSE (root mean square error) in order to express the degree of error. Although RMSE can express the degree of error, there is a limit in making relative comparison due to dimension. Therefore, it is possible to relatively compare the RMSE by dividing the standard deviation of the measured values (Moriasi et al., 2007). The simulated values effectively predict the measured values when RSR is closer to 0.

$$RSR = \frac{RMSE}{STDEV_{obs}} = \frac{\left[\sqrt{\sum_{i=1}^{n}\left(Y_i^{obs} - Y_i^{sim}\right)^2}\right]}{\left[\sqrt{\sum_{i=1}^{n}\left(Y_i^{obs} - \overline{Y^{obs}}\right)^2}\right]} \quad (16)$$

Where, $STDEV_{obs}$ is standard deviation of measured values.

d was developed by Willmott (1985) to complement the weakness of R^2. *d* means the ratio of the MSE (mean square error) and PE (potential error). *d* is affected by extreme value like R^2, but there is a merit of predicting the proportional and additive−difference (Legates and McCabe, 1999). *d* has a value in the range of 0 to 1. The closer *d* is to 1, the higher the accuracy of the model becomes. *d* is defined as in Eq. (17).

$$d = 1 - \frac{\sum_{i=1}^{n}\left(Y_i^{obs} - Y_i^{sim}\right)^2}{\sum_{i=1}^{n}\left(\left|Y_i^{sim} - \overline{Y^{obs}}\right| + \left|Y_i^{obs} - \overline{Y^{obs}}\right|\right)^2} \quad (17)$$

In this study, if the accuracy of CFD model could be sufficiently expressed using R^2, only R^2 was analyzed in the process of validation of CFD model. If it was difficult to validate using tendency analysis, d was presented for evaluating the accuracy of CFD model. Eventually, R^2, RSR, d were used for the last validation of CFD model according to all cases.

4. Results and Discussions

4.1 Wind pressure coefficients in terms of the structural design

In this section, the measured wind pressure coefficients (hereinafter C_p) of each experimental greenhouse model through wind tunnel tests are discussed in terms of the structural design as related to the wind loads and bending moments of the greenhouse's frameworks. The results were analyzed and later compared with each other according to the wind directions 0 and 90° to the side wall, while the 180° wind direction was additionally considered for the Three-quarter and Mono-span type greenhouses because of their non-symmetric structure.

4.1.1 Even-span type greenhouses

As an example, Fig. 21 (a) and (b) shows the wind-tunnel-measured (hereinafter WT-measured) wind pressure coefficients (C_p) of Even-span type greenhouses (Type-EV-D26), which had a 26° roof slope according to the location of the monitoring rows (from C01 to C15) when the wind directions were 0 and 90° to the side wall, respectively. Fig. 22 and 23 illustrate the WT-measured distribution of C_p on the surface of the Type-EV-D26 when the designed wind direction was 0 and 90°, respectively.

When wind direction was 0° to the side wall of the greenhouse, the WT-measured results of W_W showed the tendency of the biggest positive pressure at the central part of the windward sidewall surface, while the values of the C_p at C8 decreased further toward both end walls of the greenhouse (C01 and C15 rows). The positive C_p was generally found at W_W in the range of 0.15 to 0.67. Very steep inclinations were found in every monitored row (from C01 to C15) between W_W and R_W near the eaves of the greenhouse, meaning that the separation of the airflow was already generated near those

regions; thus, a relatively larger negative pressure could be formed. For the R_W region, positive C_p values were found at the central parts, including C07, C08 and C09 rows locally, and relatively larger negative C_p was observed at the end parts, including C01 and C15 rows. The R_L region showed values from −0.6 to −0.8 at the center part and values close to −1.0 at the end parts of the greenhouse. In the case of the region of W_L, the negative C_p values were found from −0.6 to −0.7 at the center parts except one measuring point; estimated C_p was 0.00 whereas, the values at the end parts of the greenhouse reached close to −1.0. This irregular tendency was also found in the other experimental cases with different roof slopes. It could be assumed that there might be experimental errors in the process of the wind tunnel test, such as an installation problem of measuring taps and a connection problem between the taps and pressure scanner. Qualitative approaches, including the gas visualization test and computational fluid dynamics, may be needed to provide the exact cause and effect of these phenomena for future study. When the designed wind direction was 90° to the side wall as shown in Fig. 21 (b), a symmetric distribution of the WT-measured results was observed. The measured C_p of the first end part at the windward (R_S1), including C13, C14 and C15, ranged from −0.8 to −1.3, while that of the R_S2 region ranged from −0.5 to −0.6 near the C12 row. That of the leeward side (R_S3) ranged from 0 to −0.3 near the rows C01 to C11. A C_p value of around −0.7 was shown for the side walls at windward first end parts (W_S1) near the C13, C14 and C15 rows, while −0.4 to −0.6 for the W_S2 region near the C12 row and 0 to −0.2 for the W_S3 region near rows C01 to C11.

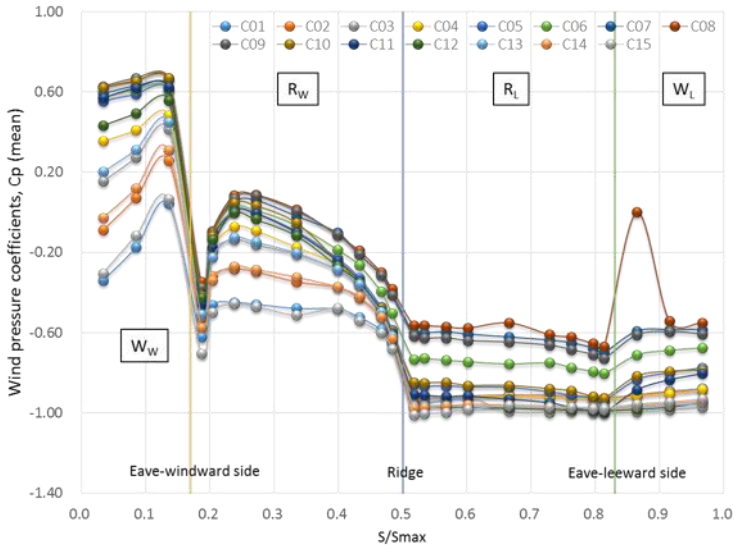

(a) Measured C_p of each monitoring row for Type-EV-D26 greenhouse when wind direction was 0°

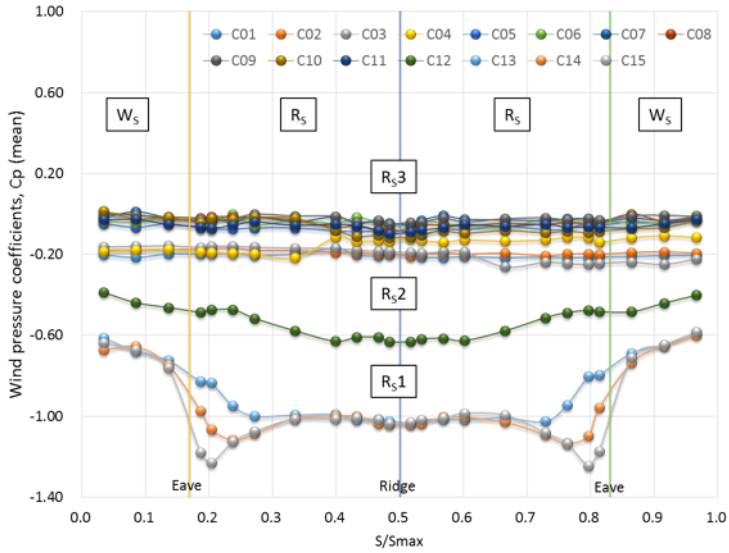

(b) Measured C_p of each monitoring row for Type-EV-D26 greenhouse when wind direction was 90°

Fig. 21 Measured wind pressure coefficients of each monitoring row for the Type-EV-D26 model when the wind directions were 0° (a) and 90° (b)

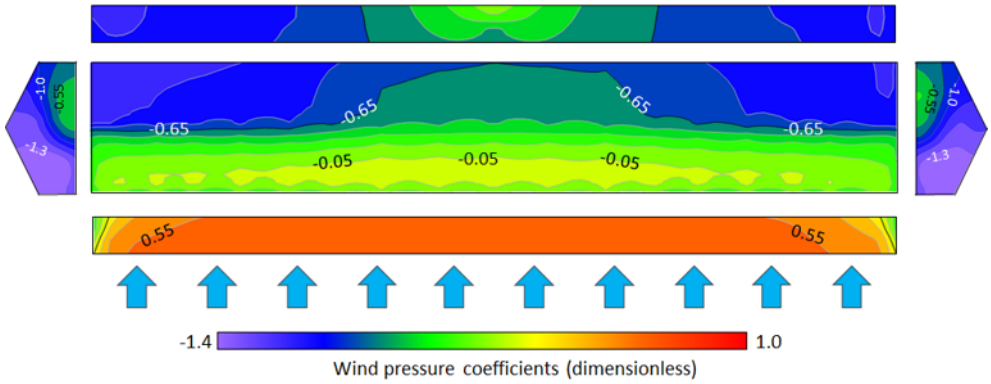

Fig. 22 Distribution of the wind pressure coefficients for Type-EV-D26 when the wind direction was 0°

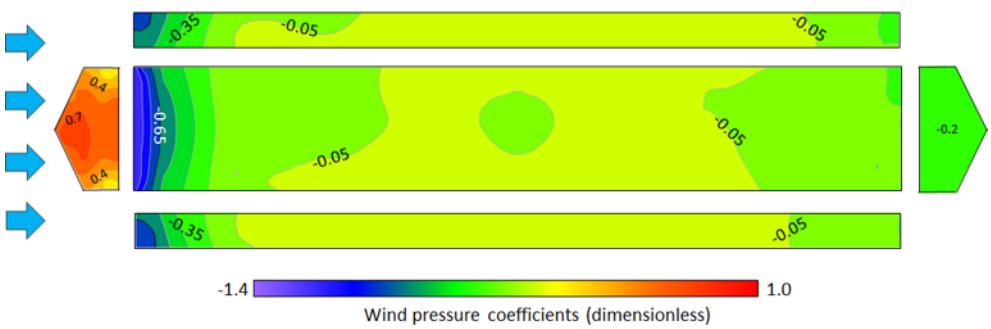

Fig. 23 Distribution of the wind pressure coefficients for Type-EV-D26 when the wind direction was 90°

Fig. 24 illustrates the area-weighted averaged C_p of each pre-defined section according to the roof slope variables of the Even-span type greenhouses when the designed wind directions were 0° (a) and 90° (b) to the side wall of the greenhouse model. The area-weighted averaging process was conducted considering the measured value, the location of the pressure measuring taps and their covered area. As shown in Fig. 24 (a), the averaged C_p values at the W_W region showed tendencies of the larger angle of the roof slope having a more positive pressure as the windward wall surface decreased. The roof slope of the greenhouse showed a reverse-linear relationship (R^2=0.99, p=7.99e-05) with the area-weighted averaged C_p at these areas. These phenomena could be explained by

the increased backflow due to the roof slope possibly generating the pressure decrease near the windward wall surface. In the case of R_W, as the slope of the roof increased, the negative pressure decreased gradually with a linear relationship (R^2=0.99, p=4.57e−05). This result may be explained by the separation point of the airflow being formed slightly further at the windward roof surface, in accordance with the increase in the roof slope of the greenhouse. However, a qualitative analysis may be helpful for explaining this phenomenon, while a visualization test or numerical approaches, such as CFD, may be good solutions. In the case of R_L, there was no specific relationship between two variables and no large differences among the WT−measured area−weighted averaged C_p. For the region of W_L, a weak reverse−linear relationship was found (R^2=0.77, p<0.05); however, the measured values did not show large differences (Avg. C_P= −0.7 and STDEV C_P= 0.02). When the designed wind direction was 90° to the side wall as shown in (b) of Fig. 24, the C_p values of the E_W only showed the relationship of a second−order polynomial function (R^2=0.97) according to the roof slope variables, whereas the values of the other sections did not show specific trends.

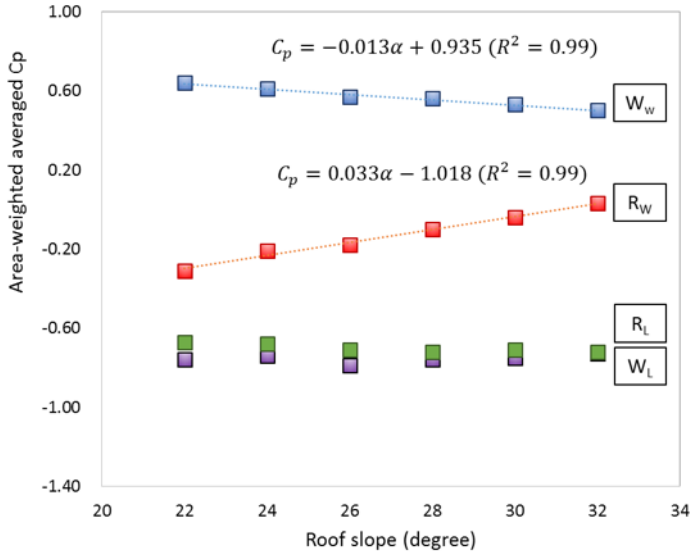

(a) Area-weighted averaged C_p according to roof slope and sections when wind direction was 0°

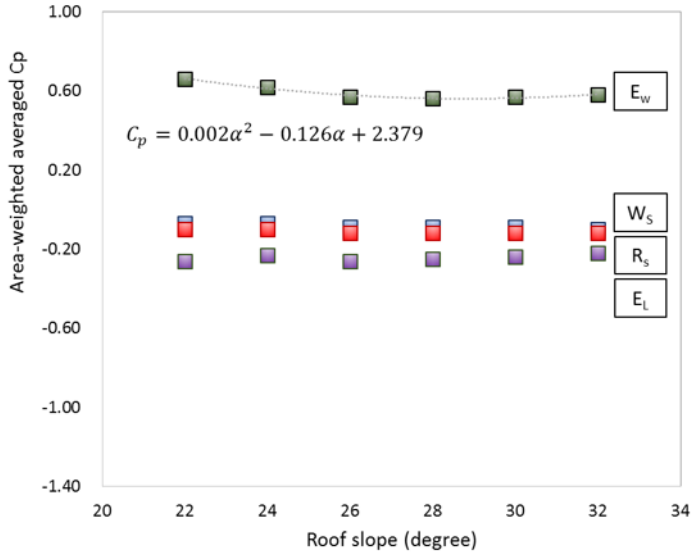

(b) Area-weighted averaged C_p according to roof slope and sections when wind direction was 90°

Fig. 24 Area-weighted averaged wind pressure coefficients according to the roof slope and section of the Even-span type greenhouses when the wind directions were 0° (a) and 90° (b)

4.1.2 Three-quarter type greenhouses

Fig. 25 describes the WT-measured results of the Three-Quarter type greenhouses (Type-TQ-D26) according to the monitored rows and designed wind directions. Fig. 26, 27 and 28 illustrate the measured distribution of C_p on the surface of the experimental Type-TQ-D26 model when the designed wind directions were 0°, 90° and 180° to the side wall of the greenhouse, respectively. When the designed wind direction was 0° to the side wall, a very steep inclination between W_W and R_W was also observed, as shown in the WT-measured results of the Even-span type greenhouses under identical wind conditions. This sudden variation of the wind pressure could cause a strong wind load and bending moment on the windward wall surface. Similar tendencies were also observed when the designed wind direction was 180° to the side wall, meaning that the structural vulnerability on strong wind should be carefully reviewed when wind blows perpendicularly to the side walls of the greenhouse. As shown in Fig. 25 (b), when the wind blows in a 90° direction to the side wall, the measured C_p values of the first end parts at the windward, including C14 and C15, did not show a symmetrical distribution in the width direction, especially for both of the eaves regions compared to the WT results of the Even-span type greenhouses when an identical wind direction was applied.

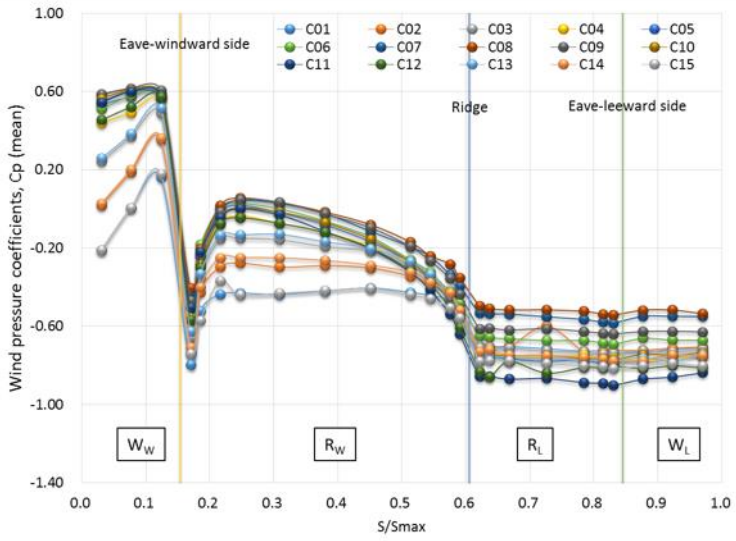

(a) Measured C_p of each monitoring row for Type-TQ-D26 greenhouse when wind direction was 0°

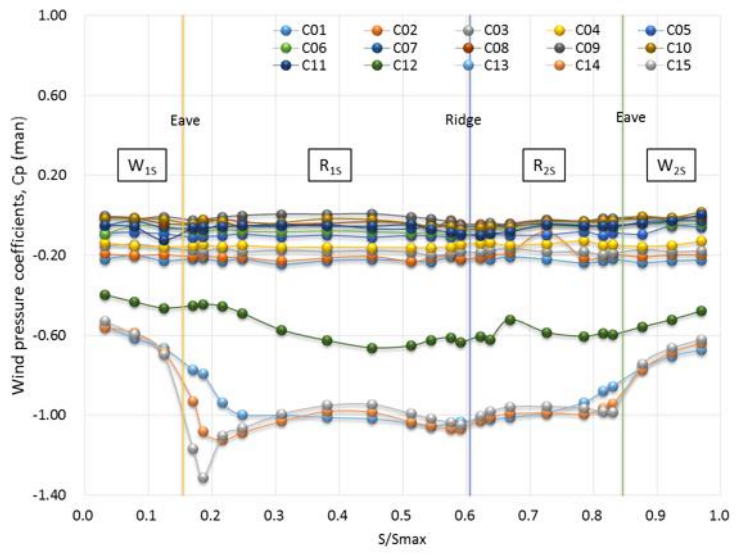

(b) Measured C_p of each monitoring row for Type-TQ-D26 greenhouse when wind direction was 90°

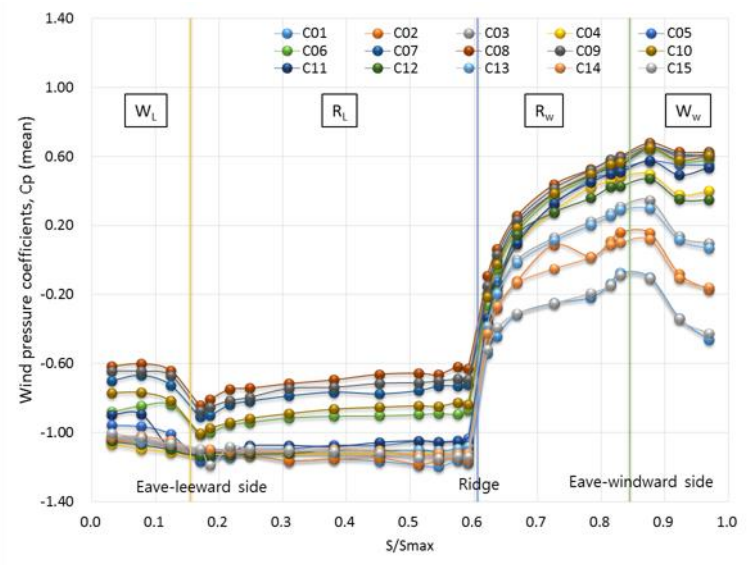

(c) Measured C_p of each monitoring row for Type-TQ-D26 greenhouse when wind direction was 180°

Fig. 25 Measured wind pressure coefficients of each monitoring row for the Type-TQ-D26 model when the wind directions ware 0° (a), 90° (b) and 180° (c)

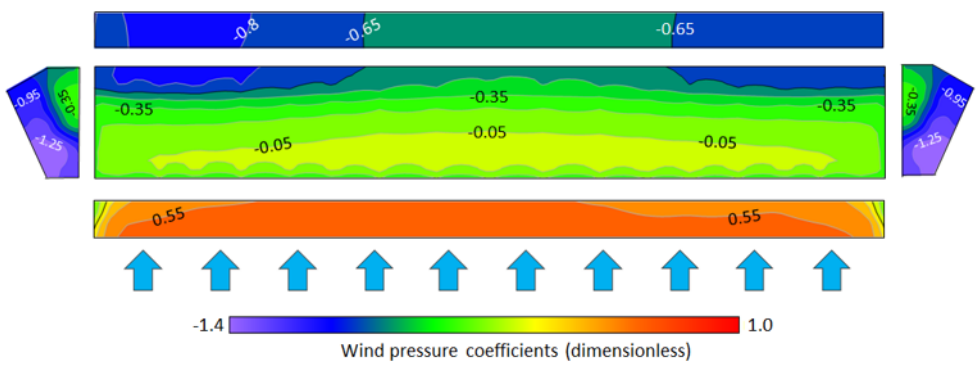

Fig. 26 Distribution of the wind pressure coefficients for Type-TQ-D26 when the wind direction was 0°

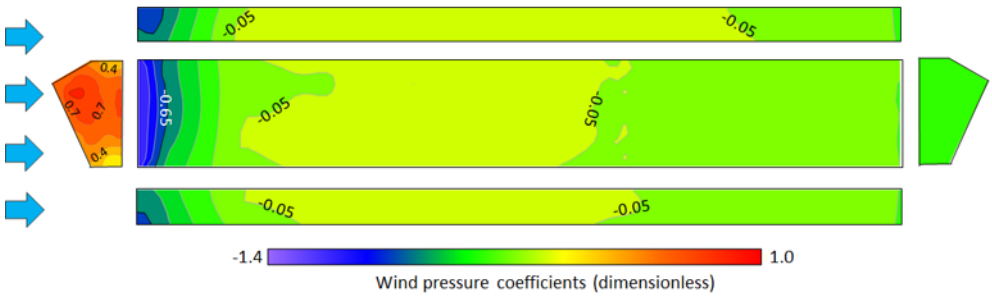

Fig. 27 Distribution of the wind pressure coefficients for Type-TQ-D26 when the wind direction was 90°

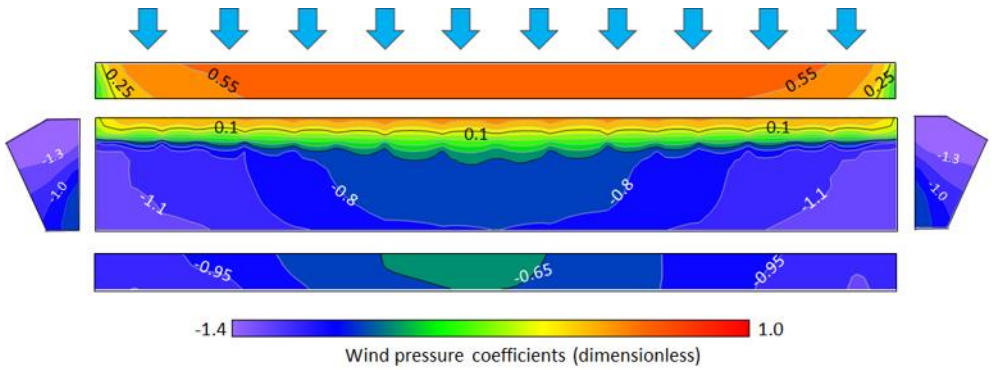

Fig. 28 Distribution of the wind pressure coefficients for Type-TQ-D26 when the wind direction was 180°

Fig. 29 shows the WT-measured results of the area-weighted averaged C_p of each section according to the roof slope of the Three-quarter type greenhouses when the designed wind directions were 0° (a), 90° (b) and 180° (c) to the side wall of the greenhouse. For a 0° wind direction, two particular linear trends were observed for the R_W region according to the variables of the roof slope. In the range between 22 and 26° roof slopes, a reverse linear relationship was found (R^2=0.99), whereas a positive linear relationship was found for the remaining ranges (R^2=0.99). However, the data were not enough to induce the general conclusions to explain the effects of the roof slope. Additional experiments with a wide range of variables of the roof slope are needed to explain these observed phenomena. In case of the results of R_L and W_L, the distribution of

the calculated area-weighted averaged values were very similar; however, no specific trends were observed (R^2=0.43 and 0.35, respectively). When the wind direction was 90° to the side wall, the C_p values as measured at E_W showed relatively larger positive values (Avg. C_p=0.63, STDEV C_p= 0.06) compared to those of the remaining sections; however, there were no particular trends.

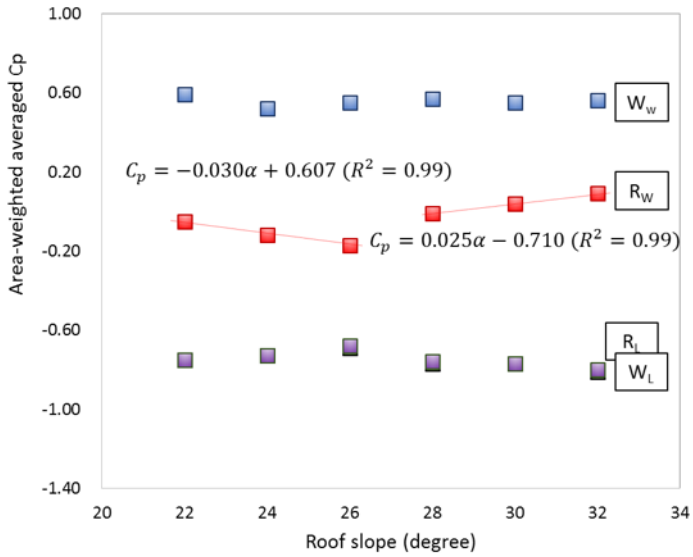

(a) Area-weighted averaged C_p according to roof slope and sections when wind direction was 0°

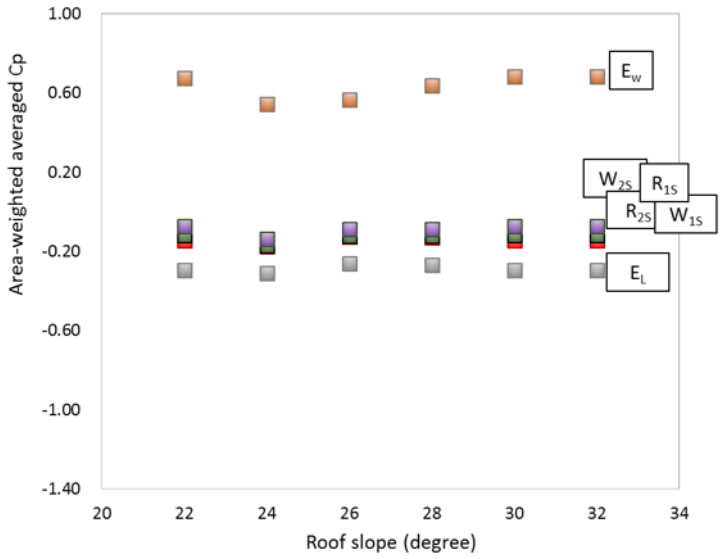

(b) Area-weighted averaged C_p according to roof slope and sections when wind direction was 90°

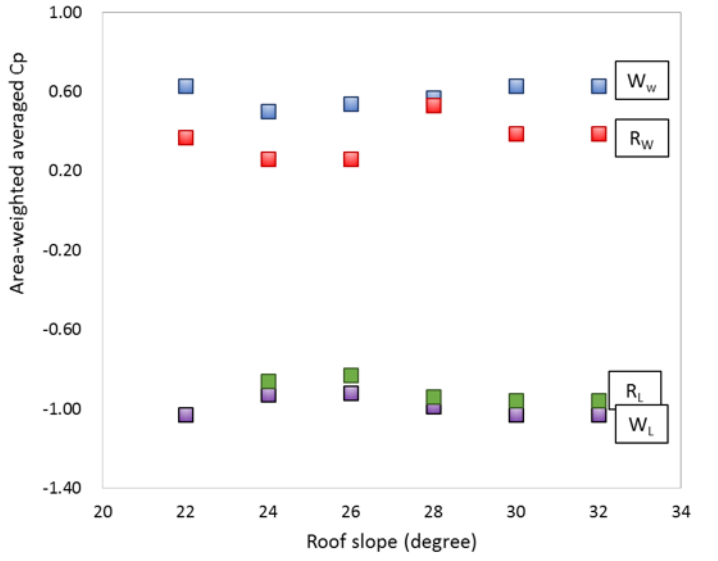

(c) Area-weighted averaged C_p according to roof slope and sections when wind direction was 180°

Fig. 29 Area-weighted averaged wind pressure coefficients according to the roof slope and section of the Three-quarter type greenhouses when the wind directions were 0° (a), 90° (b) and 180° (c)

4.1.3 Peach type greenhouses

Fig. 30 shows one of the results of measured C_p for Peach type greenhouses (Type-PC-R5000) according to the monitored rows when the designed wind directions were 0° (a) and 90° (b) to the side wall of the greenhouse. Fig. 31 and 32 show the WT-measured distribution of C_p of the Peach type greenhouses according to the wind directions. Compared to the results of the glass-covered greenhouse, such as Even-span and Three-quarter type greenhouses, which showed a steep inclination and larger decrease of C_p at the locations between the windward eaves and ridge, the variance of the measured C_p was not decreased dramatically; the values decreased slowly along the surface of the roof and showed a minimum value of -2.15 at the ridge of the greenhouse. These results could be explained by the roof of Peach type greenhouses showing a smooth arc shape; therefore, a separation of the airflow was formed more close to the arch-shaped roof surface, and relatively slow gradients of the wind pressure differences were observed alongside the roof surface. When the wind direction was 90°, as shown in (b) of Fig. 30, symmetric distribution of the C_p were observed. Among the monitored rows, the measured wind pressure coefficients of the first end part at the windward, R_S1 including C13, C14 and C15, ranged from -0.6 to -1.1, and those of the R_S2 region ranged from -0.5 to -0.7.

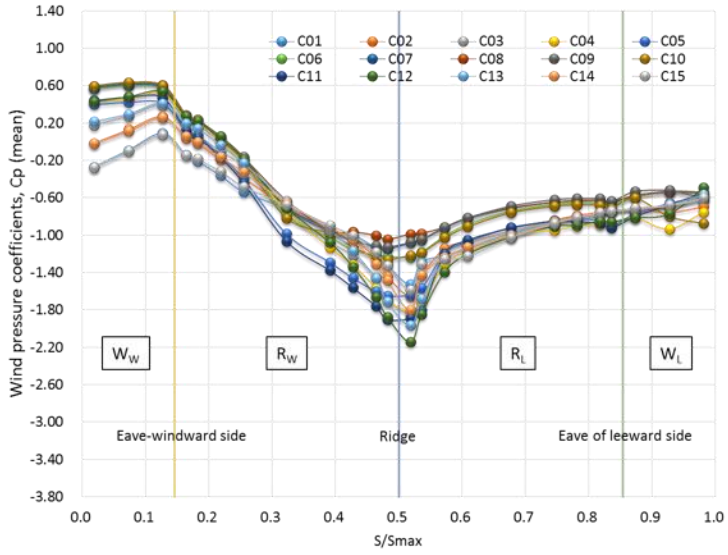

(a) Measured C_p of each monitoring row for Type-PC-R5000 greenhouse when wind direction was 0°

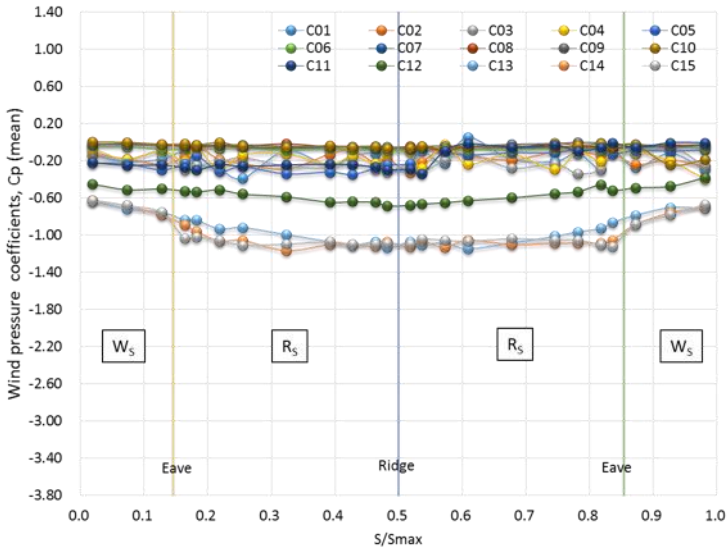

(b) Measured C_p of each monitoring row for Type-PC-R5000 greenhouse when wind direction was 90°

Fig. 30 Measured wind pressure coefficients of each monitoring row for the Type-PC-R5000 model when the wind directions were 0° (a) and 90° (b)

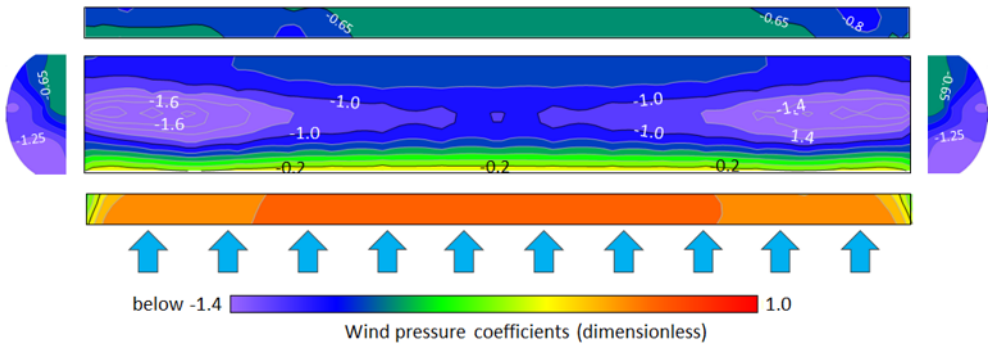

Fig. 31 Distribution of the wind pressure coefficients for Type-PC-R5000 when the wind direction was 0°

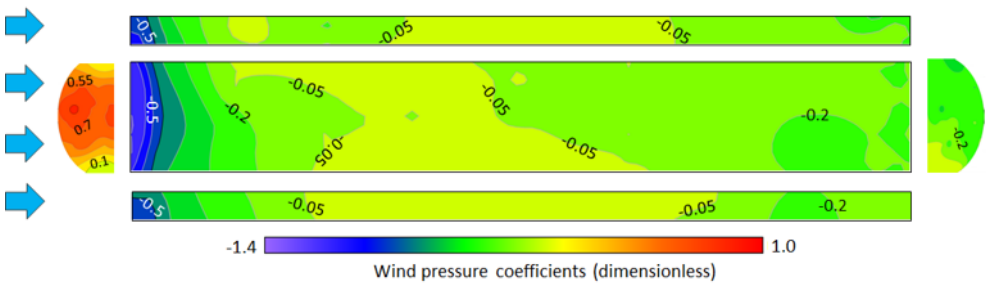

Fig. 32 Distribution of the wind pressure coefficients for Type-PC-R5000 when the wind direction was 90°

Fig. 33 shows the area-weighted averaged C_p values of each section according to the curvature radius of the roof of Peach type greenhouses when the designed wind direction was 0° (a) and 90° (b) to the side wall of the greenhouse. For the W_W, the averaged values increased according to the curvature radius of the roof (R^2=0.88, p=0.006); however, the degree of the gradient was very low. For W_L, the average values showed weak reverse-linear trends with an R^2 value of 0.85. No specific trends were found for the regions of E_W (Avg. C_p of 0.56 and STDEV C_p of 0.01) and E_L (Avg. C_p of −0.28 and STDEV C_p of 0.02) when the designed wind direction was 90° . In the case of the area-weighted averaged C_p for sections, such as the windward roof (R_W) and leeward roof (R_L) for a wind direction of 0° and the side of roof surface (R_S) for a wind direction

of 90° , the values are shown in Table 8 according to the central angle of the each “fan-shape” sector.

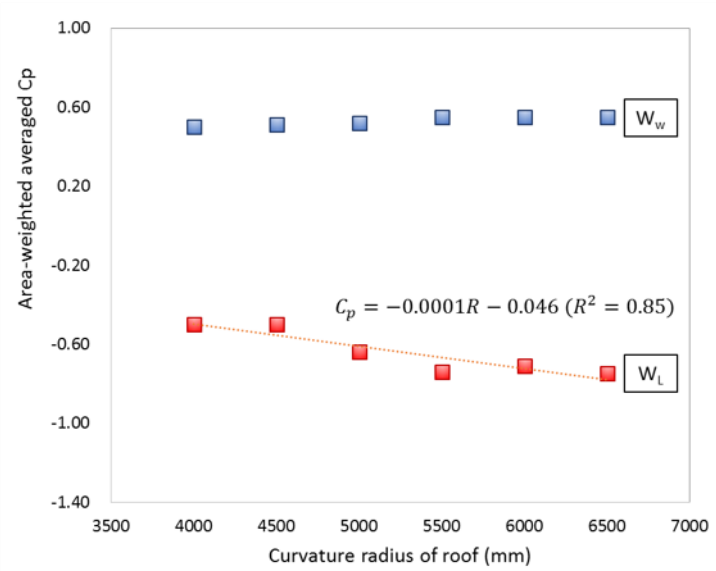

(a) Area-weighted averaged C_p according to radius of curvature of roof and sections when wind direction was 0°

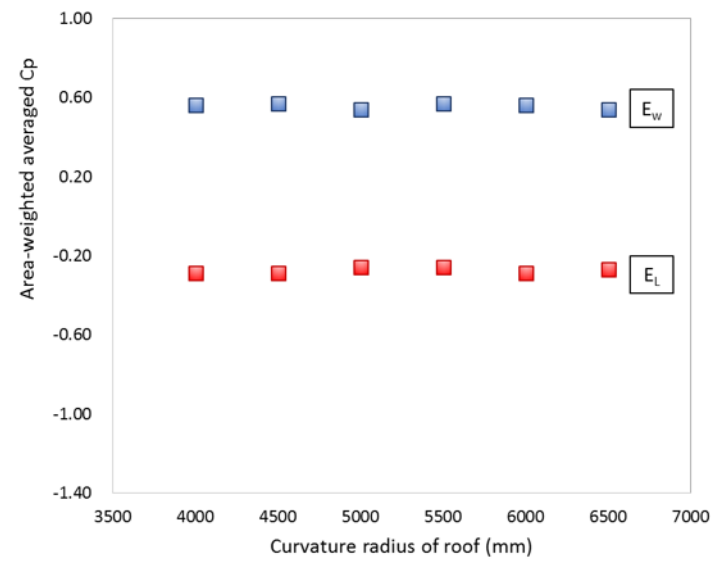

(b) Area-weighted averaged C_p according to radius of curvature of roof and sections when wind direction was 90°

Fig. 33 Area-weighted averaged wind pressure coefficients according to the radius of the curvature of roof and the section of Peach type greenhouses when the wind directions were 0° (a) and 90° (b)

Table 8 Area-weighted averaged wind pressure coefficients of the RW and RL sections (wind direction was 0°) and the RS sections (wind direction was 90°) for the Type PC-R5000 model

Area-weighted averaged wind pressure coefficients in the R_W and R_L sections				
Wind direction (°)	R_W (Windward roof surface)			
	R_W θ =0~20°	R_W θ =20~40°	R_W θ =40~65°	R_W θ =65~90°
0	−0.02	−0.79	−1.11	−1.35
Wind direction (°)	R_L (Leeward roof surface)			
	R_L θ =65~90°	R_L θ =65~90°	R_L θ =20~45°	R_L θ =0~20°
90	−1.36	−1.00	−0.81	−0.73
Wind direction (°)	R_S (Side of roof surface)			
	R_S θ =0~20°	R_S θ =20~40°	R_S θ =40~65°	R_S θ =65~90°
0	−0.16	−0.18	−0.18	−0.19
Wind direction (°)	R_S (Side of roof surface)			
	R_S θ =65~90°	R_S θ =65~90°	R_S θ =20~45°	R_S θ =0~20°
90	−0.18	−0.14	−0.13	−0.12

4.1.4 Mono-span type greenhouses

Fig. 34 shows the WT results of the Mono-span type greenhouses (Type-MS-D26) according to the monitored rows when the designed wind directions were 0° (a), 90° (b) and 180° (c) to the side wall of the greenhouse. Fig. 35, 36, and 37 illustrate the distribution of the measured C_p according to the designed wind directions, respectively. When the wind direction was 0° , the WT results of W_W showed positive values for all of the monitored rows except for the rows that were located at the end parts of the greenhouse, such as C01, C02, C14 and C15. A steep inclination was also found in every monitored row between W_W and R_W near the eaves of the greenhouse. These phenomena were also observed in every monitored row between W_W and R_L when the wind blew from the opposite direction (180°). As previously mentioned,

due to a relatively large pressure difference acting on the greenhouse surface when the wind blows perpendicularly the longitudinal of the greenhouse, strong bending moments can cause the collapse of the structure and a permanent strain of the framework. When the wind direction was 90° , the measured C_p distribution of Mono-span type greenhouses showed a skewed distribution due to its asymmetric geometry; the lowest values were observed in the regions near the ridge of the greenhouse (R_S1) with a value of −1.4 at C15 row, and the values of C14 and C13 followed.

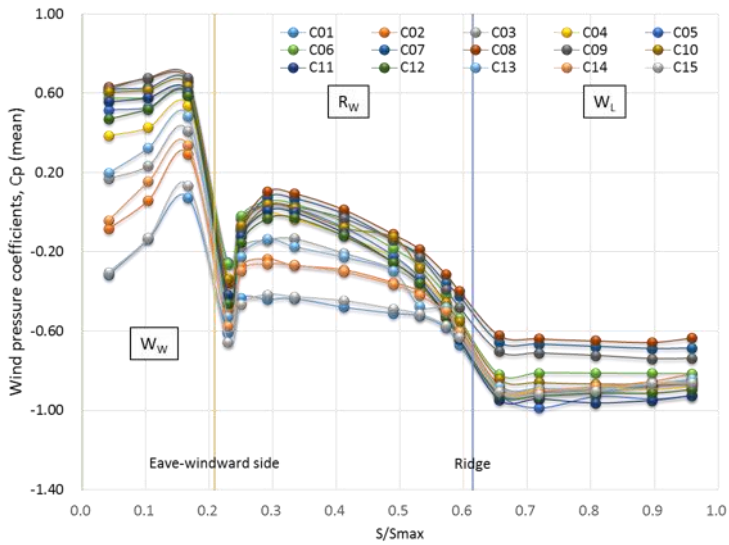

(a) Measured C_p of each monitoring row for Type-MS-D26 greenhouse when wind direction was 0°

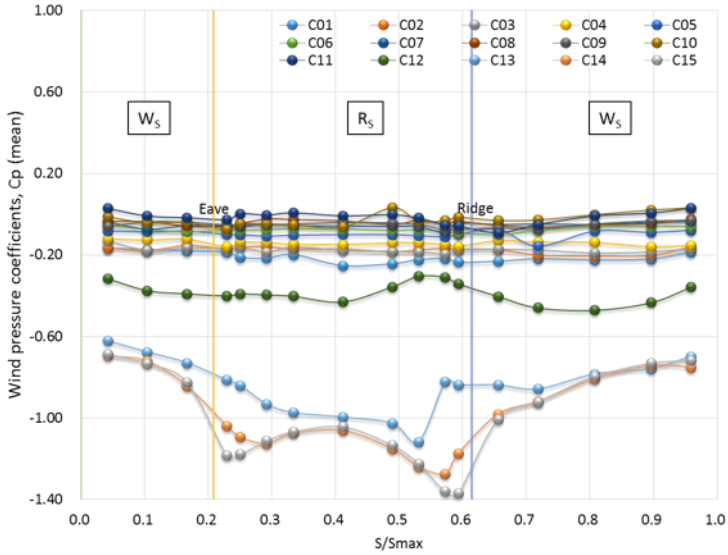

(b) Measured C_p of each monitoring row for Type-MS-D26 greenhouse when wind direction was 90°

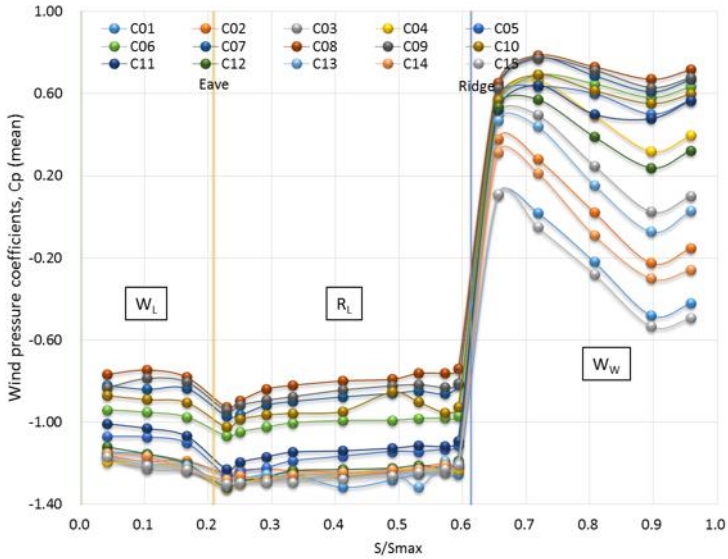

(c) Measured C_p of each monitoring row for Type-MS-D26 greenhouse when wind direction was 180°

Fig. 34 Measured wind pressure coefficients of each monitoring row for the Type-MS-D26 model when the wind directions were 0° (a), 90° (b) and 180° (c)

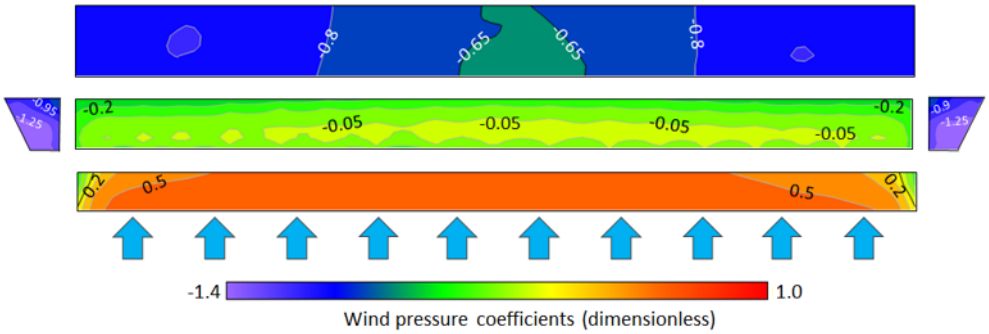

Fig. 35 Distribution of the wind pressure coefficients for Type-MS-D26 when the wind direction was 0°

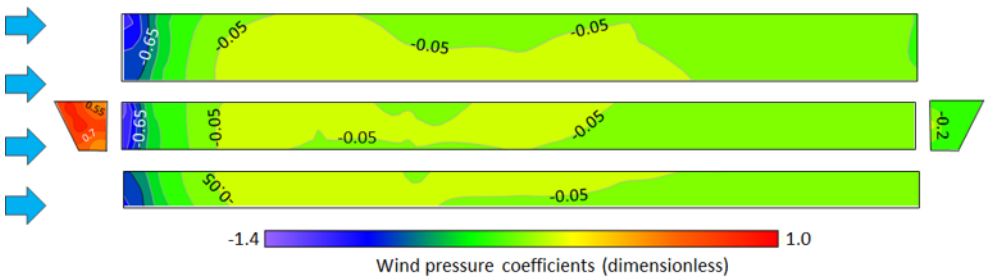

Fig. 36 Distribution of the wind pressure coefficients for Type-MS-D26 when the wind direction was 90°

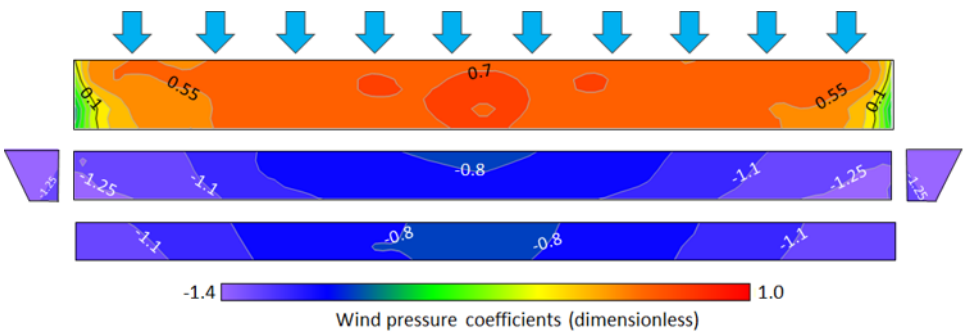

Fig. 37 Distribution of the wind pressure coefficients for Type-MS-D26 when the wind direction was 180°

Fig. 38 shows the area-weighted averaged C_p of each section according to the roof slope of Mono-span type greenhouses and the designed wind directions. For the values of R_W, a second-order

polynomial relationship (R^2=0.99) was found with increasing trends, whereas a weak reverse-linear relationship (R^2=0.81) was found for the values of the W_L according to the roof slope variables. However, no specific trends of C_p were observed for averaged sections when the wind direction was 90 and 180° to the side wall.

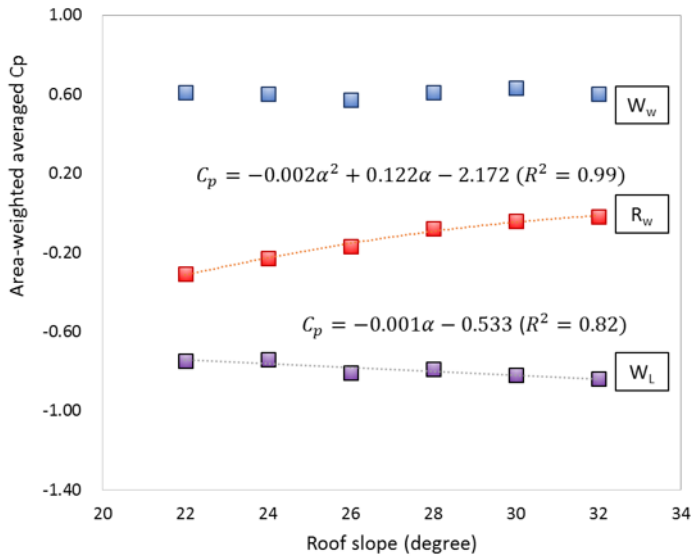

(a) Area-weighted averaged C_p according to roof slope and sections when wind direction was 0°

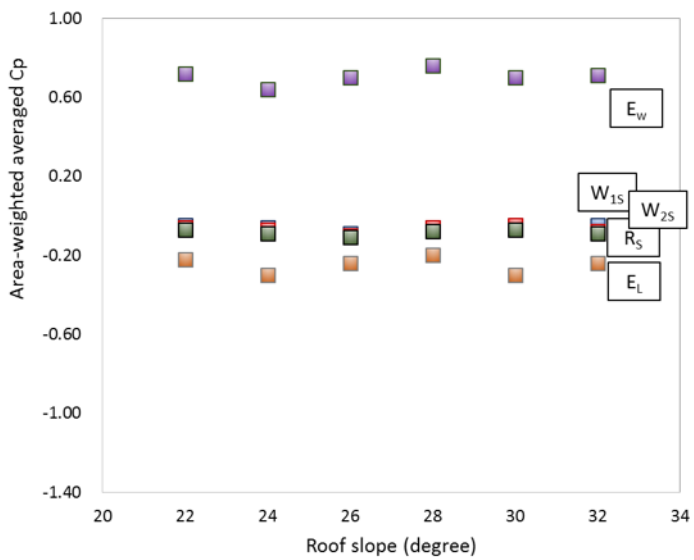

(b) Area-weighted averaged C_p according to roof slope and sections when wind direction was 90°

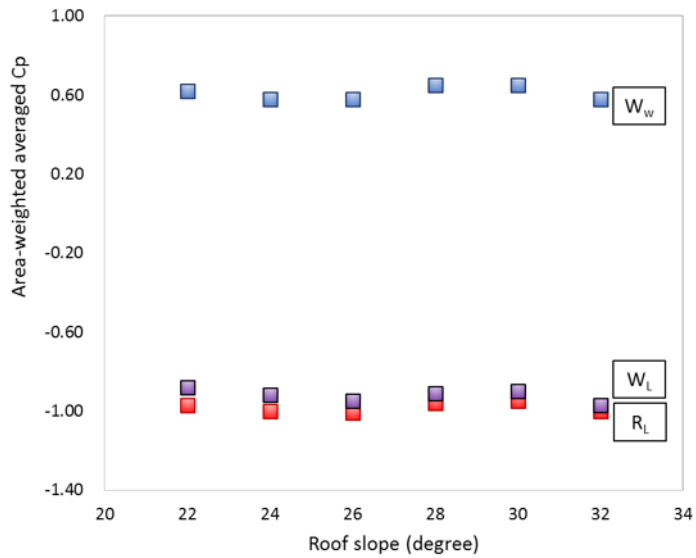

(c) Area-weighted averaged C_p according to roof slope and sections when wind direction was 180°

Fig. 38 Area-weighted averaged wind pressure coefficients according to the roof slope and section of Mono-span type greenhouses when the wind directions were 0° (a), 90° (b) and 180° (c)

4.2 Local wind pressure coefficients in terms of cladding design

To analyze the characteristics of the local wind pressure acting on the greenhouse, especially for the coverings and glazing bars, the measured C_p were evaluated according to the pre-defined local regions and various wind environmental conditions. In these sections, the results of one representative experimental case per each greenhouse model will be introduced to explain the tendencies of the distribution of the local wind pressure. Details of the measured data for all of the single-span greenhouses are available from the corresponding author upon request.

4.2.1 Even-span Greenhouses

Table 9 shows the WT-measured local C_p of Even-span type greenhouses with a roof slope of 26° (Type-EV-D26) according to the various wind directions and pre-defined local sections of the greenhouse surface. When the wind direction was 0° to the sidewall, a relatively large negative pressure at the surface of the leeward roof regions was observed due to the effect of the conical vortex of the airflow showing −0.97 and −0.95, respectively, for R_L1 and R_L2. For the surface of the end parts of the greenhouse, a large negative C_p was also shown, such as −1.36 for E_S1 and −1.04 for E_S2. As the designed wind direction changed from 0° to 45° to the sidewall, the negative pressure increased rapidly at one end part of the eaves of the leeward roof surface locally (R_L1), and the maximum value of the negative C_p was −1.78 with a wind direction of 22.5° to the sidewall. Considering the given wind directions to the geometrical surface of Even-span type greenhouse, the values of W_S1, W_S2, R_S1 and R_S2 were monitored when the wind direction was 67.5° and 90°, and a larger negative C_p of −1.14, was observed at the R_S1 region with the wind direction of 67.5°. From the mentioned results, it could be concluded that strong local wind pressure acted on the roof surface when the wind was blowing aslant to the greenhouse (e.g., results with 22.5° and 67.5° wind directions to the sidewall in Table 9). Therefore, the effect of such local effect of wind pressure on structures such as greenhouses must be carefully considered in the design of covering and glazing bars, which are strongly affected by the local wind pressure.

Table 9 Measured local wind pressure coefficients of Even-span type greenhouses (Type-EV-D26) according to the designed wind directions

Wind pressure coefficients (dimensionless)					
Sections	Wind directions (°)				
	0	22.5	45	67.5	90
R_W1	-0.35	-0.27	-0.21	-	
R_W2	-0.15	-0.18	-0.19		
R_L1	-0.97	-1.78	-1.52		
R_L2	-0.95	-1.59	-1.22		
E_S1	-1.36	-0.55	-0.29		
E_S2	-1.04	-0.54	-0.32		
W_S1	-			-0.59	-0.68
W_S2				-0.66	-0.44
R_S1				-1.14	-1.01
R_S2				-0.87	-0.56

4.2.2 Three-quarter type greenhouses

Table 10 shows the measured local C_p of Three-quarter type greenhouses with a 26° roof slope (Type-TQ-D26) according to the various wind directions and pre-defined local sections of the greenhouse surface. As mentioned in previous sections, relatively larger values of negative C_p were usually observed at the end parts of the leeward roof (R_L1), especially under slanted wind direction conditions (e.g., 22.5°, 45°, 135° and 157.5° to the side wall). For the wind direction conditions in a range from 67.5° to 112.5°, the largest negative C_p of -1.31, was found at the end corner parts of the greenhouse ($R_{1S}1$), especially with a wind direction of 112.5°.

Table 10 Measured local wind pressure coefficients of Three-quarter type greenhouses (Type-TQ-D26) according to the designed wind directions

Wind pressure coefficients (dimensionless)						
Sections	Wind directions (°)					
	0	22.5	45	135	157.5	180
R_W1	−0.42	−0.36	−0.24	0.43	0.41	0.13
R_W2	−0.21	−0.21	−0.19	0.26	0.57	0.75
R_L1	−0.74	−1.69	−1.72	−1.72	−1.96	−1.14
R_L2	−0.68	−0.80	−0.78	−1.01	−1.07	−0.90
E_S1	−1.23	−0.57	−0.29	−0.39	−0.95	−1.42
E_S2	−0.84	−0.57	−0.32	−0.42	−0.68	−1.36
Sections	Wind directions (°)					
	67.5		90		112.5	
$R_{1S}1$	−0.75		−1.01		−1.31	
$R_{1S}2$	−0.16		−0.58		−0.85	
$R_{2S}1$	−0.95		−0.97		−0.36	
$R_{2S}2$	−0.98		−0.58		−0.02	
$W_{1S}1$	−0.09		−0.61		−0.61	
$W_{1S}2$	0.15		−0.43		−0.69	
$W_{2S}1$	−0.73		−0.70		−0.04	
$W_{2S}2$	−0.88		−0.52		0.16	

4.2.3 Peach type greenhouses

Table 11 shows the measured local C_p of Peach type greenhouses with a curvature radius of roof of 5000 mm (Type-PC-R5000) according to the various wind directions and pre-defined local sections of the greenhouse surface. For the regions that were located at the end parts of the greenhouse, such as E_S1 and E_S2, relatively large C_p values were observed under conditions of a wind direction of 0° to the side wall. When the wind blows from 22.5 and 45°, not only negative pressure but also positive pressure can be distributed at the surface of the E_S1 and E_S2.

Table 11 Measured local wind pressure coefficients of Peach type greenhouses (Type-PC-R5000) according to the designed wind directions

Wind pressure coefficients (dimensionless)					
Sections	Wind directions (°)				
	0	22.5	45	67.5	90
E_S1	-1.32	-0.54	-0.33	-	
E_S2	-0.99	-0.59	-0.38		
W_S1	-			-0.61	-0.75
W_S2				-0.69	-0.49
R_S1				-0.98	-1.06
R_S2				-0.84	-0.59

4.2.4 Mono-span greenhouses

Table 12 shows the measured local C_p of Mono-span type greenhouses with a 26° roof slope (Type-MS-D26) according to the various wind directions and pre-defined local sections of the greenhouse surface. For the regions of the windward second roof walls (R_W2), the measured negative C_p slightly increased as the wind direction changed from 0 to 45° based on the side wall of the greenhouse. For the R_L1 and R_L2 regions, a relatively larger negative wind pressure acted on the local surface under conditions of 135° and 157.5° wind directions. In case of the E_S1 regions, the maximum negative wind pressure was found when the designed wind direction was 157.5° to the side wall. A strong wind pressure also acted on the surface of R_S1 and R_S2, especially when the wind direction was 112.5° to the side wall. As mentioned above, relatively larger values were locally formed when the wind blew obliquely to the greenhouse structure, meaning that some local regions, especially near the corner of the greenhouse, edge of eaves and roofs of the greenhouse, could be vulnerable to slanted strong wind conditions. Therefore, the wind pressure coefficients on the surface of the greenhouse must be carefully reviewed and determined according to the various wind directions.

Table 12 Measured local wind pressure coefficients of Mono-span type greenhouses (Type-MS-D26) according to the designed wind directions

Wind pressure coefficients (dimensionless)						
Sections	Wind directions (°)					
	0	22.5	45	135	157.5	180
R_W1 (R_L1)	−0.35	−0.20	−0.17	(−2.24)	(−2.38)	(−1.26)
R_W2 (R_L2)	−0.09	−0.12	−0.14	(−1.16)	(−1.16)	(−1.00)
E_S1	−1.31	−1.35	−0.32	−0.48	−2.28	−1.43
Sections	Wind directions (°)					
	67.5		90		112.5	
R_S1	−0.35		−0.71		−1.15	
R_S2	−0.02		−0.54		−0.80	
$W_{1S}1$	0.16		−0.53		−0.70	
$W_{1S}2$	−0.46		−0.58		−0.27	
$W_{2S}1$	−1.31		−0.62		0.22	
$W_{2S}2$	−1.45		−0.43		0.26	

4.3 Overall evaluation of the wind pressure coefficients for structural and cladding design

C_p was proposed for the design of the greenhouses that were built in the representative reclaimed lands in Korea from the WT-measured distribution characteristics of the wind pressure for a pre-defined region of the greenhouse surface according to the various wind direction conditions and design factors, such as the roof slope and the curvature radius of the roof. The values of C_p were suggested into two tracks: 1) the C_p to review the entire structural safety (conducted with wind directions of 0° and 90° to the side wall based on previous studies and international as well as domestic greenhouse standards) and 2) local C_p to design the covering and glazing bars for the target local wind pressure. For the cladding design, the maximum C_p values per each local pre-defined region were selected among the absolute value of WT-measured C_p for the whole wind direction conditions. Local wind pressure coefficients have not yet been suggested for the whole wind direction to date;

generally, only 0 and 90° wind directions to the side wall of the greenhouse have been considered in the international and domestic greenhouse standards. For the proposal of C_p of each experimental greenhouse model, 1st-order or 2nd-order regression equations were introduced when specific trends were observed between the measured values and design factors, such as the roof slope and the curvature radius of the roof; however, the area-weighted averaged C_p values were only suggested when there were no specific trends among the variables.

Table 13 and 14 show the C_p of Even-span type greenhouses for structural design and cladding design according to the location of the wind directions, pre-defined sections and roof slope angles.

Table 13 Suggestion of the wind pressure coefficients of Even-span type greenhouses for structural design

Wind direction (°)	Sections	Wind pressure coefficients (dimensionless)					
		Roof slope, α (°)					
		22	24	26	28	30	32
0	W_W	$C_p = -0.013\alpha + 0.935$					
	R_W	−0.31	−0.21	−0.18	−0.1	−0.04	0.03
	R_L	−0.76	−0.74	−0.79	−0.76	−0.75	−0.73
	W_L	−0.67	−0.68	−0.71	−0.72	−0.71	−0.72
	E_S	−0.98	−0.94	−1.00	−0.98	−0.97	−0.96
90	W_S	−0.07	−0.07	−0.09	−0.09	−0.09	−0.10
	R_S	−0.10	−0.10	−0.12	−0.12	−0.12	−0.12
	E_W	$C_p = 0.002\alpha^2 - 0.126\alpha + 2.379$					
	E_L	−0.26	−0.23	−0.26	−0.25	−0.24	−0.22

Table 14 Suggestion of the wind pressure coefficients of Even-span type greenhouses for cladding design

Wind direction (°)	Sections	Wind pressure coefficients (dimensionless)					
		Roof slope, α (°)					
		22	24	26	28	30	32
0	R_W1	$C_p = 0.051\alpha - 1.710$ (R^2=0.97)					
	R_W2	$C_p = 0.064\alpha - 1.846$ (R^2=0.98)					
22.5	R_L1	$C_p = 0.007\alpha^2 - 0.371\alpha + 3.403$ (R^2=0.92)					
	R_L2	−1.44	−1.46	−1.59	−1.66	−1.57	−1.51
45	E_S1	−1.39	−1.34	−1.36	−1.33	−1.27	−1.28
	E_S2	−1.04	−0.95	−1.04	−1.00	−1.03	−0.99
67.5	W_S1	−0.82	−0.70	−0.68	−0.66	−0.67	−0.64
	W_S2	−0.65	−0.63	−0.66	−0.65	−0.65	−0.65
90	R_S1	−1.08	−1.04	−1.14	−1.05	−1.05	−0.99
	R_S2	−0.88	−0.88	−0.87	−0.89	−0.93	−0.91

The final suggestion of C_p for the structural design and cladding design of Three-quarter type greenhouse is shown in Table 15 and 16, respectively.

Table 15 Suggestion of wind pressure coefficients of Three-quarter type greenhouses for structural design

Wind direction (°)	Sections	Wind pressure coefficients (dimensionless)					
		Roof slope, α (°)					
		22	24	26	28	30	32
0	W_W	0.59	0.52	0.55	0.57	0.55	0.56
	R_W	−0.05	−0.12	−0.17	−0.01	0.04	0.09
	R_L	−0.75	−0.73	−0.69	−0.77	−0.77	−0.81
	W_L	−0.75	−0.73	−0.68	−0.76	−0.77	−0.80
	E_S	$C_p = -0.004\alpha^2 + 0.213\alpha - 3.655$ (R^2=0.94)					
90	W_{1S}	−0.11	−0.14	−0.10	−0.10	−0.11	−0.11
	R_{1S}	−0.14	−0.18	−0.12	−0.13	−0.14	−0.14
	R_{2S}	−0.12	−0.17	−0.12	−0.12	−0.12	−0.12
	W_{2S}	−0.07	−0.14	−0.09	−0.09	−0.07	−0.07
	E_W	0.67	0.54	0.56	0.64	0.68	0.68
	E_L	−0.29	−0.31	−0.26	−0.27	−0.30	−0.30
180	W_W	0.63	0.50	0.54	0.57	0.63	0.63
	R_W	0.37	0.26	0.26	0.39	0.39	0.39
	R_L	−1.03	−0.93	−0.92	−0.99	−1.03	−1.03
	W_L	−0.96	−0.86	−0.83	−0.94	−0.96	−0.96
	E_S	−1.51	−1.24	−1.16	−1.31	−1.52	−1.52

Table 16 Suggestion of wind pressure coefficients of Three-quarter type greenhouses for cladding design

Wind direction (°)	Sections	Wind pressure coefficients (dimensionless)					
		Roof slope, α (°)					
		22	24	26	28	30	32
0	R_W1	−0.29	−0.37	−0.42	−0.18	−0.19	−0.17
	R_W2	0.18	−0.08	−0.21	0.30	0.44	0.55
22.5	R_L1	−1.98	−1.78	−1.72	−1.88	−1.87	−1.87
	R_L2	−0.91	−0.84	−0.80	−0.93	−0.91	−0.91
45	E_S1	−1.42	−1.29	−1.23	−1.38	−1.42	−1.52
	E_S2	−0.94	−0.91	−0.84	−0.93	−0.96	−1.05
67.5	$R_{1S}1$	−1.38	−1.32	−1.31	−1.33	−1.37	−1.37
	$R_{1S}2$	−1.16	−1.02	−0.85	−1.10	−1.16	−1.16
90	$R_{2S}1$	−0.98	−1.03	−0.97	−1.03	−0.99	−0.99
	$R_{2S}2$	−1.09	−1.10	−0.98	−1.13	−1.09	−1.09
112.5	$W_{1S}1$	−0.59	−0.17	−0.61	−0.66	−0.59	−0.59
	$W_{1S}2$	−0.76	−0.72	−0.69	−0.72	−0.76	−0.76
	$W_{2S}1$	−0.89	−0.81	−0.73	−0.80	−0.89	−0.89
	$W_{2S}2$	−0.95	−0.97	−0.88	−1.00	−0.95	−0.95
135	R_W1	0.67	0.49	0.43	0.60	0.66	0.66
	R_W2	0.93	0.72	0.75	1.01	1.04	1.07
157.5	R_L1	−2.12	−2.04	−1.96	−2.17	−2.11	−2.11
	R_L2	−1.26	−1.09	−1.07	−1.20	−1.26	−1.26
180	E_S1	−1.70	−1.45	−1.42	−1.46	−1.70	−1.70
	E_S2	−1.69	−1.41	−1.36	−1.44	−1.69	−1.69

Table 17 and 18 represent the C_p of Peach type greenhouses for structural design and cladding design, respectively. Considering the arch-shape of the roof surface of the target structure, the suggestion of C_p for structural design is described in detail according to the central angle of the fan-shaped sector.

Table 17 Suggestion of the wind pressure coefficients of Peach type greenhouses for structural design

Wind direction (°)	Sections	Wind pressure coefficients (dimensionless)					
		Curvature radius of roof (m)					
		4.0	4.5	5.0	5.5	6.0	6.5
0	W_W	$C_p = -0.0004\alpha^2 + 0.027\alpha + 0.088$ (R^2=0.92)					
	W_L	−0.50	−0.50	−0.64	−0.74	−0.71	−0.75
	R_W (0≤ θ ≤20)	−0.09	−0.10	−0.02	0.05	0.03	0.05
	R_W (20≤ θ ≤40)	$C_p = -0.071\alpha - 2.631$ (R^2=0.94)					
	R_W (40≤ θ ≤65)	$C_p = -0.110\alpha - 4.035$ (R^2=0.91)					
	R_W (65≤ θ ≤90)	$C_p = -0.009\alpha^2 + 0.621\alpha - 11.176$ (R^2=0.92)					
	R_L (65≤ θ ≤90)	−1.76	−1.86	−1.36	−0.87	−0.90	−0.84
	R_L (40≤ θ ≤65)	$C_p = -0.004\alpha^2 + 0.256\alpha - 4.897$ (R^2=0.96)					
	R_L (20≤ θ ≤40)	−0.61	−0.64	−0.81	−0.80	−0.79	−0.81
	R_L (0≤ θ ≤20)	$C_p = -0.004\alpha^2 - 0.240\alpha + 2.948$ (R^2=0.94)					
	E_S	−0.96	−0.90	−0.97	−1.07	−1.01	−1.11
90	W_S	−0.17	−0.14	−0.13	−0.11	−0.13	−0.12
	R_S (0≤ θ ≤20)	$C_p = -0.0002\alpha^2 + 0.014\alpha - 0.371$ (R^2=0.93)					
	R_S (20≤ θ ≤40)	−0.19	−0.17	−0.18	−0.15	−0.16	−0.16
	R_S (40≤ θ ≤65)	−0.19	−0.17	−0.18	−0.15	−0.16	−0.16
	R_S (65≤ θ ≤90)	−0.20	−0.19	−0.19	−0.16	−0.17	−0.17
	R_S (90≤ θ ≤115)	−0.20	−0.20	−0.18	−0.16	−0.19	−0.17
	R_S (115≤ θ ≤140)	−0.16	−0.16	−0.14	−0.13	−0.14	−0.14
	R_S (140≤ θ ≤160)	−0.15	−0.15	−0.13	−0.12	−0.13	−0.13
	R_S (160≤ θ ≤180)	−0.13	−0.13	−0.12	−0.11	−0.12	−0.12
	E_W	0.56	0.57	0.54	0.57	0.56	0.54
	E_L	−0.29	−0.29	−0.26	−0.26	−0.29	−0.27

Table 18 Suggestion of the wind pressure coefficients of Peach type greenhouses for cladding design

Wind direction (°)	Sections	Wind pressure coefficients (dimensionless)					
		Curvature radius of roof (m)					
		4.0	4.5	5.0	5.5	6.0	6.5
0, 22.5, 45	E_S1	$C_p = -0.030\alpha - 0.582$ (R^2=0.90)					
	E_S2	−1.03	−0.95	−0.99	−1.05	−1.09	−1.11
67.5	W_S1	−0.80	−0.83	−0.75	−0.85	−0.75	−0.76
	W_S2	−0.69	−0.64	−0.69	−0.69	−0.68	−0.72
90	R_S1	−0.99	−1.08	−1.06	−1.05	−0.99	−1.02
	R_S2	−0.83	−0.77	−0.84	−0.82	−0.86	−0.90

Table 19 and 20 show the wind pressure coefficients of Mono-span type greenhouses for structural design and cladding design according to the wind directions and roof slope angles, respectively.

Table 19 Suggestion of the wind pressure coefficients of Mono-span type greenhouses for structural design

Wind direction (°)	Sections	Wind pressure coefficients (dimensionless)					
		Roof slope, α (°)					
		22	24	26	28	30	32
0	W_W	0.61	0.60	0.57	0.61	0.63	0.60
	R_W	$C_p = 0.033\alpha - 1.026$ (R^2=0.99)					
	W_L	−0.75	−0.74	−0.81	−0.79	−0.82	−0.84
	E_S	−1.14	−1.16	−1.16	−1.20	−1.21	−1.20
90	$W1_S$	−0.05	−0.06	−0.09	−0.06	−0.05	−0.05
	$W2_S$	−0.06	−0.07	−0.10	−0.06	−0.05	−0.08
	R_S	−0.07	−0.09	−0.11	−0.08	−0.07	−0.09
	E_W	0.72	0.64	0.70	0.76	0.70	0.71
	E_L	−0.22	−0.30	−0.24	−0.20	−0.30	−0.24
180	W_W	0.62	0.58	0.58	0.65	0.65	0.58
	R_L	−0.97	−1.00	−1.01	−0.96	−0.95	−1.00
	W_L	−0.88	−0.92	−0.95	−0.91	−0.90	−0.97
	E_S	−1.37	−1.36	−1.40	−1.29	−1.30	−1.53

Table 20 Suggestion of the wind pressure coefficients of Mono-span type greenhouses for cladding design

Wind direction (°)	Sections	Wind pressure coefficients (dimensionless)					
		Roof slope, α (°)					
		22	24	26	28	30	32
0 22.5 45	R_W1	$C_p = -0.006\alpha^2 + 0.380\alpha - 6.199$ (R^2=0.96)					
	R_W2	$C_p = -0.004\alpha^2 + 0.289\alpha - 4.935$ (R^2=1.00)					
	E_S1	−1.43	−1.30	−1.35	−1.38	−1.39	−1.50
67.5	R_S1	$C_p = -0.020\alpha - 0.664$ (R^2=0.92)					
	R_S2	$C_p = -0.019\alpha - 0.351$ (R^2=0.91)					
90	$W_{1S}1$	−0.71	−0.73	−0.70	−0.73	−0.74	−0.77
	$W_{1S}2$	−0.53	−0.54	−0.58	−0.62	−0.58	−0.60
112.5	$W_{2S}1$	$C_p = -0.027\alpha - 0.559$ (R^2=0.91)					
	$W_{2S}2$	$C_p = -0.035\alpha - 0.523$ (R^2=0.98)					
135 157.5 180	R_L1	−2.24	−2.32	−2.38	−2.32	−2.37	−2.55
	R_L2	$C_p = -0.012\alpha - 0.841$ (R^2=0.91)					
	E_S1	$C_p = 0.007\alpha^2 - 0.384\alpha + 3.096$ (R^2=0.95)					

4.4 Development of CFD model for predicting distribution of wind pressure on greenhouse

4.4.1 Comparison of wind pressure coefficients according to y^+ value

Fig. 39 shows the distribution of y^+ values on Even-span greenhouse (Type-EV-D22) according to the first grid heights when the wind direction was 0° to the side wall. y^+ values near eaves and ridges were larger than in other regions due to the separation of airflow in the Even-span type greenhouses. As the first grid heights were 1.5×10^{-4} m, 1.5×10^{-3} m and 1.5×10^{-2} m, average y^+ value was 0.85, 7.67 and 52.66, respectively. Even though the distribution of y^+ values were irregular on the surface of the greenhouse, y^+ values at the first grid height 1.5×10^{-4} m generally were satisfied with standard of grid ($y^+ < 5$) in FLUENT. In the case of first grid height of 1.5×10^{-3} m, average y^+ value was a little larger than the standard of grid, but y^+ values were locally

satisfied with the standard of grid in FLUENT. On the contrary, average y^+ value was far larger than the standard of grid when first gird height was 1.5×10^{-2} m.

Fig. 40 shows the compared results between CFD computed and WT measured C_p of Even-span type greenhouses (Type-EV-D22) according to variations of y^+ values. The results in the central row (C08) were representatively presented in the condition of SST k-ω. As the first grid heights were 1.5×10^{-4} m and 1.5×10^{-3} m, the computed C_p almost exactly corresponded with the measured C_p except a little difference at the windward eaves. The reasons were that the separation points were slightly different in CFD simulation and the wind tunnel test. In the case of 1.5×10^{-2} m of the first grid height, the computed results were out of line with the measured results with a divergent trend. These results could be explained by the failure of CFD simulation, and the difference in results at the windward roof was especially noticeable.

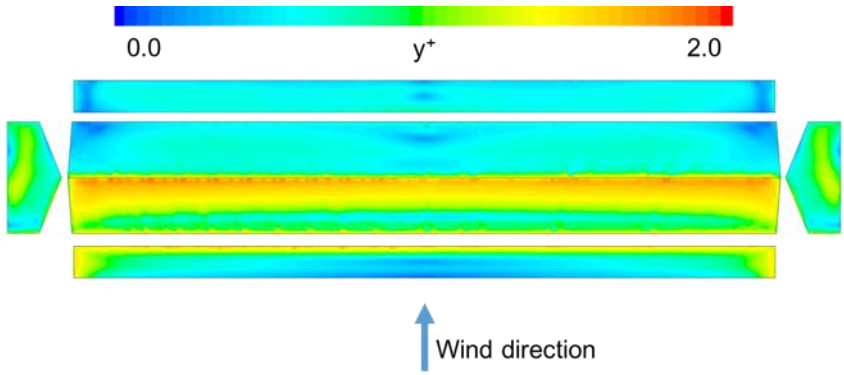

(a) Distribution of y^+ value (1.5×10^{-4} m of first grid height)

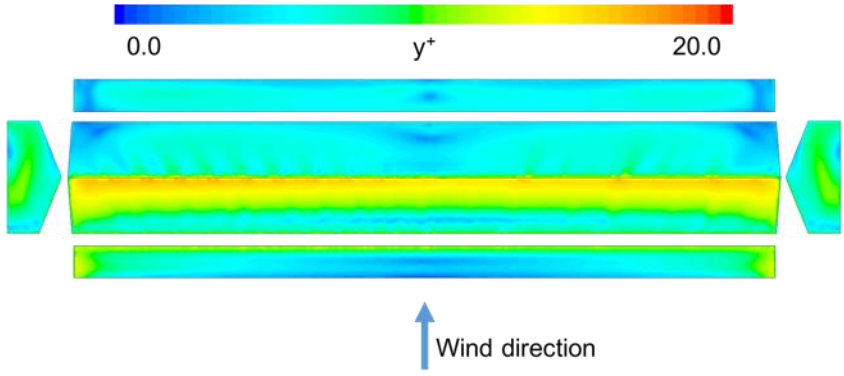

(b) Distribution of y^+ value (1.5×10^{-3} m of first grid height)

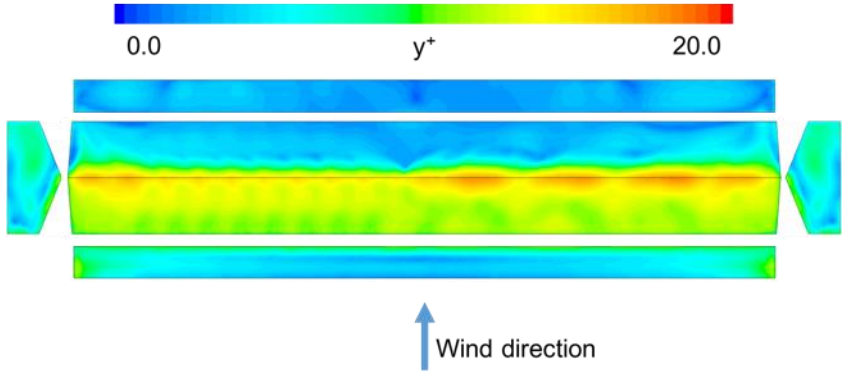

(c) Distribution of y^+ value (1.5×10^{-2} m of first grid height)

Fig. 39 Distributions of y^+ value of Type-EV-D22 as first grid heights were 1.5×10^{-4} m (a), 1.5×10^{-3} m (b) and 1.5×10^{-2} m (c) when the wind direction was 0°

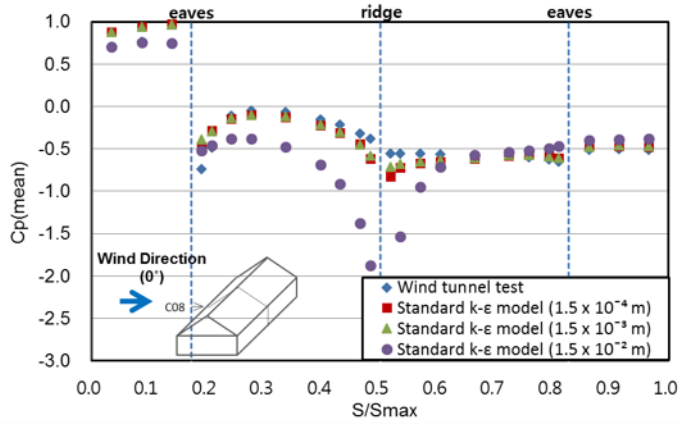

(a) Wind pressure coefficients according to y^+ value (Standard k-ε model)

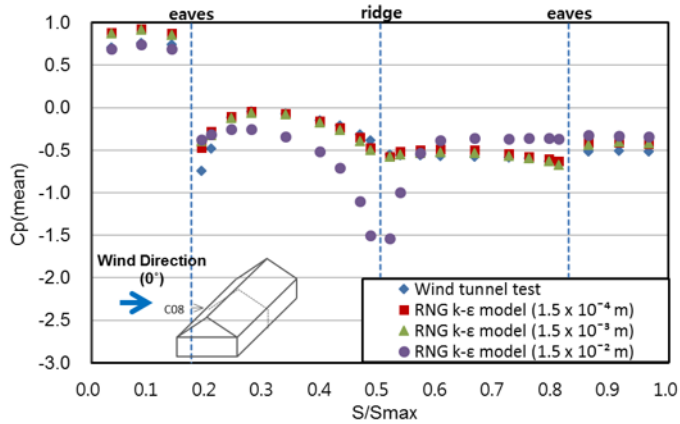

(b) Wind pressure coefficients according to y^+ value (RNG k-ε model)

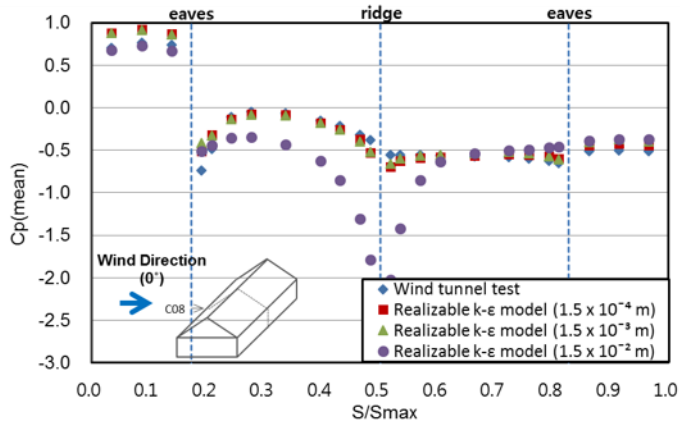

(c) Wind pressure coefficients according to y^+ value (Realizable k-ε model)

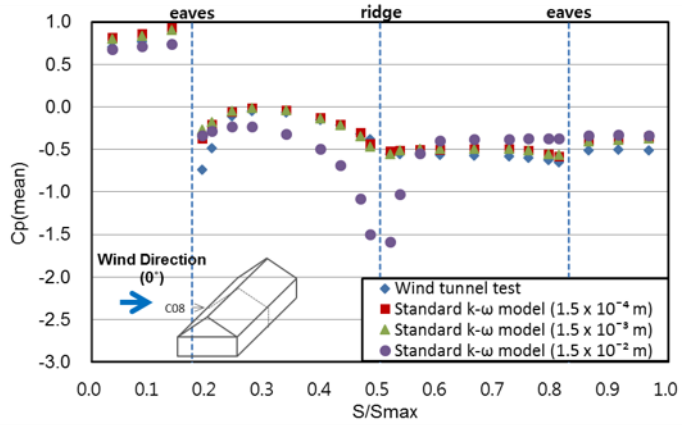

(d) Wind pressure coefficients according to y^+ value (Standard k-ω model)

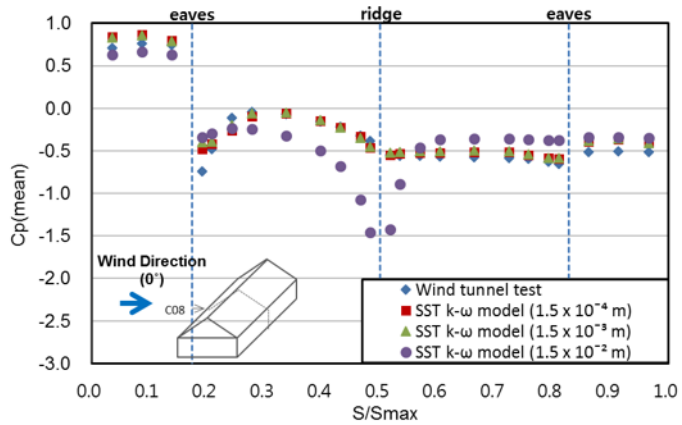

(e) Wind pressure coefficients according to y^+ value (SST k-ω model)

Fig. 40 Comparison between CFD computed and WT measured wind pressure coefficients of Type-EV-D22 according to first grid heights when the wind direction was 0°
(a) Standard k-ε model (b) RNG k-ε model (c) Realizable k-ε model (d) Standard k-ω (e) SST k-ω model

R^2 was used in order to quantitatively express the difference between the computed and the measured results according to variations in y^+ value (Table 21). When the first grid heights were 1.5×10^{-4} m and 1.5×10^{-3} m, there was a high correlation between the computed and the measured results in all turbulence models, and R^2 values ranged from 0.91 to 0.94. As the first grid

height increased to 1.5×10^{-2} m, R^2 values decreased remarkably from 0.39 to 0.46. From these results, it was determined that the air flow in the near wall region was important for predicting the wind pressure of greenhouses, and the grid in the near wall region need to be sophisticatedly designed. In this study, the first grid height was selected as 1.5×10^{-4} m in consideration of the standard of grid in FLUENT and results correlation.

Table 21 R^2 values between CFD computed and WT measured wind pressure coefficients of Type-EV-D22 according to first grid height when the wind direction was 0°

Turbulence model	First grid height (m)	R^2
Standard k-ε	1.5×10^{-4}	0.92
	1.5×10^{-3}	0.92
	1.5×10^{-2}	0.39
RNG k-ε	1.5×10^{-4}	0.91
	1.5×10^{-3}	0.92
	1.5×10^{-2}	0.43
Realizable k-ε	1.5×10^{-4}	0.93
	1.5×10^{-3}	0.92
	1.5×10^{-2}	0.41
Standard k-ω	1.5×10^{-4}	0.92
	1.5×10^{-3}	0.91
	1.5×10^{-2}	0.46
SST k-ω	1.5×10^{-4}	0.94
	1.5×10^{-3}	0.94
	1.5×10^{-2}	0.44

4.4.2 Comparison of wind pressure coefficients for decision of domain size

The wind velocity vector at the central surface of domain was illustrated according to the length of downstream part in the case of Even-span type greenhouse (Type-EV-D22) when the wind direction was 0° to the side wall (Fig. 41). When the length of the downstream part was in the range of 10H to 25H, the backflow was formed inside the computational domain, and the shape of backflow

was similar to each other. On the other hand, when the length of the downstream was 5H, the wind flowed in from outlet of domain, while the backflow was not formed inside the computational domain.

CFD computed C_p were compared with the WT measured C_p in the central row according to the length of the downstream part (Fig. 42). The computed results mostly agreed with the measured results irrespective of the length of the downstream in the range of 10H to 25H. The reason was that the length of the downstream part was long enough that the shape of backflow could be formed inside the domain. As the length of the downstream was 5H, the computed C_p had a similar tendency with the measured C_p, but the computed results were overestimated in comparison with the measured results. These results could be explained by the instability of computations due to short length of the downstream part.

Fig. 43 and Fig. 44 shows a comparison between the CFD computed C_p and the WT measured C_p in the central row according to the length of the side part (Fig. 43) and the upper part (Fig. 44). The computed results agreed with each other in all cases because the airflows weren't influenced by the side and the upper boundary when the length of the side and the upper parts were greater than 5H.

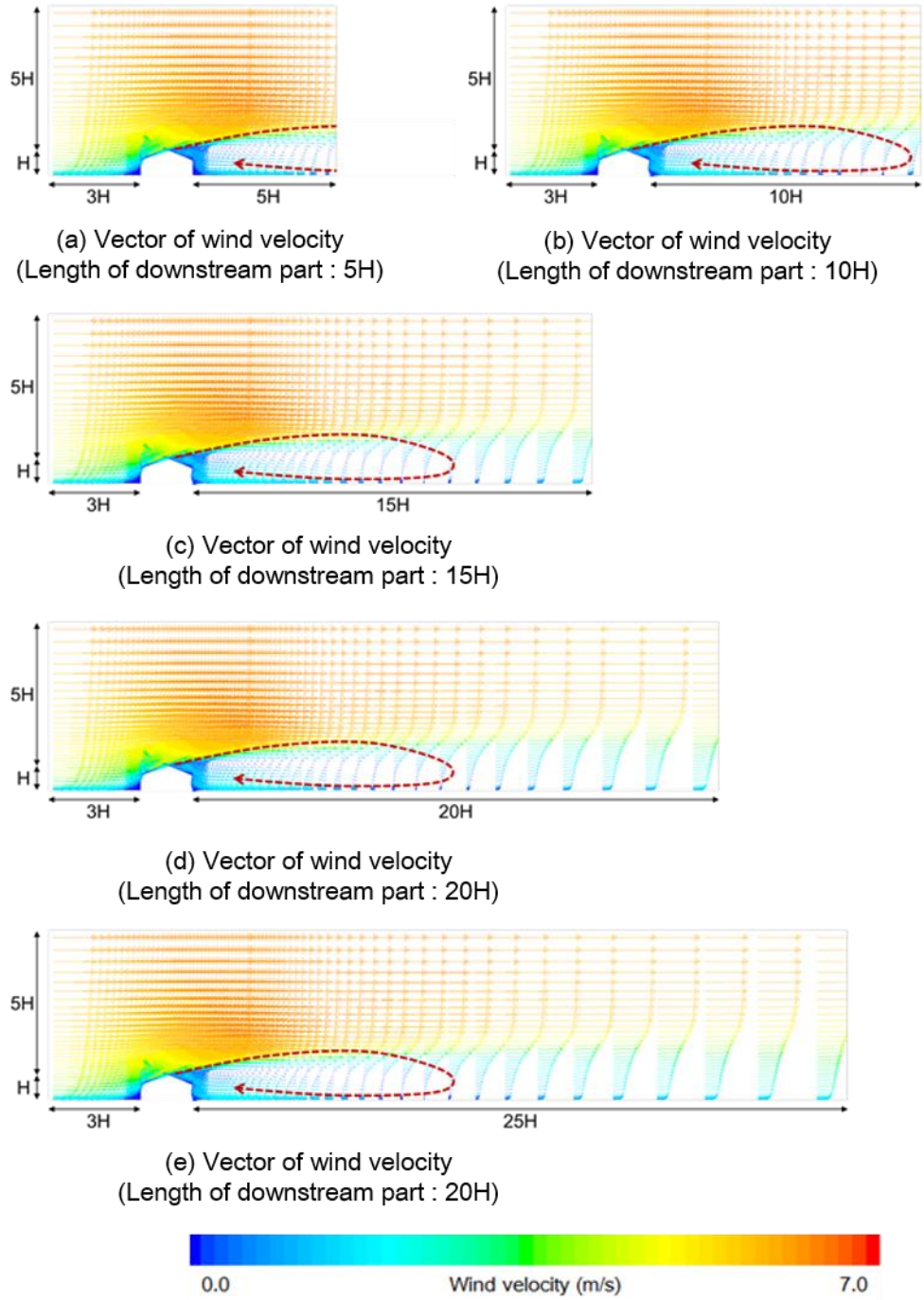

Fig. 41 Vector of wind velocity at central surface of computational domain according to length of downstream part when greenhouse type was Type-EV-D22, and the wind direction was 0°
(a) 5H, (b) 10H, (c) 15H, (d) 20H and (d) 25H

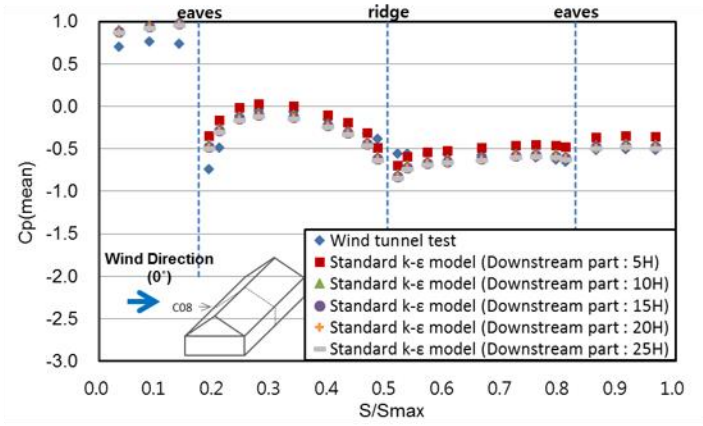

(a) Wind pressure coefficients according to length of downstream part (Standard k-ε model)

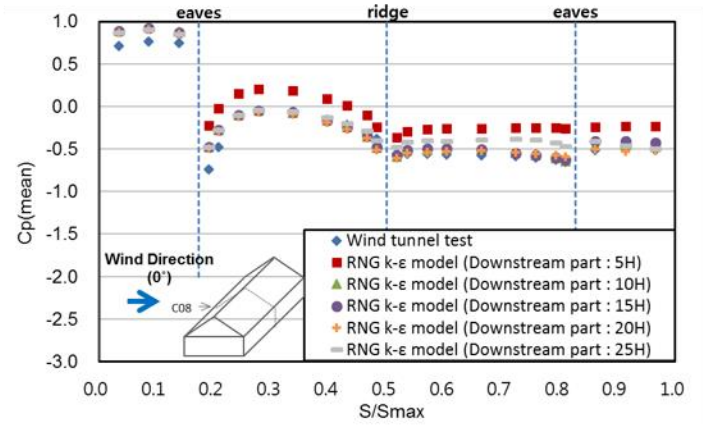

(b) Wind pressure coefficients according to length of downstream part (RNG k-ε model)

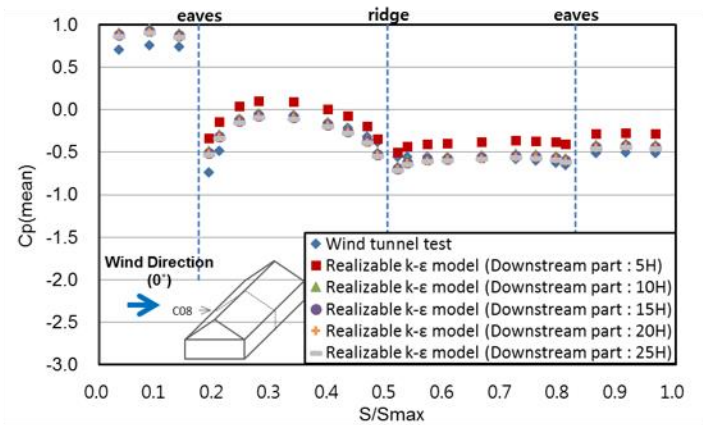

(c) Wind pressure coefficients according to length of downstream part (Realizable k-ε model)

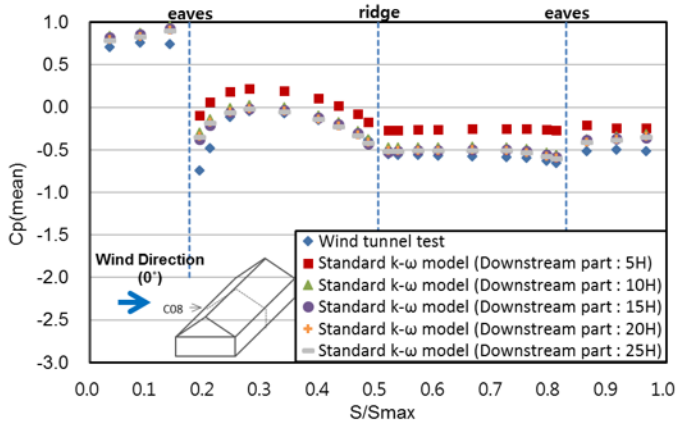

(d) Wind pressure coefficients according to length of downstream part (Standard k-ω model)

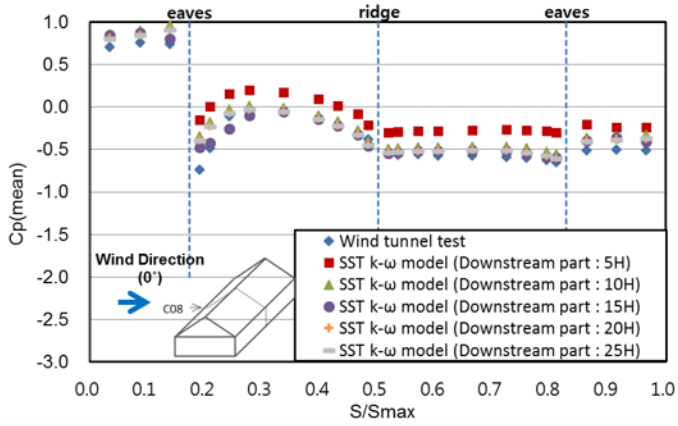

(e) Wind pressure coefficients according to length of downstream part (SST k-ω model)

Fig. 42 Comparison between CFD computed and WT measured wind pressure coefficients of Type-EV-D22 according to length of downstream part when the wind direction was 0°
(a) Standard k-ε model (b) RNG k-ε model (c) Realizable k-ε model (d) Standard k-ω (e) SST k-ω model

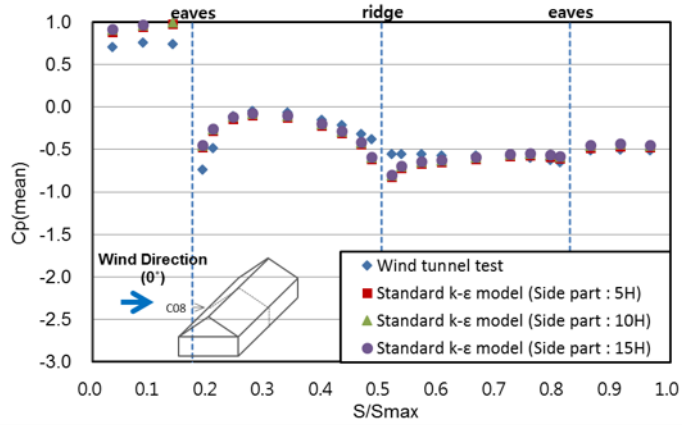

(a) Wind pressure coefficients according to length of side part (Standard k-ε model)

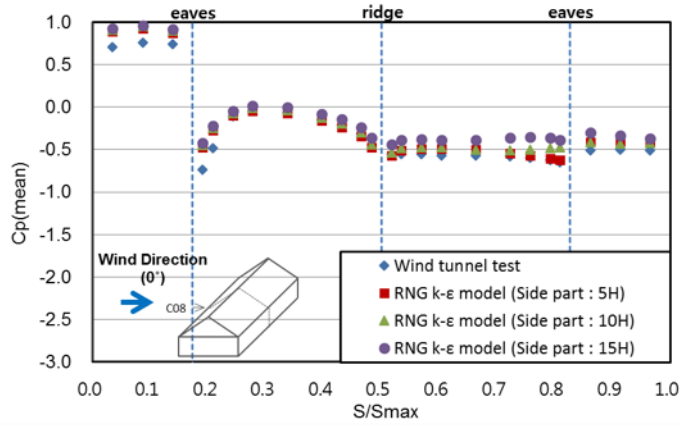

(b) Wind pressure coefficients according tolength of side part (RNG k-ε model)

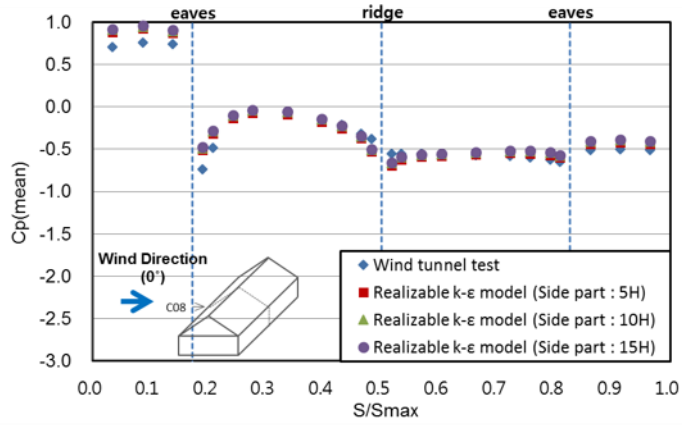

(c) Wind pressure coefficients according to length of side part Realizable k-ε model)

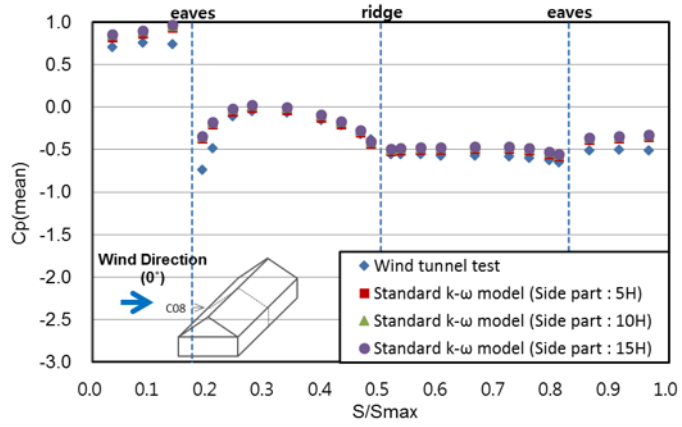

(d) Wind pressure coefficients according to length of side part (Standard k-ω model)

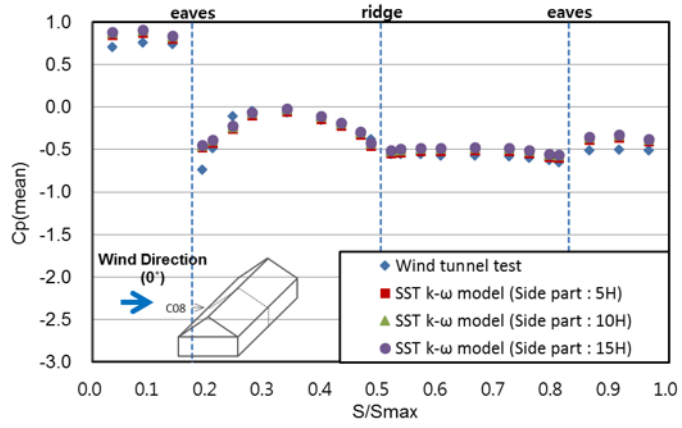

(e) Wind pressure coefficients according to length of side part (SST k-ω model)

Fig. 43 Comparison between CFD computed and WT measured wind pressure coefficients of Type-EV-D22 according to length of side part when the wind direction was 0°
(a) Standard k-ε model (b) RNG k-ε model (c) Realizable k-ε model (d) Standard k-ω (e) SST k-ω model

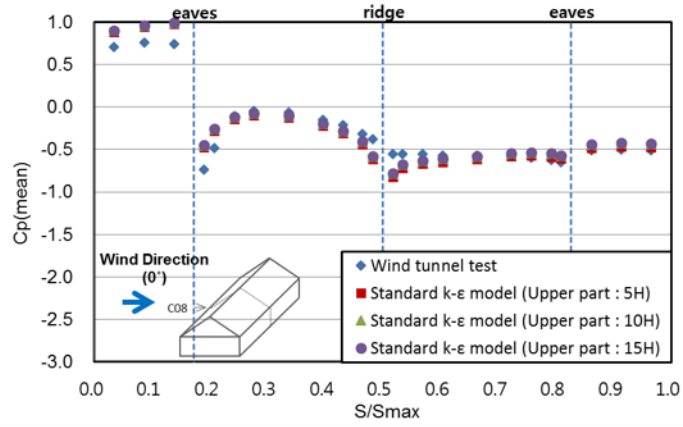

(a) Wind pressure coefficients according to length of upper part (Standard k-ε model)

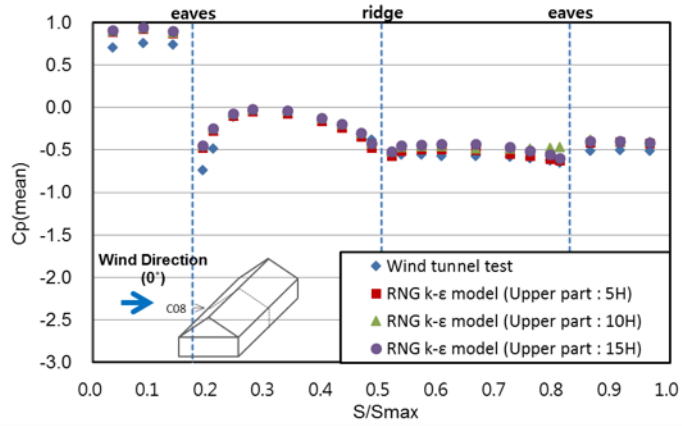

(b) Wind pressure coefficients according to length of upper part (RNG k-ε model)

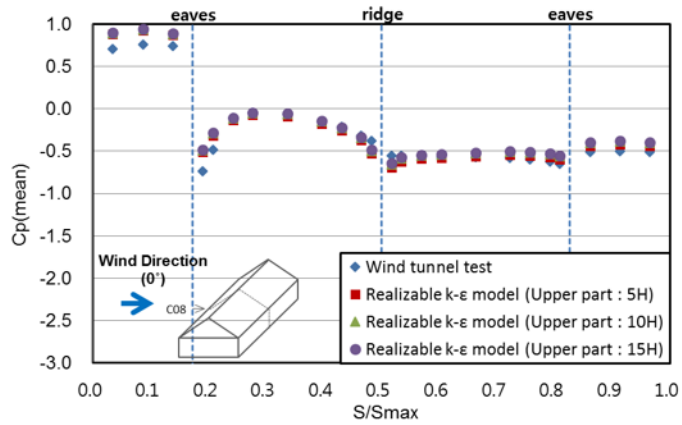

(c) Wind pressure coefficients according to length of upper part (Realizable k-ε model)

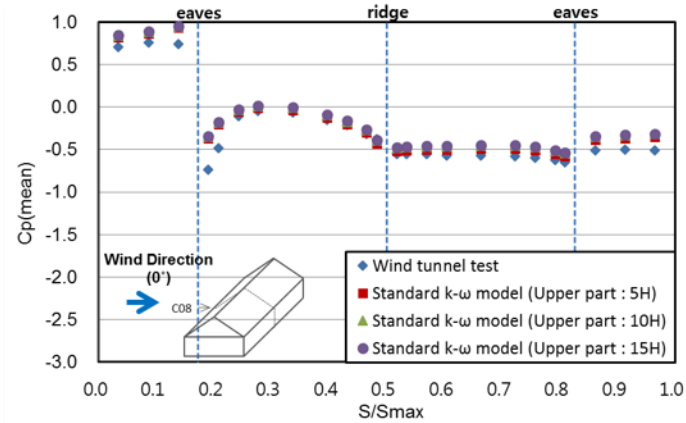

(d) Wind pressure coefficients according to length of upper part (Standard k-ω model)

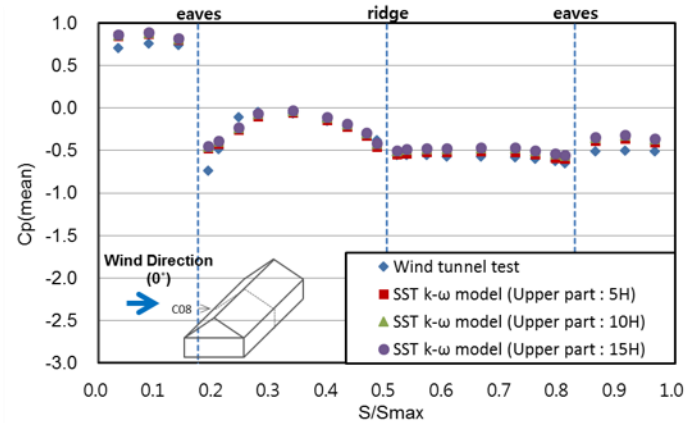

(e) Wind pressure coefficients according to length of upper part (SST k-ω model)

Fig. 44 Comparison between CFD computed and WT measured wind pressure coefficients of Type-EV-D22 according to length of upper part when the wind direction was 0°
(a) Standard k-ε model (b) RNG k-ε model (c) Realizable k-ε model (d) Standard k-ω (e) SST k-ω model

R^2 and d values were used for quantitatively comparing the computed and the measured results according to the length of the downstream, side and upper parts (Table 22 and Table 23). R^2 value was approximately consistent with the maximum difference of 0.02 in the case of the length of the downstream part. These were the reasons why the CFD computed C_p agreed with the WT measured C_p

as the length of the downstream was from 10H to 25H. When the length of the downstream part was 5H, R^2 was pretty high like in other cases. These results were caused by the fact that the tendency was similar between the computed and the measured results, even though the computed results were larger than the measured results. On the contrary, d value was the smallest in length in the downstream part of 5H, and especially the maximum difference of d value according to the length of the downstream part was about 0.15 when the turbulence model was RNG $k-\varepsilon$ model. R^2 and d values were pretty high in all turbulence models irrespective of the length of the side and the upper parts. These results were caused by the facts that the airflows weren't influenced by the side and the upper boundary. From these results, the length of the downstream, side and upper part were determined as 15H, 5H and 5H with consideration for effectiveness and the accuracy of computation, and finally determined the size of the computational domain illustrated in Fig. 45.

Table 22 R^2 and d values between CFD computed and WT measured wind pressure coefficients of Type-EV-D22 according to length of downstream parts when the wind direction was 0°

Turbulence model	Length of downstream part	R^2	d
Standard k-ε	5H	0.92	0.94
	10H	0.92	0.97
	15H	0.92	0.98
	20H	0.92	0.98
	25H	0.92	0.98
RNG k-ε	5H	0.90	0.81
	10H	0.91	0.95
	15H	0.91	0.95
	20H	0.91	0.96
	25H	0.91	0.96
Realizable k-ε	5H	0.93	0.90
	10H	0.93	0.97
	15H	0.93	0.97
	20H	0.93	0.98
	25H	0.93	0.98
Standard k-ω	5H	0.91	0.85
	10H	0.91	0.95
	15H	0.92	0.96
	20H	0.91	0.96
	25H	0.91	0.96
SST k-ω	5H	0.92	0.87
	10H	0.92	0.96
	15H	0.94	0.98
	20H	0.92	0.97
	25H	0.92	0.97

Table 23 R^2 and d values between CFD computed and WT measured wind pressure coefficients of Type-EV-D22 according to length of side and upper parts when the wind direction was 0°

Turbulence model	Length of side part	R^2	d	Length of upper part	R^2	d
Standard k-ε	5H	0.92	0.98	5H	0.92	0.98
	10H	0.92	0.97	10H	0.92	0.97
	15H	0.92	0.97	15H	0.92	0.97
RNG k-ε	5H	0.91	0.95	5H	0.91	0.95
	10H	0.93	0.96	10H	0.91	0.95
	15H	0.92	0.95	15H	0.91	0.94
Realizable k-ε	5H	0.93	0.97	5H	0.93	0.97
	10H	0.93	0.97	10H	0.93	0.97
	15H	0.93	0.97	15H	0.93	0.96
Standard k-ω	5H	0.92	0.96	5H	0.92	0.96
	10H	0.92	0.96	10H	0.92	0.95
	15H	0.92	0.95	15H	0.92	0.95
SST k-ω	5H	0.94	0.98	5H	0.94	0.98
	10H	0.94	0.98	10H	0.94	0.97
	15H	0.94	0.98	15H	0.94	0.97

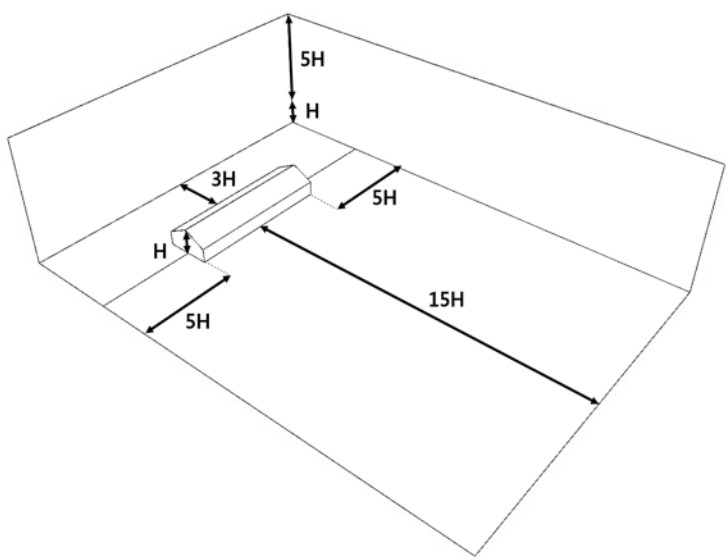

Fig. 45 Finally determined computational domain size in CFD simulation

4.4.3 Comparison of wind pressure coefficients for grid independence

The correlation analyses between the computed and the measured C_p were conducted for a grid independence test for Even-span type greenhouse (Type-EV-D22) when the wind direction was 0° to the side wall (Fig. 46). The highest correlations (R^2=0.94) between the computed and the measured results were observed when the grid size was 1.0×10^{-2}, and R^2 value decreased to 0.85 as grid size increased to 5.5×10^{-2} m. These results could be explained by the computing systems at the center of grid in CFD simulation. Therefore, the accuracy of the computed results increased when the grid size became smaller. These principles were more important in predicting the wind pressure because the variations in the wind pressure were from surface to surface.

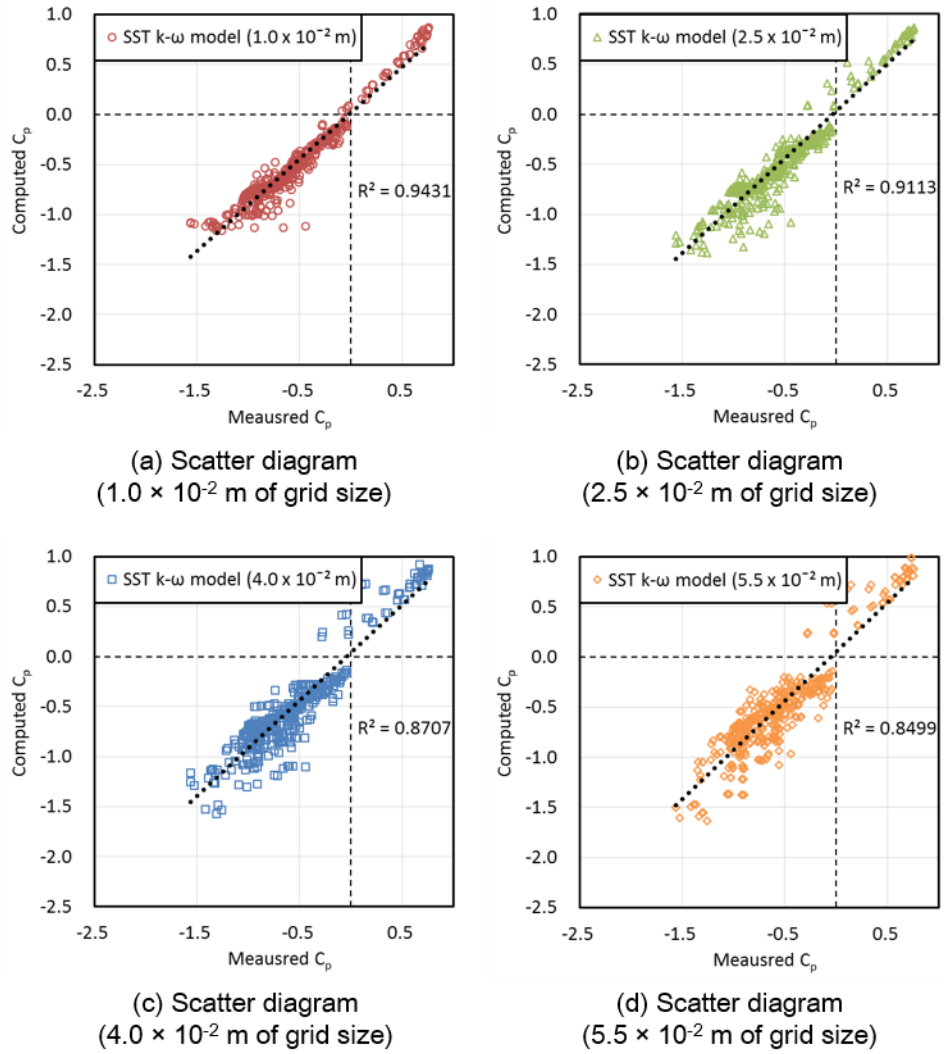

Fig. 46 Scatter diagram between CFD computed and WT measured wind pressure coefficients of Type-EV-D22 as grid sizes were 1.0 × 10^{-2} m (a), 2.5 × 10^{-2} m (b), 4.0 × 10^{-2} m (c) and 5.5 × 10^{-2} m (d) when the wind direction was 0°

R^2 values were presented for a grid independence test according to turbulence model (Table 24). In the case of grid size of 1.0 × 10^{-2} m, R^2 values were the highest among all turbulence models. As the grid size increased, R^2 values also decreased generally. R^2 value, for example, was about 0.71 for the grid size of 1.0 × 10^{-2} m. In this study, the gird size was designed by 1.0 × 10^{-2} m in consideration of design of grids and the accuracy of computations for CFD model

of multi-span greenhouses.

Table 24 R^2 values between CFD computed and WT measured wind pressure coefficients of Type-EV-D22 according to grid size when the wind direction was 0°

Turbulence model	gird size (m)	R^2
Standard k- ε	1.0×10^{-2}	0.92
	2.5×10^{-2}	0.84
	4.0×10^{-2}	0.76
	5.5×10^{-2}	0.71
RNG k- ε	1.0×10^{-2}	0.91
	2.5×10^{-2}	0.89
	4.0×10^{-2}	0.86
	5.5×10^{-2}	0.84
Realizable k- ε	1.0×10^{-2}	0.93
	2.5×10^{-2}	0.88
	4.0×10^{-2}	0.83
	5.5×10^{-2}	0.75
Standard k- ω	1.0×10^{-2}	0.92
	2.5×10^{-2}	0.88
	4.0×10^{-2}	0.83
	5.5×10^{-2}	0.79
SST k- ω	1.0×10^{-2}	0.94
	2.5×10^{-2}	0.91
	4.0×10^{-2}	0.87
	5.5×10^{-2}	0.85

4.4.4 Comparison of wind pressure coefficients according to turbulence model

The first grid size, domain size, and grid size were designed on the basis on previous results, and the results were analyzed using R^2, RSR and d in all types of Even-span and Peach type greenhouses. Firstly, the statistical indices between the computed and the measured results of Even-span type greenhouses were analyzed according to turbulence model when the wind directions were 0° and 90° to the side wall (Table 25). The CFD computed C_p agreed quite well with the WT measured C_p regardless of turbulence model,

wind direction and roof slope. Especially, the statistical indices indicated the outstanding predictability of CFD model when the wind direction was 90° to the side wall. When the wind direction was 0°, the correlation between the computed and the measured were almost high in all turbulence models except RNG k−ε model. Therefore, Standard k−ε model, Realizable k−ε model, Standard k−ω model and SST k−ω model were determined as appropriate turbulence models for predicting the wind pressure of Even-span type greenhouses.

Table 25 Statistical indices between CFD computed and WT measured wind pressure coefficients of Even-span type greenhouses according to turbulence model when the wind directions were 0 and 90°

Roof slope / Wind direction	Statistical index	Standard k−ε	RNG k−ε	Realizable k−ε	Standard k−ω	SST k−ω
22° / 0°	R^2	0.92	0.91	0.93	0.92	0.94
	RSR	0.32	0.42	0.33	0.38	0.27
	d	0.98	0.95	0.97	0.96	0.98
22° / 90°	R^2	0.91	0.93	0.93	0.91	0.93
	RSR	0.32	0.27	0.28	0.31	0.31
	d	0.97	0.98	0.98	0.98	0.97
26° / 0°	R^2	0.95	0.91	0.96	0.95	0.95
	RSR	0.30	0.44	0.32	0.37	0.28
	d	0.98	0.95	0.98	0.97	0.98
26° / 90°	R^2	0.94	0.95	0.95	0.94	0.94
	RSR	0.30	0.23	0.25	0.28	0.27
	d	0.98	0.99	0.99	0.98	0.98
30° / 0°	R^2	0.97	0.93	0.97	0.97	0.96
	RSR	0.32	0.38	0.28	0.32	0.24
	d	0.98	0.96	0.98	0.98	0.99
30° / 90°	R^2	0.92	0.95	0.94	0.93	0.95
	RSR	0.36	0.22	0.29	0.33	0.24
	d	0.97	0.99	0.98	0.98	0.98

Next, the statistical indices among the computed and the

measured C_p of Peach type greenhouse were analyzed according to turbulence model when the wind direction was 0° and 90° to the side wall. (Table 26). When the wind direction was 90°, there was a high correlation between the computed and the measured C_p in common with the results of Even-span type greenhouses. On the contrary, the statistical indices between the computed and the measured results fluctuated greatly with the experimental conditions of Peach greenhouse when the wind direction was 0°. The predictability of the turbulence model based on k-ε model was better than that of the turbulence model based on k-ω model for Peach type greenhouse (Type-PC-R4000). In the case of Peach type greenhouse (Type-PC-R5000), a correlation between the computed and the measured C_p was similar among the most of turbulence models even though the statistical indices were slightly low in Standard k-ε model. As a Peach type greenhouse (Type-PC-R6000), the turbulence model based on k-ω model made more accurate estimations than a turbulence model based on k-ε model in contrast to the Peach type greenhouse (Type-PC-R4000). These were the reasons that a Peach type greenhouse was similar to Arch type greenhouse in Type-PC-R4000, but it was similar to Even-span type greenhouse in Type-PC-R6000. In other words, the predictabilities of each turbulence model for separation of the airflow were different according to the shape of greenhouse. From these results, RNG k-ε model, Standard k-ω model and SST k-ω model were determined as appropriate turbulence model because this turbulence model had higher statistical indices than others.

Table 26 Statistical indices between CFD computed and WT measured wind pressure coefficients of Peach type greenhouses according to

turbulence model when the wind directions were 0 and 90°

Curvature radius of the roof / Wind direction	Statistical index	Standard k−ε	RNG k−ε	Realizable k−ε	Standard k−ω	SST k−ω
4000mm / 0°	R^2	0.94	0.96	0.97	0.84	0.80
	RSR	0.30	0.23	0.22	0.44	0.46
	d	0.98	0.99	0.99	0.95	0.94
4000mm / 90°	R^2	0.90	0.94	0.92	0.91	0.94
	RSR	0.40	0.29	0.35	0.37	0.29
	d	0.97	0.98	0.97	0.97	0.98
5000mm / 0°	R^2	0.83	0.88	0.88	0.87	0.87
	RSR	0.58	0.41	0.47	0.51	0.43
	d	0.93	0.96	0.96	0.93	0.95
5000mm / 90°	R^2	0.91	0.92	0.93	0.92	0.91
	RSR	0.37	0.31	0.31	0.33	0.33
	d	0.97	0.97	0.98	0.97	0.97
6000mm / 0°	R^2	0.67	0.81	0.78	0.94	0.94
	RSR	0.78	0.50	0.60	0.41	0.31
	d	0.88	0.94	0.93	0.96	0.98
6000mm / 90°	R^2	0.91	0.94	0.93	0.92	0.94
	RSR	0.37	0.28	0.32	0.35	0.28
	d	0.97	0.98	0.98	0.97	0.98

As results of Even−span and Peach type greenhouse, Standard k−ω model and SST k−ω model were determined as optimum turbulence model for predicting the wind pressure. In this study, SST k−ω model was finally determined as turbulence model for CFD validation model since statistical indices in SST k−ω model were generally higher than that in Standard k−ω model.

4.5 Wind pressure coefficient computed from CFD validation model

C_p of all experimental conditions was computed from CFD validation model designed by determined first grid size, domain size, grid size and turbulence model. CFD computed C_p of Even-span type greenhouse was analyzed according to wind direction and roof slope (Fig. 47). The computed results in the central row of Even-span type greenhouses were presented as representative values when the wind direction was 0°, and the computed results at the end row of Even-span type greenhouse, which had a large negative pressure, were represented when the wind direction was 90°. The CFD computed C_p agreed with the WT measured C_p in all experimental conditions because the eaves and the ridges of Even-span type greenhouse were so angulated that the separation point was clear. CFD validation model could predict wind pressure of Even-span greenhouses with an approach to perfection.

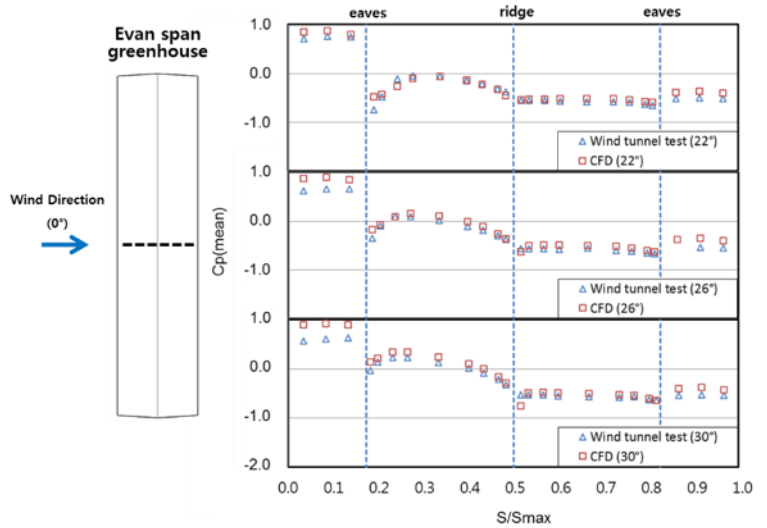

(a) Wind pressure coefficients of Even-span type greenhouses when the wind direction was 0°

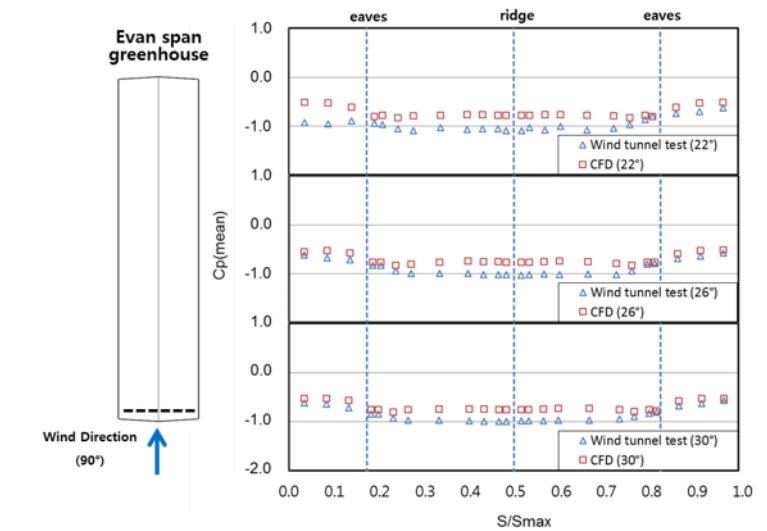

(b) Wind pressure coefficients of Even-span type greenhouses when the wind direction was 90°

Fig. 47 Comparison between CFD computed and WT measured wind pressure coefficients of Even-span type greenhouses using CFD validation model when the wind directions were 0° (a) and 90° (b)

Next, the CFD computed C_p of Peach type greenhouse was presented according to the wind direction and the curvature radius of the roof (Fig. 48). When the wind directions were 0° and 90° to the side wall, the computed C_p in the central and end row of Peach

type greenhouse was presented as representative values, respectively. The computed results agreed with the measured results when the wind direction was 90°. When the wind direction was 0°, CFD validation model properly predicted the wind pressure coefficient in the case of Peach type greenhouse (Type-PC-R5000 and Type-PC-R6000). However, the difference between the computed and the measured C_p existed in case of Peach type greenhouse (Type-PC-R4000). The reasons for these were that Peach type greenhouse (Type-PC-R4000) was similar to the Arch type greenhouse, and the separation point of the curved surface was determined from the Reynolds number. Although the air flow was designed for a wind tunnel with an approach focusing on accuracy, the air flow near the greenhouse model might be unstable since the greenhouses were low building. As seen in Fig. 48(a), the Reynolds number near the greenhouse model was larger in the wind tunnel test than in CFD simulation. For these reason, CFD validation model produced successful results in all experimental conditions. In conclusion, it was determined that CFD validation model was very appropriate for estimation of the wind pressure for single-span greenhouses.

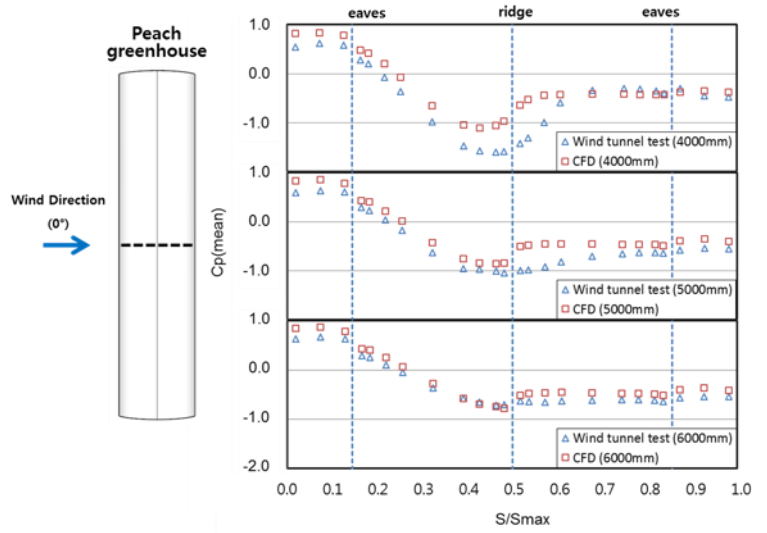

(a) Wind pressure coefficients of Peach type greenhouses when the wind direction was 0°

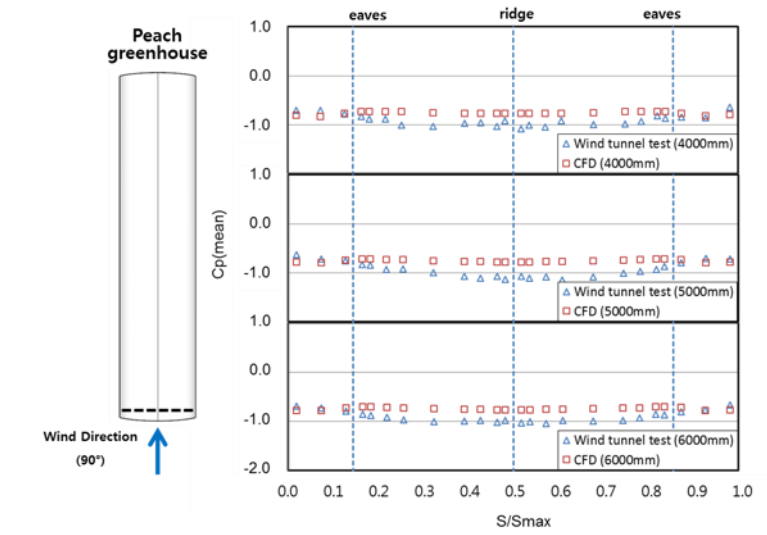

(b) Wind pressure coefficients of Peach type greenhouses when the wind direction was 90°

Fig. 48 Comparison between CFD computed and WT measured wind pressure coefficients of Peach type greenhouses using CFD validation model when the wind directions were 0° (a) and 90° (b)

5. Conclusions

It has been a long time since the greenhouse standards of the countries in the world were updated. Many new types of greenhouse structures have been developed; meanwhile, accuracies of the measuring devices for wind pressure has also been greatly enhanced.

To establish the newly modified greenhouse design standard, especially for reclaimed lands, wind pressure coefficients of 4 representative single-span greenhouse in Korea were evaluated through large-sized wind tunnel tests. In addition, a CFD validation model was developed to estimate wind pressure coefficients of single-span greenhouses.

As a first step, the wind environment was designed inside the wind tunnel using ESDU, and the vertical wind and turbulence intensity profiles were designed inside the wind tunnel. With the boundary condition, the wind pressure distribution of single-span greenhouses was measured through the wind tunnel tests, and then they were compared to the CFD computed results to improve the reliability of CFD model.

The measured wind pressure coefficients were proposed in this study in terms of structural safety and cladding design according to the pre-defined sections of the greenhouse surface, wind environment and design factors, such as the roof slope angle, for Even-span, Three-quarter and Mono-span type greenhouses and the radius of the curvature of the roof for Peach type greenhouses. From the wind tunnel measurement, when the wind blows perpendicularly to the sidewall of the greenhouse (0 and 180° wind directions), a relatively large pressure variation was generated near the eaves of the greenhouse because of the separation phenomena of the airflow; these large pressure differences can cause the collapse and permanent strain of the framework of the greenhouse. The effects of wind directions on the distribution of local wind pressure were very significant, especially at the end corner parts and regions near the eaves of the greenhouse, and these instantaneous

concentrations of strong wind pressure can cause the tearing of cover materials, the destruction of glazing bars and local framework, etc., of the greenhouse facility. Therefore, it could be concluded that detailed consideration and suggestion of not only the structural design but also local the wind pressure for cladding design are significantly important in securing the structural safety and economically stable operation of the greenhouse in response to a strong wind environment.

CFD validations according to y^+ value, computational domain and grid independence tests were conducted by comparing the CFD computed and the wind tunnel measured results of Even-span greenhouse (Type-EV-D22), which has a 22° roof slope when the wind direction was 0° to the side wall. The CFD computed y^+ value corresponded precisely to the WT measured results as the first grid height was 1.5×10^{-4}. From these results, the first grid height was selected to be 1.5×10^{-4} m. In the case of computational domain test, the length of the upstream part was maximally reduced to 3H for preventing the development of an internal boundary layer. The length of the side and the upper side was fixed at 5H in range that airflows were not influenced by the side and the upper boundary. The length of the downstream was determined to be 15H because the CFD model predicted accurately the value to be above 10H. The grid independence test was conducted for determining the grid size around the greenhouse. The accuracy of the CFD model was improved as the grid size decreased. The grid size was designed by 1.0×10^{-2} m based on grid independence test. From the CFD model designed by a given first grid height, domain size and grid size, the results of Even-span and Peach type greenhouses were relatively compared in order to find optimum conditions of turbulence model. SST k-ω model was determined as turbulence model for CFD validation model because the statistical indices in SST k-ω model were generally higher in other turbulence models. Finally, the wind pressure coefficients of all experimental conditions were computed from CFD validation model designed by a given first grid size, domain

size, grid size and turbulence model. It was determined that CFD validation model was appropriate for estimation of the wind pressure coefficient.

References

Blocken. B., T. Stathopoulos, J. Carmeliet. 2007. CFD simulation of the atmospheric boundary layer: wall function problems. *Atmospheric Environment*, *41*(2), 238-252.

Bournet. P.E., S.O. Khaoua, T. Boulard. 2007. Numerical prediction of the effect of vent arrangements on the ventilation and energy transfer in a multi-span glasshouse using a bi-band radiation model. *Biosystems Engineering*, 98(2), 224-234.

Bournet. P.E., T. Boulard. 2010. Effect of ventilator configuration on the distributed climate of greenhouses: A review of experimental and CFD studies. *Computers and Electronics in Agriculture*, 74(2), 195-217.

Cebeci. T., P. Bradshaw. 1977. Momentum transfer in boundary layers. W*ashington, DC, Hemisphere Publishing Corp.; New York, McGraw-Hill Book Co.*, 407 p., 1.

Castro. I.P., A.G. Robins. 1977. The flow around a surface-mounted cube in uniform and turbulent streams. *Journal of Fluid Mechanics*, 79(02), 307-335.

Comite Europeen de Normalisation. 1995. Eurocode-1: Basis of design and actions on structures- Part 2-4: Actions on structures 'Wind actions', Brussels.

Comite Europeen de Normalisation. 1999. prEN 13031-1-Final Draft 'Greenhouses: Design and construction Part 1: Commercial production greenhouses', Brussels.

Drew. D.R., J.F. Barlow, S.E. Lane. 2013. Observations of wind speed profiles over greater London, UK, using Doppler lidar. *Journal of*

Wind Engineering and Industrial Aerodynamics, 121, 98-105.

ESDU. 1993. Wind speed profiles over terrain with roughness changes. Engineering Science Data Unit. ESDU Data Item: 84011.

ESDU. 1993. Longitudinal turbulence intensities over terrain with roughness changes. Engineering Science Data Unit. ESDU Data Item: 84030.

ESDU. 2002. Strong winds in the atmospheric boundary layer Part 2: discrete gust speeds. Engineering Science Data Unit. ESDU Data Item: 83045.

ESDU. 2005. Computer program for wind speeds and turbulence properties: flat or hilly sites in terrain with roughness changes. Engineering Science Data Unit. ESDU Data Item: 01008.

Franke. J., C. Hirsch, A.G. Jensen, H.W. Krus, M. Schatzmann, P.S. Westbury, S.D. Miles, J.A. Wisse, N.G. Wright. 2004. Recommendations on the use of CFD in wind engineering. *Cost action C*, 14, C1.

Harris. R.I., D.M. Deaves. 1980. The structure of strong winds. *Proceedings of the CIRIA conference held on,* 12-13.

Hefny. M.M., R. Ooka. 2008. Influence of cell geometry and mesh resolution on large eddy simulation predictions of flow around a single building. *Building Simulation*, 1, 251-260.

Hoxey. R.P., A.P. Robertson, B. Basara, B.A. Younis. 1993. Geometric parameters that affect wind loads on low-rise buildings: full-scale and CFD experiments. *Journal of Wind Engineering and Industrial Aerodynamics*, 50, 243-252.

Hoxey. R.P., G.M. Richardson. 1983. Wind loads on film plastic

greenhouses. *Journal of Wind Engineering and Industrial Aerodynamics*, 11(1), 225-237.

Hoxey. R.P., G.M. Richardson. 1984. Measurements of wind loads on full-scale film plastic clad greenhouse. *Journal of Wind Engineering and Industrial Aerodynamics*, 16(1), 57-83.

Irwin. H.P.A.H. 1981. The design of spires for wind simulation. *Journal of Wind Engineering and Industrial Aerodynamics*, 7(3), 361-366.

Irwin. J.S. 1979. A theoretical variation of the wind profile power-law exponent as a function of surface roughness and stability. *Atmospheric Environment* (1967), 13(1), 191-194.

Jackson. P.S. 1981. On the displacement height in the logarithmic velocity profile. *Journal of Fluid Mechanics*, 111, 15-25.

Korea Meteorological Administration. 2014. http://www.kma.go.kr.

Launder. B.E., D.B. Spalding. 1974. The numerical computation of turbulent flows. *Computer Methods in Applied Mechanics and Engineering*, 3(2), 269-289.

Lee. I.B., C. Kang, S. Lee, G. Kim, J. Heo, S. Sase. 2004. Development of vertical wind and turbulence profiles of wind tunnel boundary layers. *Transactions of the ASAE*, 47(5), 1717-1726.

Lee. I., S. Sase, A. Okushima, K. Ikeguchi, J. Yun. Choi. 2003. A wind tunnel study of natural ventilation for multi-span greenhouse scale models using two-dimensional particle image velocimetry (PIV). *Transactions of the ASAE*, 46(3), 763-772.

Lee. I.B., T.H. Short. 2000. Two-dimensional numerical simulation of natural ventilation in a multi-span greenhouse. *Transactions of the*

ASAE, 43(3), 745-753.

Legates. D.R., G.J. McCabe Jr. 1999. Evaluating the use of" goodness-of-fit" measures in hydrologic and hydroclimatic model validation. *Water Resources Research*, 35(1), 233-241.

Li. L., A. Kareem, J. Hunt, Y. Xiao, C. Zhou, L. Song. 2015. Turbulence spectra for boundary-layer winds in tropical cyclones: A conceptual framework and field measurements at coastlines. *Boundary-Layer Metrology*, 154, 243-263.

Manual, A. U. S. 2012. Ansys Inc. *Cannonsburg, PA*.

Mathews. E.H., C.P. Crosby, J.A. Visser, J.P. Meyer. 1988. Numerical prediction of wind loads on buildings. *Journal of Wind Engineering and Industrial Aerodynamics*, 31(2), 241-250.

Mathews. E.H., J.P. Meyer. 1987. Numerical modelling of wind loading on a film clad greenhouse. *Building and Environment*, 22(2), 129-134.

Mathews. E.H., J.P. Meyer. 1988. Computation of wind loads on a semicircular greenhouse. *Journal of Wind Engineering and Industrial Aerodynamics*, 29(1), 225-233.

Mehta. K.C., M.L. Levitan, R.E. Iverson, J.R. McDonald. 1992. Roof corner pressures measured in field on a low building. *Journal of Wind Engineering and Industrial Aerodynamics*, 41(1), 181-192.

Ministry of Agriculture, Food and Rural Affairs of Korea. 1995. Standards and Explanations of Greenhouse Structural Design.

Ministry of Agriculture, Food and Rural Affairs of Korea. 2010. Specification and Drawing of Horticulture facility, 2010-128.

Ministry of Agriculture, Food and Rural Affairs of Korea. 2014. Specification and Drawing of Horticulture facility, 2014-78.

Ministry of Agriculture, Food and Rural Affairs of Korea. 2014. http://english.mafra.go.kr/main.jsp.

Ministry of Public Safety and Security of Korea. 2012. http://mpss.go.kr.

Ministry of Land, Infrastructure and Transport of Korea. 1997. Korean Greenhouse design standards for glass type greenhouse. 1997-451.

Ministry of Land, Infrastructure and Transport. 2009. Korean Building Code Structural.

Mistriotis. A., D. Briassoulis. 2002. Numerical estimation of the internal and external aerodynamic coefficients of a tunnel greenhouse structure with openings. *Computers and electronics in Agriculture*, 34(1), 191-205.

Mistriotis. A., T. De Jong, M.J.M. Wagemans, G.P.A. Bot. 1997. Computational fluid dynamics (CFD) as a tool for the analysis of ventilation and indoor microclimate in agricultural buildings. *NJAS wageningen Journal of Life Sciences*, 45(1), 81-96.

Moriasi. D.N., J.G. Arnold, M.W. Van Liew, R.L. Bingner, R.D. Harmel, T.L. Veith. 2007. Model evaluation guidelines for systematic quantification of accuracy in watershed simulations. *Transactions of the ASAE*, 50(3), 885-900.

Moriyama. H., S. Sase, Y. Uematsu. T. Yamaguchi. 2010. Wind tunnel study of the interaction of two or three side-by-side pipe-framed greenhouses on wind pressure coefficients. *Transactions of the ASABE*.

Nuederlandse Norm. 2002. Greenhouses : Design and construction – part 1: commercial production greenhouses.

Prandtl. L. 1925. Über die ausgebildete turbulenz (investigations on turbulent flow). *Z. Angew. Math. Mech*, *5*, 136-139.

Reichrath. S., T.W. Davies. 2002. Computational fluid dynamics simulations and validation of the pressure distribution on the roof of a commercial multi-span Venlo-type glasshouse. *Journal of wind engineering and industrial aerodynamics*, *90*(3), 139-149.

Richards. P.J. 1989. Computational modelling of wind flows around low rise buildings using PHOENIX. Report for the ARFC Institute of Engineering Research Wrest Park, Silsoe Research Institute, Bedfordshire, UK.

Richards. P.J., R.P. Hoxey. 1993. Appropriate boundary conditions for computational wind engineering models using the k–e turbulence model. Journal of Wind Engineering and Industrial Aerodynamics, 46, 145–153.

Richards. P.J., R.P. Hoxey, B.D. Connell. D.P. Lander. 2007. Wind-tunnel modelling of the Silsoe Cube. *Journal of Wind Engineering and Industrial Aerodynamics*, *95*(9), 1384-1399.

Richards. P.J., R.P. Hoxey. Pressures on a cubic building-Part 1 : Full-scale results. *Journal of Wind Engineering and Industrial Aerodynamics*, 102(2012), 72-86.

Richards. P.J., R.P. Hoxey. Pressures on a cubic building-Part 2 : Quasi-steady and other processes. *Journal of Wind Engineering and Industrial Aerodynamics*, 102(2012), 87-96.

Richardson. G.M. 1993. Full-scale wind load measurements on a

single-span film plastic-clad livestock building. *Journal of Agricultural Engineering Research*, 55, 251-264.

Robertson. A.P., Ph. Roux, J. Gratraud, G. Scarascia, S. Castellano, M. Dufresne de Virel, P. Palier. 2002. Wind pressures on permeably and impermeably-clad structures. *Journal of Wind Engineering and Industrial Aerodynamics*, 90(4), 461-474.

Rural Development Administration. 2007. Guide book of horticulture facilities for reducing meteorological disaster.

Rural Research Institute. 1995. Design Guide for Greenhouse Structures.

Shademan. M., R.M. Barron, R. Balachandar, H. Hangan. 2014. Numerical simulation of wind loading on ground-mounted solar panels at different flow configurations. *Canadian Journal of Civil Engineering*, 41, 728-738.

Statistics of Korea. 2014. http://kostat.go.kr/portal/english/index.action.

Tahouri. B., N. Toy, E. Sabory. Surface pressures and wake flows associated with highly curved agricultural buildings. *Journal of Wind Engineering and Industrial Aerodynamics*, 36(1990), 319-327.

Tominaga. Y., A. Mochida, S. Murakami, S. Sawaki. 2008. Comparison of various revised k–ε models and LES applied to flow around a high-rise building model with 1: 1: 2 shape placed within the surface boundary layer. *Journal of Wind Engineering and Industrial Aerodynamics*, 96(4), 389-411.

Uematsu. Y., K. Nakahara, S. Tanaka, H. Moriyama, S. Sase. 2009. Effects on sidewall opening on the wind loads on pipe-framed greenhouses. *Wind Engineering*.

Wang. K. 2005. Modeling terrain effects and application to the wind loading of low buildings, Ph.D Thesis, Concordia University.

Wells. D.A., R.P. Hoxey. 1980. Measurements of wind loads on full-scale glasshouses. *Journal of Wind Engineering and Industrial Aerodynamics*, 6(1), 139-167.

White. F.M. 2007. Fluid Mechanics. Sixth edition, McGraw-Hill.

Wieringa. J. 1992. Updating the Davenport roughness classification. *Journal of Wind Engineering and Industrial Aerodynamics*, 41(1), 357-368.

Wilcox. D.C. 2006. Turbulence Modelling for CFD. Third Edition, DCW Industries.

Willmott. C.J., S.G. Ackleson, R.E. Davis, J.J. Feddema, K.M. Klink, D.R. Legates, J. O'donnell, C.M. Rowe. 1985. Statistics for the evaluation and comparison of models. *Journal of Geophysical Research: Oceans (1978–2012)*, 90(C5), 8995-9005.

국문 초록

풍동 실험과 수치 모델에 의한 온실 풍압 계수 평가

김락우
생태조경 · 지역시스템공학부 지역시스템공학 전공
서울대학교 대학원

우리나라는 1990년대부터 정부의 시설현대화 정책에 힘입어 시설 재배가 보편화되고 있으며, 시설 재배 면적이 지속적으로 증가하고 있다. 또한, 최근 정부에서는 국내 시설 원예 산업의 경쟁력을 확보하고자 새만금을 포함한 화웅, 시화 등 국내 간척지 총 12지구에 첨단수출 원예단지, 일반 원예단지 등 대규모 시설농업 단지 조성 계획을 수립하였다. 그러나, 온실은 일반 건축물보다 낮은 안전율로 설계되고 경량구조물이기 때문에 매년 돌발성 강풍 및 태풍으로 온실이 붕괴되는 피해를 겪고 있다. 이에 따라, 다양한 형태의 원예시설에 대한 구조안전 설계기준 정립이 필요하며, 특히 간척지에서의 강풍 피해를 대비하여 원예 시설물의 풍하중에 대한 구조 안정성 평가 및 대책 마련은 필수적이다.

본 연구에서는 풍하중에 대한 원예 시설물의 구조적 안정성을 평가하기 위하여 국내 대표적 단동 온실인 단동 양지붕형, 단동 3/4형, 단동 복숭아형, 단동 편지붕형 온실의 풍압 계수를 분석하였다. 또한, 폐쇄율, 센서수 등의 한계로 실험에 제약이 있는 연동형 온실의 풍압 분포를 예측하기 위하여 전산유체역학 모델을 설계하였으며 단동 양지붕형, 단동 복숭아형 온실의 풍동 실험 결과와 비교를 통하여 검증을 실시하였다.

먼저, ESDU를 통하여 간척지의 지표면 거칠기를 계산하여 풍속 프로파일과 난류 강도 프로파일을 도출하고 풍동 실험장 풍상측에 풍환경을

조성하였다. 이후, 단동형 온실의 풍향, 지붕경사, 지붕곡률반경에 따라서 풍압 계수를 측정하였으며 온실 표면에 최대 444개의 풍압공을 설치하여 풍압 계수를 지역적으로 분석하였다. 풍동 실험 결과, 바람이 온실의 측벽에 수직으로 불어올 때 (풍향 0, 180°) 처마에서 박리점이 형성되기 때문에 압력 차이가 크게 나타났다. 이러한 결과로부터, 바람이 온실의 측벽에 수직으로 불어올 때 온실 구조 안정성에 큰 영향을 미칠 것으로 판단되었다. 또한, 풍향에 따라서 온실에 국부적으로 높은 압력이 발생하였으며 이는 온실의 외장재의 파괴를 야기할 수 있다고 판단되었다. 따라서, 본 연구에서는 측정된 결과를 바탕으로 구조 설계용 풍압계수와 외장재 설계용 풍압 계수로 구분하여 풍압 계수를 제안하였다.

본 연구에서는 전산유체역학 모델의 검증을 위하여 풍동 실험의 결과와 비교 분석하였으며 y^+ 비교, 계산 영역 시험, 격자 독립성 시험, 난류 모델 비교를 통하여 첫 셀 격자 크기, 계산 영역, 격자 크기, 난류 모델을 결정하였다. 분석 결과, 첫 셀 격자 크기가 1.5×10^{-4} m 일 때 전산유체역학 시뮬레이션으로부터 모의한 풍압 계수가 풍동 실험 결과와 일치하였기 때문에 첫 셀 격자 크기를 1.5×10^{-4} m로 결정하였다. 계산 영역의 경우, 상류 길이는 3H, 측면과 상부 길이는 5H로 결정하였으며 후류의 길이는 연산의 수렴성과 정확성을 고려하여 15H로 결정하였다. 격자 독립성 시험을 바탕으로 격자의 크기를 1.0×10^{-2} m로 결정하였으며 전체적으로 높은 통계적 변량 ($d > 0.94$)을 갖는 SST $k-\omega$ 난류 모델 최종 난류 모델으로 선정하였다. 결정된 기준을 바탕으로 최종 전산유체역학 모델을 설계하였으며 모든 검증용 온실에 대하여 풍압계수 예측을 하고 풍동 실험 결과와 비교하였다. 본 연구에서는 통계적 변량을 통하여 결과를 보다 정량적으로 비교하였으며 단동 양지붕형 온실의 경우 모든 환경조건에 대하여 R^2 가 0.93 이상, d 가 0.97 이상으로 높은 상관성을 보였다. 또한, 단동 복숭아형 온실에서는 모든 환경조건에 대하여 R^2 가 0.80 이상, d 가 0.94 이상의 통계적 수치를 보였다. 이러한 결과로부터 전산유체역학 검증 모델은 풍압 분포를 적절하게 모의한다고 판단하였으며 전산유체역학 검증 모델은 다양한 형태의 단동

형 온실뿐만 아니라 연동형 온실의 풍압 분포 예측에 활용될 수 있을 것으로 판단된다.

주요어 : 단동형 온실, 전산유체역학, 전산유체역학 모델 검증, 풍동 실험, 풍압 계수
학 번 : 2013-23257